DESIGN AND MANUFACTURE OF A HIGH-G UNMANNED AERIAL VEHICLE STRUCTURE

by

Seth Stovack Kessler

S.B. Aeronautics and Astronautics
Massachusetts Institute of Technology, 1998

Submitted to the Department of Aeronautics and Astronautics in Partial Fulfillment of the Requirements for the Degree of

MASTER OF SCIENCE IN AERONAUTICS AND ASTRONAUTICS
AT THE
MASSACHUSETTS INSTITUTE OF TECHNOLOGY

DECEMBER 1999

Signature of Author…….
Department of Aeronautics and Astronautics
December 16th, 1999

Approved by…….
Gregory A. Kirkos
Charles Stark Draper Laboratory
Thesis Supervisor

Certified by……..……..
S. Mark Spearing
Associate Professor of Aeronautics and Astronautics
Thesis Advisor

Accepted by……..……..
Nesbitt Hagood, IV
Associate Professor of Aeronautics and Astronautics
Chairman, Department Graduate Committee

[This page intentionally left blank]

DESIGN AND MANUFACTURE OF A HIGH-G UNMANNED AERIAL VEHICLE STRUCTURE

by

Seth Stovack Kessler

Submitted to the Department of Aeronautics and Astronautics
on December 16th, 1999 in Partial Fulfillment of the
Requirements of for the Degree of Master of Science in
Aeronautics and Astronautics

ABSTRACT

In 1997, the Charles Stark Draper Laboratories commenced a project with the objectives of reducing the risk, cost and time associated with obtaining time critical battlefield reconnaissance data. The Wide Area Surveillance Projective, or WASP, is a small autonomous flyer, which is launched contained in an artillery shell, and then deployed over the battlefield to capture images. The first phase of this project involved identifying and solving the challenges associated with designing a device capable of surviving launch loads of 15,000 g's. The second phase of WASP is currently addressing the manufacturing and flight control issues. The focus of this thesis is on the structural design and manufacture of the WASP vehicle, particularly the aft fuselage section and the wings. The aft section is not only subjected to high impulsive inertial loads, but its weight (being aft of the center of pressure) has a substantial effect on the controllability of the vehicle. Finite element models of this section as well as test specimens are produced to optimize the design. The wings are required to be stiff aerodynamic surfaces, and are folded along the side of the vehicle so as to take up minimal volume. Several different manufacturing procedures are explored to provide a robust set of wings that match all of the specified requirements. All of these pieces need to be as light as possible; therefore they are manufactured in advanced composite materials.

Thesis Supervisor: Gregory A. Kirkos
Charles Stark Draper Laboratory

Thesis Advisor: S. Mark Spearing
Associate Professor of Aeronautics and Astronautics
Massachusetts Institute of Technology

FOREWORD

12/16/99

This thesis was prepared at The Charles Stark Draper Laboratory, Inc., under IRAD funds.

Publication of this thesis does not constitute approval by Draper or the sponsoring agency of the findings or conclusions contained herein. It is published for the exchange and stimulation of ideas.

Permission is hereby granted by the Author to the Massachusetts Institute of Technology to reproduce any or all of this thesis.

_____

Seth S. Kessler

This Work was performed in the Technology Laboratory for Advanced Composites (TELAC) in the Department of Aeronautics and Astronautics at the Massachusetts Institute of Technology. This work was sponsored by the Charles Stark Draper Laboratory.

ACKNOWLEDGMENTS

There are many people I would like to thank for their help and support on this project. Without their help, I would not have been able to accomplish this milestone so quickly, efficiently and with such good results. First of all, I need to thank Draper Labs for funding my research and providing continuous support. In particular, I would like to thank Neil Barbour and Brent Appleby who were the first to believe in the potential of my work, and my advisors at Draper Greg Kirkos and Jamie Anderson. This project would not have been possible without their help along with the rest of the Draper WASP team, Rich, Sean, Jake, Don, Byron, Will, and Frank.

Next I would like to acknowledge everyone who provided technical support for this project at MIT, Draper and elsewhere. Thanks to Al Supple for teaching me almost everything I know about composite manufacturing, and John Kane, Dick Perdichizzi, Don Weiner, John Mahoney and Ed McCormack for provided invaluable assistance with testing and machining throughout my the project. From the Aero/Astro faculty I have received help countless times from Prof. Carlos Cesnik, Prof. Paul Lagace and Prof. Mark Drela, and my advisor Prof. Mark Spearing, who has always trusted in my abilities and pointed me in the right direction. Lastly I would like to thank Alex Plotkin and Don Babcock for their help at Picatinny Arsenal.

Many friends and co-workers at TELAC contributed to this work by helping with research, analysis, writing and providing support. Thank you DJ, Ariela, Torrey, Dennis, Randal and especially Chris Dunn, who has been giving me wonderful advice and inspiration for years, and Staci Jenkins who literally worked by my side. A special thanks goes to all of my UROP's who made this project work: Thad Matuszeski, Ryan Peoples, Larry Pilkington and Caroline Twomey.

Lastly, I would of course like to thank my loving family—Dad, Mom, Bree and Moira—who have always given me their support.

[This page intentionally left blank]

TABLE OF CONTENTS

TABLE OF FIGURES

CHAPTER 1

INTRODUCTION

The Wide Area Surveillance Projectile project, or WASP, was commenced as a cooperative venture between the Massachusetts Institute of Technology (MIT) and the Charles Stark Draper Laboratories in 1997. The goal was to develop a small autonomous flyer that would reduce the risk and time associated with obtaining time-critical battlefield reconnaissance data, for instance regarding mobile tactical formations in the field. WASP was to be a low cost expendable vehicle, which would be launched in an artillery shell and deployed over the battlefield, using visual and infrared cameras to track ground targets. This mission profile required a g-hardened vehicle that was extremely light and sufficiently maneuverable to perform its reconnaissance mission with acceptable endurance. This is a very challenging combination to implement simultaneously.

For the first two years of this project, Draper and the MIT jointly worked to develop the Phase I prototype of WASP as seen in **Figure 1.1**. During this initial "proof of concept" phase, the Draper/MIT team aimed to meet the

geometric constrains of the proposed 5" naval shell, as well as to construct vehicle components that could survive the 15,000-g acceleration load of the launch. Through a combination of cost, fabrication, and time concerns the design team decided to manufacture the prototype largely of aluminum. This design, which can be followed in a previous MIT thesis[1], survived the high-g tests however was unable to achieve controlled flight due to its high weight and poor center-of-gravity placement. A second phase of the program commenced in 1999 to design a second WASP vehicle, incorporating the knowledge gained from the first phase of the project to achieve a successful mission.

Phase II of WASP, the "integrated vehicle demonstration" phase, added some new requirements to the design, and established an end goal of a functional test article able to demonstrate its components while remaining "g-hardened credible." The following is a list of the revised key mechanical requirements for the WASP vehicle:

- Ability to track ground targets at 60 mph
- Steady wind 35 knots, gust 10 knots (upper bound)
- Altitude <1000 feet
- Temperature = 20 - 130° F
- Endurance = 30 minutes (minimum)
- Round = M83 series, 155 mm diameter
  - Payload length 21 inches max
  - Payload diameter 5 inches max
  - Final design may be wider and shorter with XM898 round
  - Round gyro stability > 1.6
- Gun launch
  - Set-back acceleration = 16,000 g
  - Set-forward acceleration = 4,000 g
  - Balloting acceleration = 2,000 g
  - Spin = 270 Hz
  - Barrel soak temperature = 300° F for 15 minutes
- Expulsion pressure = 3,000 psi

Key changes from the original design include using an electric motor in place of the original internal combustion engine, placing the folded wings against the body instead of internally stowed, and making the tail more aerodynamically efficient. The overall design of the WASP II, as seen in **Figure 1.2** is outside the scope of the present thesis but is described in the project's final report[2]. A parallel research program was conducted to explore the use of composites for the wing sections, which is described in a separate thesis[1].

One of the key modifications from the original design was the introduction of carbon fiber reinforced polymer composites as the principal structural material in place of aluminum alloys. Composites have some of the highest values of specific strength and stiffness of any materials, making them prime candidates for the WASP vehicle. However, these potential performance advantages are incurred at the expense of increased cost, and increased complexity of analysis and manufacturing. In addition the heterogeneous nature of composites increases the risk of unanticipated failure modes. The rationale for the work presented in this thesis was to mitigate the programmatic risk of using composites, by providing validated design codes and developing manufacturing processes prior to committing to the use of composites in the WASP II vehicle.

The focus of the first several chapters of this research is on the tail-section of the vehicle. One method of resolving many of the control issues of the original vehicle was by reducing the overall weight of the vehicle as well as shifting the center of gravity further forward. Since the tail-section is located

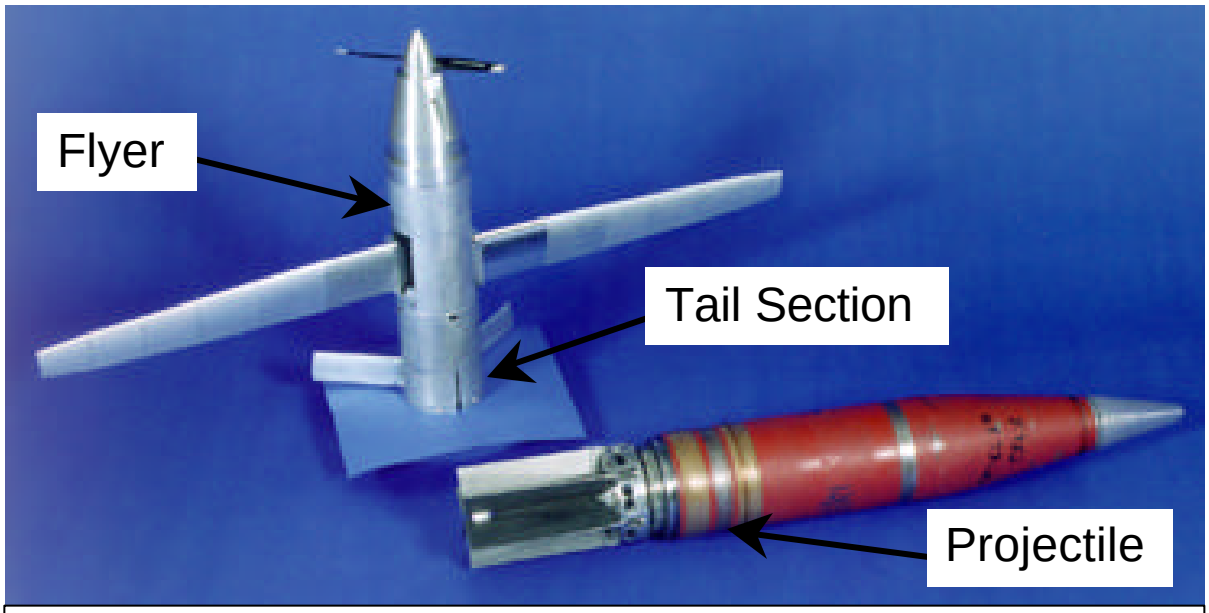

Figure 1.1: Original WASP flyer and projectile[2]

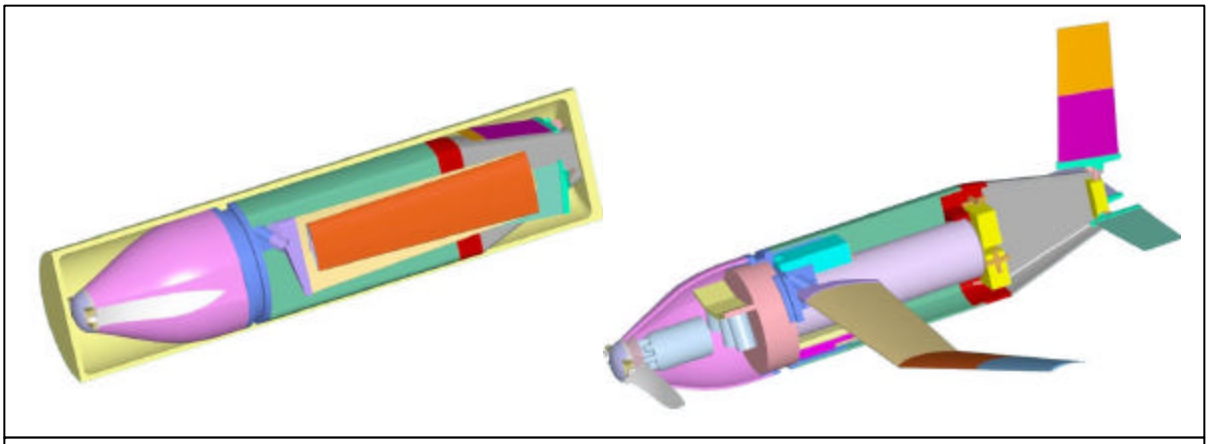

Figure 1.2: CAD representation of WASP II flyer[2]

in the very rear of the vehicle, its weight is crucial to the controllability of the WASP. This section, under the original Phase I WASP design, would also experience the highest axial compressive load since it would have to support the accelerated mass of all the other parts of the vehicle. Thus the design of the tail section was buckling critical in addition to being able to survive the static fracture loads.

Chapter 2 discusses previous research in the buckling of composite cylinders and stress concentrations around slots and cutouts in shells. Chapter 3 goes on to discuss the specific requirements of the tail section, as well as delineating and contrasting the previous design to the current one. Chapters 4 through 7 explain the analysis and testing procedures used to design and verify the g-hardness of the composite tail section, and discuss the different trade-offs associated with the variables involved. Chapters 8 and 9 describe some of the other issues that arose with a composite design, such as adhesive joints and the manufacturing of composite airfoil section and hinge mechanisms. Finally the last chapter concludes with future recommendations for this line of specialized composite research.

[This page intentionally left blank]

CHAPTER 2

BACKGROUND

This chapter presents the findings of a literature search of previous work relevant to this thesis. There were no reports found which directly involved failure of composite cylinders with cutouts under acceleration loading; however, there were several papers that presented many aspects of this topic, including buckling of composite cylinders, compression of cylinders with cutouts, and stress concentrations due to cutouts in shells. These papers were separated into three categories, which are explored further in this chapter: analytical studies, computational studies, and experimental studies.

2.1 Analytical Studies

The analytical methods used to investigate these problems range from solving complex differential equations to finite element analysis. These papers, some of which date back to 1965, cover a broad range of topics relevant to this

thesis including stress concentrations, buckling, compression of cylinders and failure of composite laminates. The three most pertinent topics are described in the following sections.

2.1.1 Stress concentrations

When a section is cut out of a structure under load, such as the slots removed in the WASP vehicle for the tail fins, stress concentrations are introduced. The most common cutout analyzed for cylindrical shells were circular holes. In one technique[3], linear shallow shell differential equations were used to formulate the governing stress functions of the cylindrical shell. After applying an axial tensile load to the system, the equations were solved using the boundary condition that the stress field had to reach zero at the hole. The results of this study can be seen in **Figure 2.1**. The dimensionless curvature parameter β was defined by the equation $\beta^2 = a^2[12(1-\nu^2)]^{1/2}/8Rt$, where *a* was the radius of the hole, *R* was the radius of curvature of the shell, and *t* was the shell thickness. These curves show that as the parameter β is increased, the circumferential membrane stresses at the top of the hole increased as well. Solutions of stress concentrations for more complicated configurations can be found in recently published handbooks[4,5].

2.1.2 Buckling of cylindrical shells

Few analytical studies have been published on the buckling of cylinders. Hoff presented a closed-form solution for the axial loading of a thin-walled cylindrical shell of finite length by representing the boundary at the circular edges with simple supports[6]. His solution, which can be seen in **Figure 2.2**, plotted the normalized shell length $\lambda = [12(1-\nu^2)^{1/4} L/(ah)^{1/2}$ (where a was the shell radius and h the thickness) versus the buckling stress ratio $p=\sigma/\sigma_{cl}$, where $\sigma_{cl} = Eh/a[3(1-\nu^2)]^{1/2}$. The interesting result drawn from this figure is the fact that for a symmetric buckling mode with this boundary condition, the buckling load was determined to be about half of the classical value, regardless of the cylinder length, radius or thickness. The author was unable however, to find close-form solutions for several other boundary conditions he investigated in this paper. Generally, the dynamics of buckling are too complicated to solve analytically, and are usually analyzed using finite element techniques over differential equations, as described in the following section.

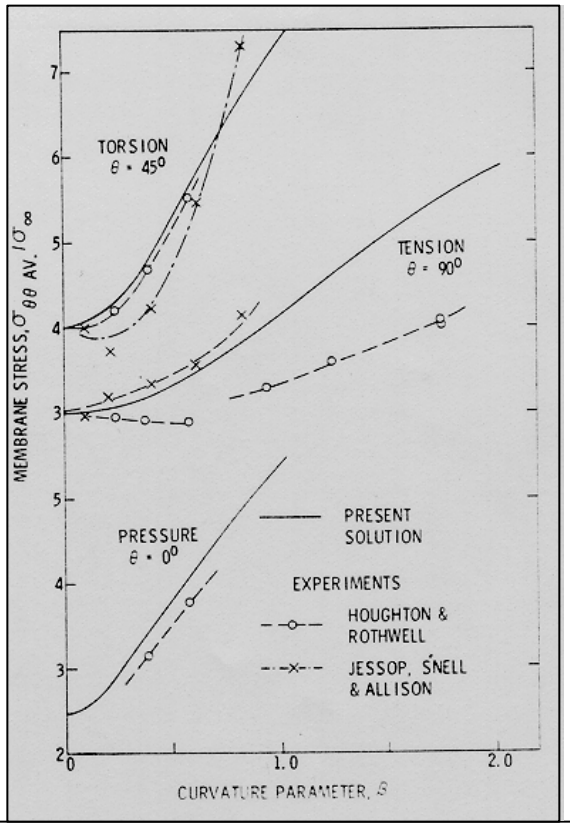

Figure 2.1: Variation of stress concentration due to cutout geometry[3]

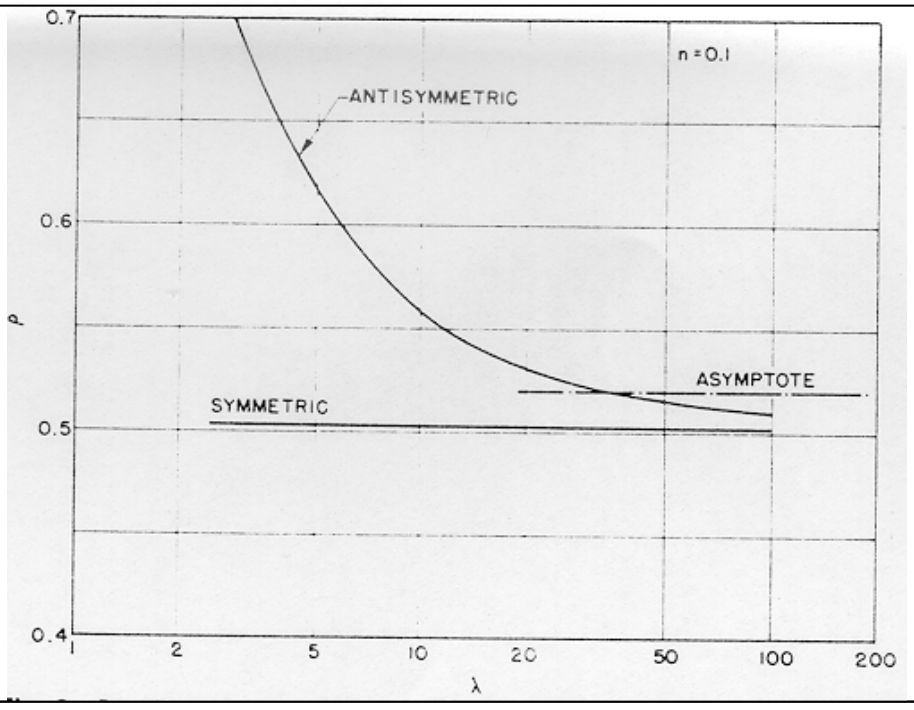

Figure 2.2: Buckling stress ratio versus normalized shell length[6]

2.1.3 Composite cylinders with cutouts

Other studies have used more sophisticated methods to solve analytical problems, such as the finite element analysis presented in this thesis. Hilburger[7] analyzed the response of composite cylindrical shells with cutouts using a non-linear finite element code called STAGS (STructural Analysis of General Shells). The results, as shown in **Figure 2.3**, indicated that a nonlinear interaction between in-plane stresses and out-of-plane deformations in a compression loaded shell caused local buckling near the cutout. These results also indicated that increasing the area of the cutout significantly reduced the initial buckling load of the shell. Also covered in this paper were the effects of internal pressure on the buckling of composite shells. Much of this research has been in collaboration with NASA Langley Research Center.

2.2 Computational Studies

A few papers were found that chose a computational approach to solving problems concerning buckling of cylinders and failure of composite laminates. This involved solving recursive series on a computer to predict stresses and displacements, and writing codes to optimize fiber orientation in laminates under certain loading conditions. The following sections describe in more detail some of the computational work found.

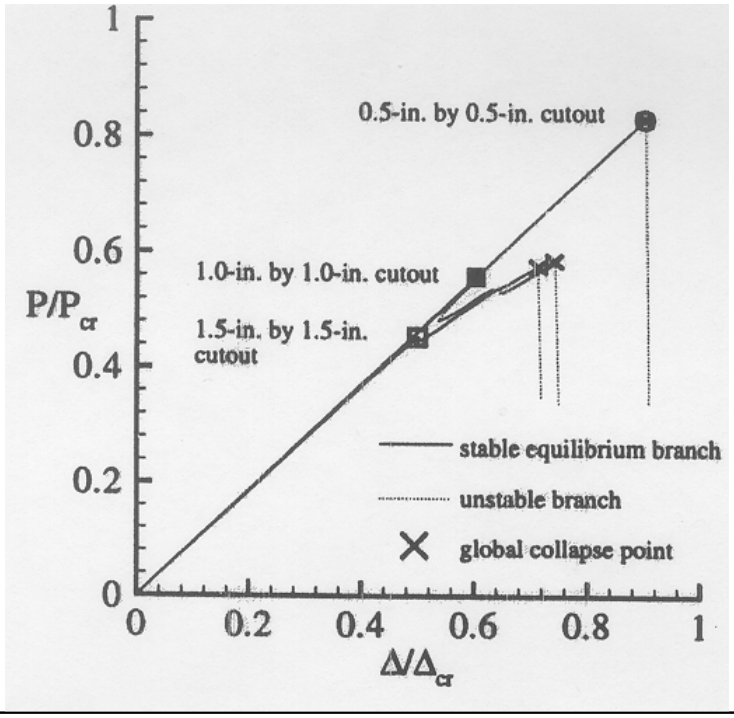

Figure 2.3: Effect of cutout size on shell response[7]

2.2.1 Composite shells

Noor and Burton[8] presented an assessment of several computational models for multi-layered composite shells. Although the results were not directly relevant to this thesis, four interesting general conclusions were drawn. First, the authors stated that transverse shear deformation had a much greater effect on the response than that of transverse normal strain and stress that became noticeable only in regions of high localized loading. Secondly, the accuracy of the first-order shear deformation theory depended strongly on the values of the composite shear correction factors selected. Thirdly they concluded that the accurate prediction of the stress and displacements through the thickness of a shell required 3-D equilibrium and constitutive relations. Lastly, the authors confirmed that predictor-corrector approaches to determining the response characteristics of shells appeared to be a very effective procedure for global as well as detailed results.

2.2.2 Buckling of composite cylinders

A computational procedure for evaluating the buckling of a multi-layered cylinder was explored by Noor in a subsequent paper[9]. In this paper, the author presented an efficient procedure that was based on linear 3-D elasticity theory including the orthotropic material properties of the composite layers. The code would approximate the buckling response of the cylinder associated with a certain range of Fourier harmonics using a two-field mixed finite element models in the thickness direction and successive applications of the Rayleigh-Ritz technique. This method reduced the number of arithmetic operations involved in the solution, and presented comparable results to traditional methods.

2.2.3 Buckling resistance in composite shells with cutouts

Some of the more advance research in computational methods has been performed in the area of buckling resistance in composite cylinders. One technique[10] presented a sequential linear programming method, which optimized fiber orientation and cutout geometry for buckling resistance in composite shells. The paper concluded that the buckling of a composite shell is strongly influenced by fiber orientation and the presence of cutouts. As demonstrated in **Figure 2.4** by the results of a $[\pm\theta/90_2/0]_{10s}$ laminate, given a

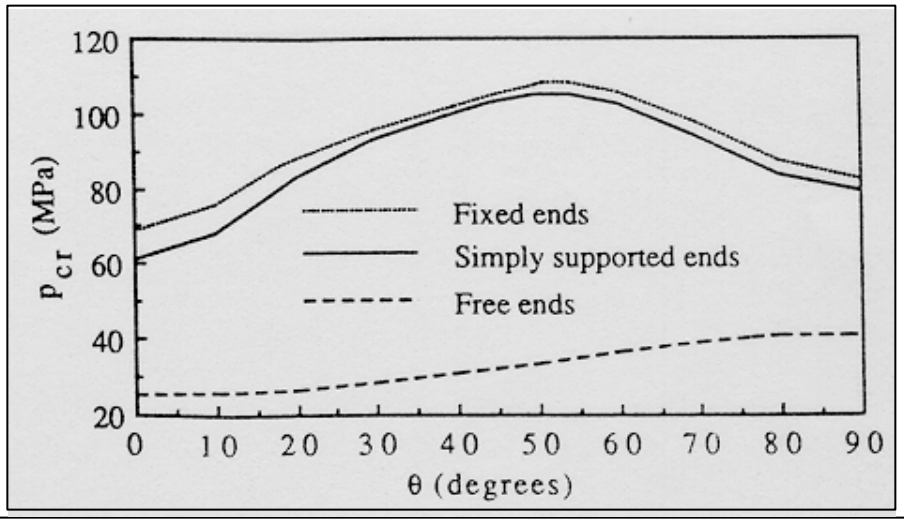

Figure 2.4: Critical shell pressure as a function of ply angle[10]

geometry and laminate pattern, an optimum ply angle could be determined using this method to maximize the critical buckling pressure. Also, it was determined that for an optimized laminate, a cutout with an elliptical geometry oriented with its long axis parallel to the hoop direction would minimize the reduction of the cylinder's critical buckling load.

2.3 Experimental Studies

Probably the most applicable papers to the research presented in this thesis concerned experimentally determining the effects of composite material and cutouts on the buckling of cylinders. While the buckling of thin walled cylinders for fuselage sections had been investigated experimentally as early as 1934, it was not until much more recently that composite materials had been introduced to these tests. Presented in the following sections are experimental works with direct applications to the WASP fuselage structure design.

2.3.1 Buckling of thin cylinders

The phenomenon of buckling in both thick and thin walled cylinders has been thoroughly explored over the years, and is well documented in several papers and textbooks[11,12]. Early works in the century attempted to explore the boundary between thick and thin solutions, and found that the

discrepancy between the theoretical failure stresses increases with the radius to thickness ratio. It was also discovered that this trend behaves differently for different metals. Later it was revealed that this phenomenon was governed by a ratio of the metal's modulus to its yield strength[13]. This topic will not be explored further here though, since it is not directly relevant to the topic of this thesis.

2.3.2 Buckling of composite cylinders

Probably the most germane of all of the papers reviewed here were the ones in which the authors manufactured composite cylinders and buckled them under axially compressive load. The main difference between most of these experiments was the manufacturing procedure that was utilized—about half the specimens tested were filament wound and half were hand laid-up. One particularly interesting work[14] explored the effect of varying the winding angle of a filament wound cylinder on its buckling load as well as investigating the effects of cyclic buckling. Carbon fiber cylinders of three lay-ups were tested, and it was found that the laminates with angles closer to 90°, i.e. the circumferential direction, failed at a lower buckling load as expected due to the reduced laminate stiffness. It was also found, as demonstrated in **Figure 2.5**, that when a cylinder was repeatedly loaded in the buckling regime, its buckling load would lower with each successive cycle due to post buckling damage.

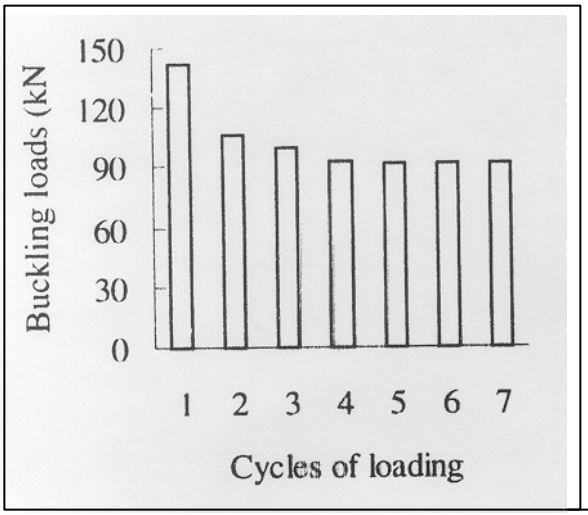

Figure 2.5: Effects of cyclic buckling with applied displacement of 1.5 mm[14]

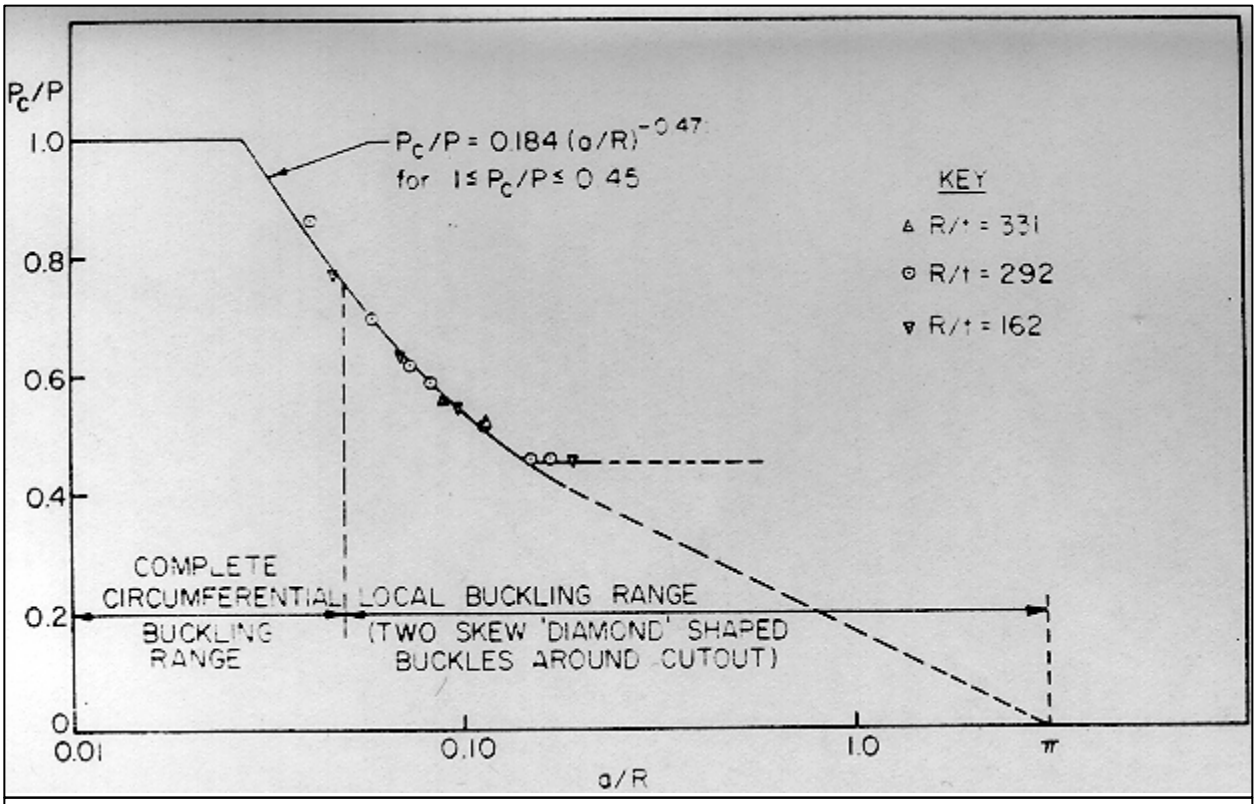

Figure 2.6: Variation of buckling load ratio with radius of circular cutouts[17]

Another article also discovered this same phenomenon in hand laid-up composite cylinders, however the manufacturing of these specimens proved much more critical since initial defects would cause them to fail prematurely[15]. Finally, in a paper that evaluated two sets of comparable composite cylinders[16]—one filament wound and one hand laid-up with a material of the same stiffness—it was found that there was little difference in the failure strain of cylinders fabricated by these various techniques. Furthermore, it was found that they buckled in identical modes. The only difference observed between the two sets of specimen was the greater variation found in the results for the hand laid-up specimen, apparently due to the more inconsistencies in that manufacturing technique.

2.3.3 Buckling of cylinders with cutouts

Experimental work investigating the buckling of cylinders with cutouts has found general agreement between theory and test results. In a particularly innovative test[17], which used a photoelastic plastic cylinder to identify strains in the shell, it was found that the buckling load was consistently within few percent of the value predicted by classical mechanics. Furthermore, it was discovered that the critical buckling load was significantly reduced by the presence of relatively small unreinforced holes in the structure, as seen in **Figure 2.6**. When doublers were placed around the cutouts in the

cylinder, it was found that the buckling load again approaches the value of the complete cylinder[18]; however it was also determined that over-stiffening can occur, which again reduced the buckling load of the specimen.

2.4 Conclusions

While none of the papers found directly related to the design of g-hardened composite fuselage section, several of them laid paths to appropriate analytical and experimental techniques. After reviewing the analytical and computational papers presented in this section, it was determined that for the level of complexity to be examined in this thesis only finite element methods would provide accurate solutions. Some of the analytical solutions for stress concentrations and shell buckling from the textbooks[4,5,11,12] listed above were used however on simplified cylindrical models in order to check the bounds on the finite element solutions.

The experimental studies reviewed provided two important pieces of information for this thesis. First, they detailed many important issues for the manufacturing of specimen for a buckling investigation of composite cylinders, including an excellent comparison of multiple manufacturing techniques. Secondly, they emphasized the use of reinforcements or doublers to negate the stress concentration effect of cutouts in composite cylinders, which was an important consideration in the assembly of the WASP II demonstration flyer.

CHAPTER 3

TAIL SECTION DESIGN

The following chapter elaborates on the design requirements of the tail section of the WASP vehicle. This includes the specific shape and loading constraints imposed on this section, as well as a comparison to the previous all aluminum design. This chapter also includes a trade study, based on the original design, performed to quantify the advantages of a composite design.

3.1 Tail Section Requirements

The specifications for the tail section of the WASP vehicle were dictated by the MK64 5" Navy gun shell that it was designed to be contained within. In the following sections, the critical specifications of this round are described and their implications for the WASP tail section design are assessed.

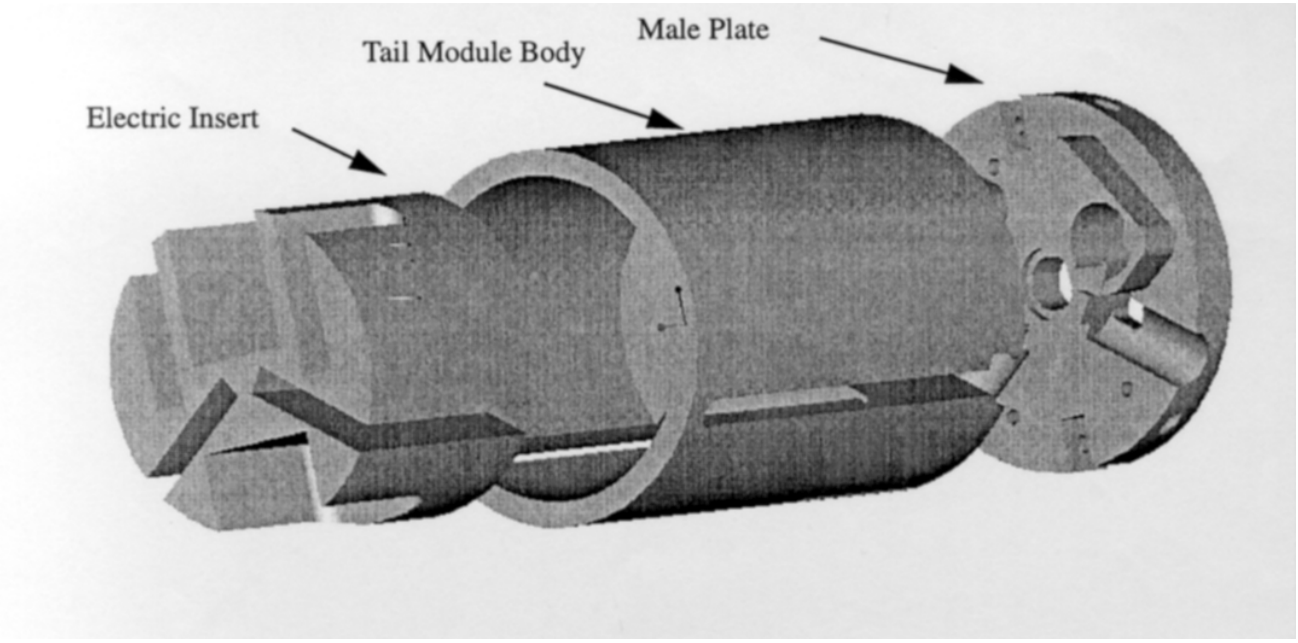

Figure 3.1: Tail section of the original WASP vehicle[19]

3.1.1 Geometry

The tail section of the WASP vehicle, as seen in **Figure 3.1**, housed the tail servos, much of the electronic components of the vehicle (which were attached to the "male plate"), and was where the tail fins stowed. It had an outside diameter of 3.8" in order to give it clearance with the shell wall, which was 3.9" in diameter. The inner wall thickness varied throughout the section and was machined from a solid block of aluminum. There were two long slots cut out of the back of the section, each about ¼" wide and 2" long, which allowed the tail fins to deploy, as well as several bolt holes to connect this section to the wing module. The geometrical requirements for this section were to maximize the volume while not exceeding the maximum internal diameter of the shell, and to provide appropriate cutouts for the fins and bolts.

3.1.2 Loading

The loading of the tail section, as with the rest of the structure, was derived from the acceleration loads of the shell launch. The major design load was the set-back of 16,000 g's pushing the entire mass of the vehicle against the tail section. This acceleration load was distributed evenly across the upper cross-sectional face of the tail section.

3.1.3 Boundary Conditions

The back of the tail section was bolted to the male plate, which housed the electronics. This boundary effectively clamped the back of the section. The other constraint on the tail section was the wall of the shell surrounding the flyer, which restricted the radial expansion of the section.

3.2 WASP I Design

The WASP I vehicle was designed to be fabricated mostly out of aluminum for ease of manufacturing and to save the time and expense of developing more complicated parts[19]. Consequently, the tail section of the vehicle weighed almost 4 lbs. The design was very conservative to ensure g-survivability without any yielding; however the excessive weight of the aft section proved to be a major factor in the uncontrolled crash of the subsequent test flyer.

3.3 Composite Trade Study

The first part to be re-designed for the WASP II flyer was the aft section with the objective of further reducing its weight while still retaining g-survivability. In order to achieve this, a trade study was performed, comparing

several different possible configurations of the flyer. The first configuration was the baseline design in 7075 aluminum. The second was an optimized aluminum design, which accounted for the fact the loading was directly proportional to the weight of the section. Therefore, it was derived parametrically by varying both the load and cross-section as a function of thickness, producing the minimal weight section to meet the design stress of twice the yield stress, 70 Ksi. This optimization equality yielded a thickness of .48", which therefore dictated the inertial load. The next two configurations modeled were both in graphite/epoxy composite. Both were quasi-isotropic AS4/3501-6 laminates; the first consisted of a constant section of 20 plies $(0_2/+45/0_2/-45/0_2/90/0)_s$ and the second consisted of 40 plies $(0_2/+45/0_2/-45/0_2/90/0)_{2s}$. Their weight was calculated based upon their volume and a density of .06 lbs/in^3.

For the analysis, the aluminum parts were modeled in I-DEAS™ as solid elements and processed in I-DEAS™ as a linear model. The composite parts were also modeled in I-DEAS™ but as thin shell elements, and were processed in ABAQUS™ as a non-linear model since this FEA package is much more accurate for advanced materials. All post-processing was performed in I-DEAS™, a finite element analysis tool, which has a simple graphical interface. The two areas of Von Mises stress chosen for comparison were the far-field stresses at the center of the cylinder between the slots, and the maximum stress concentration at the tip of the large slot. The stresses are tabulated in **Figure 3.2** along with the margin of safety (MOS) over the design stress.

Material	Comment	Von Mises Stresses (ksi) Far Field	Max	Axial Strain (microstrain) Far Field	Max	Stress MOS	Strain MOS
7075 AL	Optimized	36	52	-	-	1%	-
AS4 Gr/Ep	20 Ply	70	84	2450	2770	0%	2%
AS4 Gr/Ep	40 Ply	36	42	1290	1400	**49%**	**48%**

Figure 3.2: Table of stresses found in tail section material trade-study

Material	Comment	Weight (g)	Savings over Original AL Aft	Savings over Original AL Overall	Savings over Optimized AL Aft	Savings over Optimized AL Overall
7075 AL	Original	1860	-	-	n/a	n/a
7075 AL	Optimized	1138	39%	10%	-	-
AS4 Gr/Ep	20 Ply	143	92%	23%	87%	15%
AS4 Gr/Ep	40 Ply	277	**85%**	**21%**	**76%**	**13%**

Figure 3.3: Table of weight savings over original WASP design

The stress margins of safety listed were calculated by taking the difference between twice the far field stress and the yield stress, and dividing it by the yield stress. The far field stress was used to tabulate these margins of safety along with an assumed stress concentration of two to be more conservative over the traditional use of the maximum stress in the model. A yield stress of 73 Ksi was used for the aluminum design; for the composite designs, a first ply failure was assumed to occur at a laminate stress of 140 Ksi, which was found using classical laminated plate theory (CLPT). For the composite sections, a strain margin of safety was also calculated using 5000 microstrain (.5%) as the strain limit.

These results show that a significant weight savings can be achieved over the original vehicle design by optimizing the aluminum configuration. As shown in **Figure 3.3**, a significant additional weight savings can be achieved if composites are used as the primary material. Furthermore, an additional margin of safety can be achieved as a result. The first pair of percentages displayed compare the weight of the three new designs to the original design for both overall vehicles as well as just the weight of the aft section. The second set of percentages demonstrates the additional savings of a composite design over the optimized aluminum design, again comparing both the weight of the entire vehicle as well as the weight of just the aft section. In Chapter 4, an analytical procedure will be introduced to further investigate the advantages of composite material in the WASP design.

[This page intentionally left blank]

CHAPTER 4

ANALYTICAL PROCEDURES

The following chapter outlines the analytical procedures that were used to predict the response of composite tube sections with cutouts to high-g loading. This includes the use of Classical Laminated Plate Theory (CLPT), as well as the implementation of both static and dynamic structural finite element models.

4.1 Overview

The general procedure for analyzing the WASP composite sections can be followed in the flow chart in **Figure 4.1**. The analysis commenced with selecting a candidate laminate to be examined. A CLPT code (explained further in the following section) was written in Matlab™, which would iterate the acceleration load until first ply failure as determined by the Tsai-Wu failure criterion[20]. This failure theory, which can be found in **Figure 4.2**, uses the anisotropic ultimate strength properties of the composite material to calculate

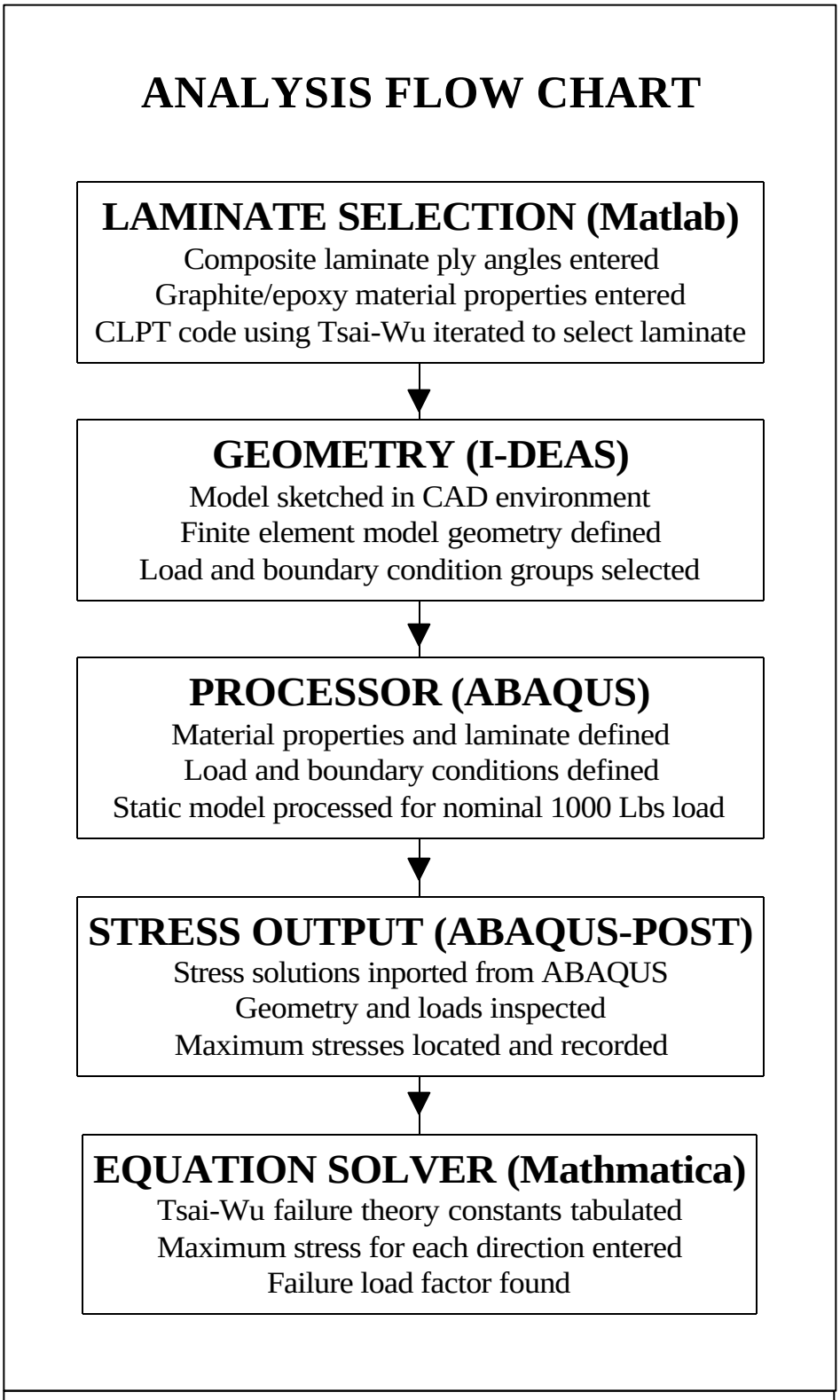

Figure 4.1: Analysis flow chart

failure constants, which are then equated with several combinations of the stress components. The next step was to use I-DEAS™ as a pre-processor and mesh generator.

There were two distinct configurations investigated; one with two long slots where the V-tail was stowed, and the other with two short slots where electronic inserts were placed. The geometry of the section to be studied was modeled and meshed, and then sets of boundary elements and nodes were grouped to be exported together into ABAQUS™. Once in ABAQUS™, material properties, boundary conditions and a nominal 1000 lbs axial compressive load were imposed via an input "script," an outline of which can be seen in **Figure 4.3**. After being processed by ABAQUS™, ABAQUS-Post™ was used to examine the stress contours of the section for static models, and the message file was analyzed for the convergence of a buckling load factor (the load multiplier that causes the out-of-plane deformation to diverge) for dynamic models. Both a static and dynamic analysis was performed for each model.

For the static models, the three stress components—axial, circumferential and shear—were extracted from the elements with the highest stress state near the slot tip. These stresses along with the tabulated Tsai-Wu failure constants were then entered into Mathmatica™. Since the laminate was assumed to behave linearly until first ply failure, the stresses in the cylinder would therefore scale linearly with the load applied to the model. Using this fact, the equation solver in Mathmatica™ was used to solve for the critical load

$$F_1\sigma_1 + F_2\sigma_2 + F_{11}\sigma_1^2 + F_{22}\sigma_2^2 + F_{66}\sigma_3 + 2F_{12}\sigma_1\sigma_2 = 1$$

$$F_1 = \frac{1}{X_t} + \frac{1}{X_c} \qquad F_{11} = \frac{-1}{X_t X_c} \qquad F_2 = \frac{1}{Y_t} + \frac{1}{Y_c} \qquad F_{22} = \frac{-1}{Y_t Y_c}$$

$$F_{66} = \frac{1}{S^2} \qquad F_{12} = \frac{-0.5}{\sqrt{X_t X_c Y_t Y_c}}$$

Figure 4.2: Tsai-Wu failure criterion and constants

GEOMETRY
- Points
- Shells
- Groups

DEFINITION
- Element Definitions
- Material Definitions
- Laminate Definitions

CONSTRAINTS
- Boundary Conditions
- Loads

OUTPUTS
- Results export
- Custom Routines

Figure 4.3: ABAQUS™ code outline

factor to be multiplied by the nominal load entered in ABAQUS™, which would yield the first ply failure load as determined by the Tsai-Wu criterion.

4.2 Classical Laminated Plate Theory

CLPT was implemented by ABAQUS™ in this analysis to calculate the stresses in each ply layer. This theory assumes that all of the layers in a composite laminate are perfectly bonded together, and that each ply strains equally in the laminate coordinate system when subjected to a pure tensile or compressive load. A stress or strain is applied to the laminate, and using the above assumptions and a couple coordinate transformations, the stress in each ply can be calculated. Several books have been written explaining CLPT, including *Mechanics of Composite Materials* by Jones[21]. A Matlab™ code implementing this theory into a ply-by-ply failure analysis can be found in **Appendix A**. Given cylinder dimensions and a laminate, this code would continuously increase the acceleration load until first ply failure, using the Tsai-Wu theory as a failure criterion. Since this code could only analyze uniform cylindrical bodies without cut-outs and did not taking bending into account, it was only used as a preliminary laminate selection tool.

4.3 Static Model

This section describes how I-DEAS™ and ABAQUS™ were used to form a static finite element model. The generic geometry of the model was first created, and then supplemented with a loading scheme, boundary conditions and specific material properties in the ABAQUS™ input (.inp) file as described in the following sections. A sample of this file can be found in **Appendix B**. Once the edited file was run in ABAQUS™, the restart (.res) file was viewed in ABAQUS-Post™ to observe the stress contours.

4.3.1 Geometry

Before the finite element analysis could be performed, it was necessary to model the shape of the section in I-DEAS™. I-DEAS™ is a graphical program, which uses points, lines, curves and surfaces to define a model. The tail sections were drawn 3.5" in diameter and 5.5" in length. Next, depending on which of the two geometries was being worked on, a pair of ¼" rounded slots were cut from the geometry, either 2" or 5" in length. A semi-circle ¼" in diameter was also drawn at the top of the slot to accurately model the rounded edges of the WASP vehicle machined slots. These models' geometries can be seen in **Figure 4.4**.

Once the outline of the tube had been completed, the next step was to form surfaces from the boundaries. These surfaces were meshed with 8-noded S8R5 shell elements, whose properties were prescribed in a future step. A convergence study was performed to find the appropriate refinement for each curve, which in the end was limited by the scratch space available on the computer. The general rules followed were first to keep the scale in each direction constant so as to create square elements, and secondly to refine the mesh in the area around the slot tip to provide more accurate stress contours. For the same reason, 8-noded elements were selected since they quadratically interpolate displacement fields with the mid-side nodes as opposed to 4-noded quadrilateral elements that use linear interpolations.

Lastly, a surface mesh was formed on the top of the tube model, as seen in **Figure 4.5**. This was to provide a uniform pressure load on the structure, which will be described more in greater detail in the next section. The elements of this top plate were grouped as “force” to be exported in a special separated section, and the nodes around the bottom ring of the structure were exported in a group called “fixed.” The entire meshed model along with these specially selected sections were then exported into an ABAQUS™ format to be edited and processed.

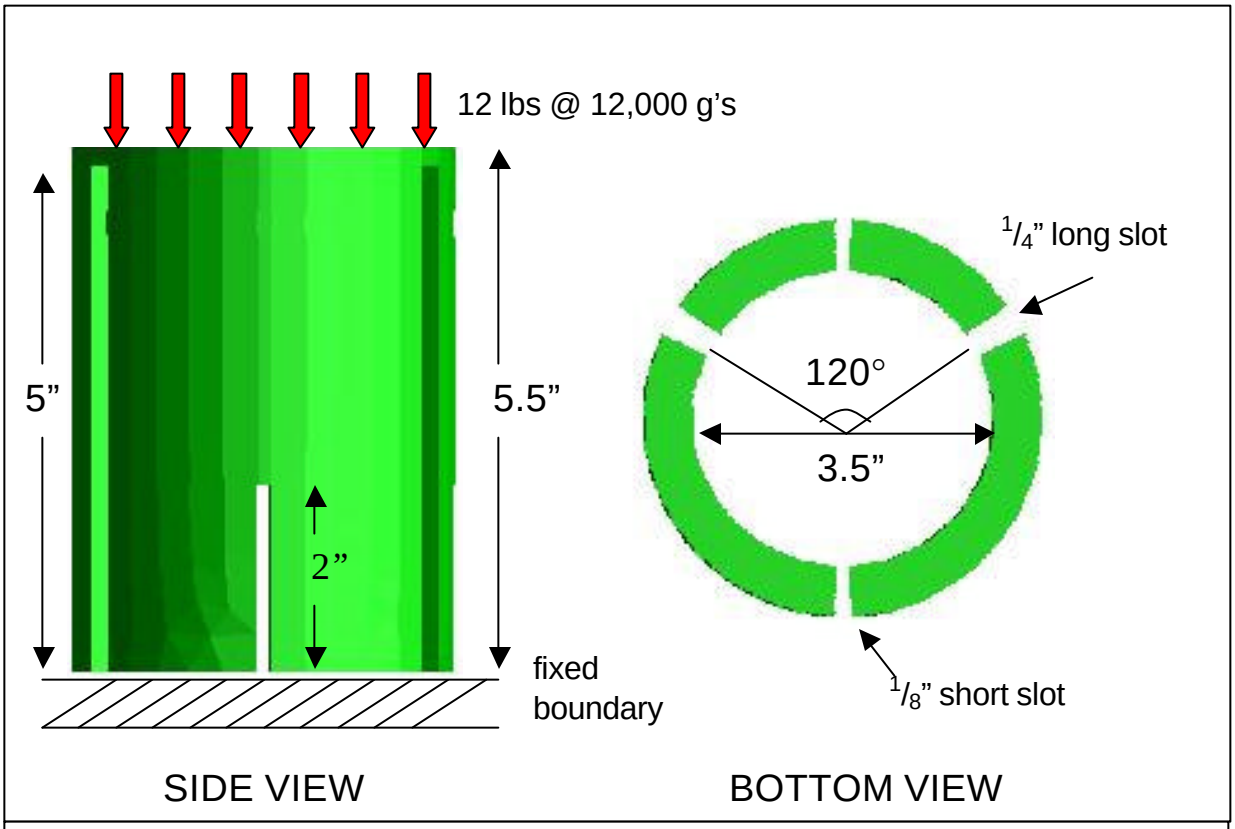

Figure 4.4: Model geometry, applied load and boundary conditions

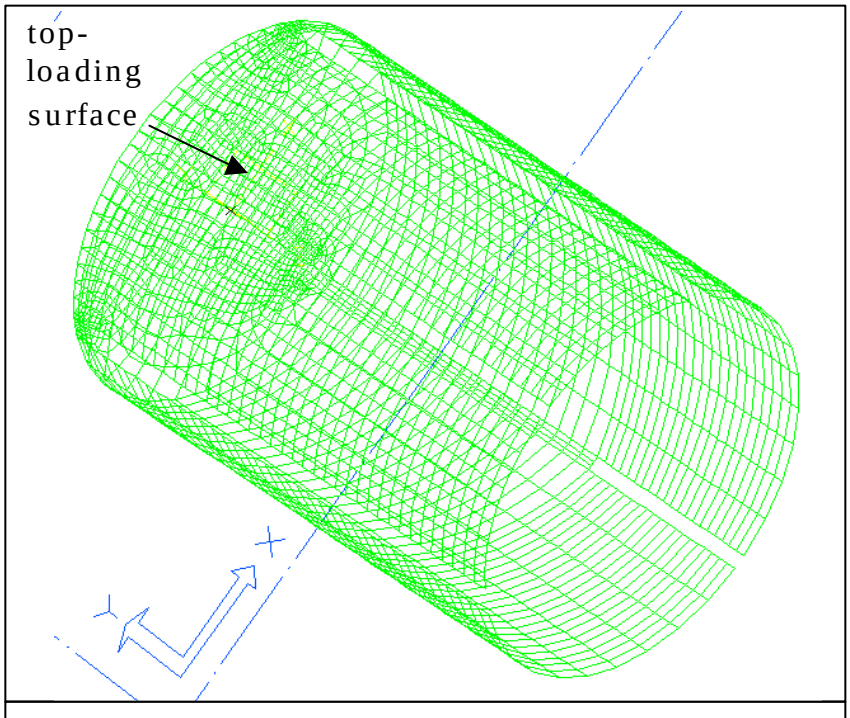

Figure 4.5: Mesh of cylindrical model in I-DEAS™

4.3.2 Loading

The loading used in ABAQUS™ attempted to simulate the effect of the rest of the vehicle being accelerated into the tail section. To accomplish this, as described in the previous section, a top surface was meshed onto the finite element model. This surface was given a very stiff modulus so that it would not deform significantly under the load, and was meshed freely by I-DEAS™. A uniform axial compression pressure load of 1000 psi was then applied in the ABAQUS™ input file to the "force" element set. Since the material properties entered (as described below) were linear, the stresses outputted by ABAQUS-Post™ could then be easily scaled by this magnitude of pressure.

4.3.3 Boundary Conditions

Using a similar method to how the load was applied, the boundary conditions were inserted into the ABAQUS™ input file. The boundary to be modeled was a clamp formed by the "male plate" which is attached to the bottom end of the tail section. To simulate this, in the input file the set of nodes referred to as "fixed" was restrained in all six degrees of freedom using the encastre command, thus modeling the plate as infinitely stiff. Some other boundary conditions were experimented with, such as restraining the hoop

Ply Property	Value	Units	Ply Property	Value	Units
E11	142	GPa	Xt	2356	GPa
E22	9.81	GPa	Xc	1468	GPa
E33	9.81	GPa	Yt	49.4	GPa
G12	6	GPa	Yc	186	GPa
G23	3.773	GPa	S	105	GPa
G13	6	GPa	Thickness	.134	mm
V12	.3		Density	1580	Kg/m^3
V23	.34				
V13	.3				

Figure 4.6: Table of AS4/3501-6 prepreg material properties

deformation at the top of the tube, although this had minimal effect on the model solutions.

4.3.4 Material Properties

The ABAQUS™ input files as exported by I-DEAS™ had only generic properties, which were then edited while in text format. The thin shell elements were given a laminate material card, which allows several layers of materials of different orientations to be attached together. Each of the ply layers were given the material properties as given by **Figure 4.6**, which were supplied by the manufacturer Hexcel. There were 18 plies in the laminate, arranged $[0/\pm45]_{3s}$. This ABAQUS™ material card used CLPT, and assumes that each ply layer is perfectly bonded to the next.

4.4 Dynamic model

Since there were relatively long slots in the length of the structure, it was uncertain whether the tubes would fail by fracture or buckling; therefore a dynamic model was also analyzed in ABAQUS™. The dynamic model followed the same procedure as described above for the static model, using identical geometry, materials, loads and boundary conditions. The only difference occurred in the solution section of the input file, where linear buckling

(eigenvalue buckling) was specified instead of a static solution. A sample of this input file can also be found in **Appendix B**. The subspace iteration method was used to find the buckling load factor, and the number of vectors and iterations could also be specified in the input file. For the tail section, 3 vectors were chosen for quick convergence, and 30 iterations were chosen so the rate of convergence could be calculated. These solutions could be found in the message (.msg) file after the buckling problem had been processed in ABAQUS™. Several different variations were experimented with in the buckling model, which will be further discussed in the results section. These variations included changing the elastic properties of the material, the tube's length and diameter, and the layup. In the following chapter, the experimental techniques used to validate this analytical model will be discussed.

CHAPTER 5

EXPERIMENTAL PROCEDURES

The following chapter outlines the experimental procedures that were used to investigate the response of composite tube sections with cutouts to high-g loading. These sections are an idealization of the tail section of the WASP I vehicle, as described in Chapter 3. Both the manufacturing method implemented and a description of the two testing phases are included in this chapter.

5.1 Manufacturing Process

This section delineates the manufacturing process used to fabricate composite fuselage sections. This includes the material used, a detailed description of the processes implemented for curing, and subsequent machining. The procedure described produces three tubes each 14” long that are then machined into six 5½” long specimens.

5.1.1 Graphite/Epoxy Pre-Preg

All of the experiments were performed using AS4/3501-6 graphite epoxy pre-preg. This is TELAC's standard composite material, so the procedures drawn up by the lab[22] formed the basis for the manufacturing conducted here. First the roll of pre-preg, which is initially stored in a freezer, has to be thawed to room temperature before being removed from its plastic bag in order to prevent wrinkles due to moisture absorption. The roll is then placed on a wooden roller and unwound onto a cutting table, prior to being cut to the required lengths.

Since a 3.5" diameter mandrel has an 11" circumference, the standard TELAC templates could be used, yielding 12x14" sections of pre-preg. The 0° direction of fibers here is defined as axial, or in the 14" direction. The layup investigated was $[0/\pm45]_{3s}$ so for each tube manufactured six of each 0°, +45° and -45° plies had to be cut out. Since each layer increases the circumference of the layup around the mandrel, the outer-most uncured layer has a circumference of 12", so a different procedure than the one described in this section would have to be used for any mandrel with diameter greater than 3.5". The plies here were cut to identical lengths, and placed separated with backing paper in a vacuum bag in a freezer until they were used.

5.1.2 Cylindrical Mandrel

The hollow mandrel used for these cures was purchased from TW Metals[23], and was custom machined in the student machine shop. It was 3.5" in diameter 2024 aluminum and 48" long. Aluminum was chosen because of its high thermal expansion, which would cause it to shrink more then the composite tube during cool down from the cure temperature, making it easier to remove the tube from the mandrel, which will be described later. Legs were constructed on the water-jet for the mandrel, which consisted of a square aluminum plate with 3.5" diameter hole cut out of the middle that was cut in half. A 1" diameter steel threaded rod was then passed through both plates to add rigidity, which was held in place by 2 steel bolts on either side of each plate. A vacuum port was then machined into the mandrel by drilling and tapping a hole 1" from the end of the tube. The threads were formed from the inside of the tube since the pipe fittings would be screwed in from that side. In order to attach the autoclave's vacuum hose to the mandrel, a three part vacuum fitting assembly was threaded in the mandrel, sealed with Teflon™ tape. It consisted of a short piece of pipe stock screwed into the hole, an elbow, and a long piece of pipe stock protruding from the tube and ending in a swage-lock fitting.

MATERIAL	SIZE	PIECES
Guaranteed Non-Porous Teflon™	11” x 15”	3
	12” x 4”	4
	14” x 5”	3
Porous Teflon	13” x 16”	3
Cork	11”	6
Bleeder paper	16” x width	3
	4” x width	6
Glass bag	16” x width	3
Vacuum Bag	64” x width	1

Figure 5.1: Table of required cure bagging materials

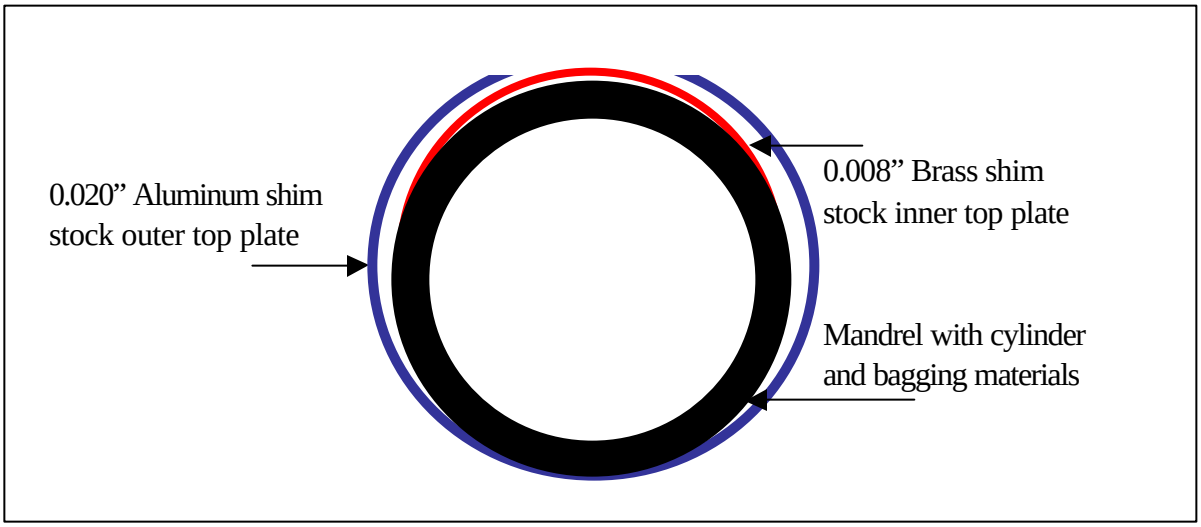

Figure 5.2: Schematic of cure top-plate configuration

5.1.3 Pre-cure setup

Manufacturing closed cylindrical shapes with pre-preg composite introduced many complexities. This forced a deviation from the standard cure setup, which had been explored in the Draper "micro-satellite" project[24] through trial and error of many cures. **Figure 5.1** shows a checklist of materials that were needed to perform each cure of 6 specimens. Once these materials were cut out, the mandrel was scrubbed using methanol and scouring pads to give it a smooth surface. Masking tape was then wrapped around 2" at either end, and Mold Wiz™ was sprayed over the mandrel's surface to protect it from epoxy. The tape was then removed and the area it was covering was cleaned with methanol. From this point on, handling of the mandrel was minimized. When it was necessary, latex gloves were worn.

Probably the most important part of the setup was the top plates. The top plates wrap around the pre-preg, and control the surface finish of the specimens. Often top plates are not used due to the additional complexity they add, and they can be replaced by using more bagging materials such as excessive bleeder paper. However, this approach can introduce surface wrinkles. Furthermore, having a metallic top plate present during the cure increases the consolidation of the epoxy compared to that achieved with more compliant bagging materials. Here, a two-part top plate system was used to minimize the effect on the gap where the two sides meet, as demonstrated in **Figure 5.2**. The first part was a 20 mil thick piece of sheet aluminum cut into

three 10x14” pieces, and rolled into a curvature of 3.5” diameter. This would wrap snugly around the pre-preg leaving a 2” gap between its ends. This gap would then be filled by the second part, which consisted of 15 mil thick brass shim stock, cut to 4x14”. All of these pieces were sprayed with Freekote™ on all sides and allowed to dry before using them. Additionally, the aluminum pieces were coated with guaranteed non-porous teflon (GNPT) on the inside, which was attached using 3M Spray Adhesive™.

The first cure performed only used a butt-joined piece of aluminum as the top plate, which created a large ridge in the cured specimens. This resulted in the selection of a two-part system. The various thicknesses and materials were chosen based on experiments performed trying to minimize the resulting ridges in the specimen. This final procedure still yielded some indented lines, however from inspection they were considered superficial.

5.1.4 Laying-up

The process for hand laying-up composite tubes is very time consuming. Originally it was thought that the pre-preg could be layed-up on a flat surface in a stair step fashion, however when implemented the variation in wrapping tension was too great and the radius was too small to correctly line up all of the ply layers. The alternative selected was to lay-up each ply layer individually on the mandrel. Since each of the 45° plies is cut into two trapezoidal parts, each pair of ±45 plies were stuck together in order to better

preserve the ply angles. This was done by removing one side of the backing from each piece of pre-preg, and pressing them together on a flat, hard surface.

The prepared mandrel was placed without its legs on a clean glass table covered with GNPT. First three 0° plies were cut to 11" width, the backings were removed, and they were wrapped onto the mandrel separated by 1½" each to start each tube. Next a ±45° ply group was applied with the backing still attached in order to measure the length which needed to be trimmed. This ply group was then removed, and the three groups were trimmed to the proper length. After the backings had been removed, a 1" section of each ply group was pressed onto the underlying 0° ply, offset from the butt joint, and the rest of the ply group was left resting on the glass table. Pressure was then applied to the mandrel, and it was rolled across the table until the ply groups had been completely stuck to the previous layer. This process is then repeated for each ply until the final 0° ply, which does not need to be trimmed and the backing was not removed until the bagging materials were applied. A picture of the layed-up mandrel can be seen in **Figure 5.3**.

5.1.5 Cure Process

After the pre-preg was wrapped around the mandrel, the bagging materials that where cut out previously were placed on the mandrel as shown in the **Figure 5.4**. Again, many of these layers are non-standard, and were determined by an experimental process. The most important layers to the

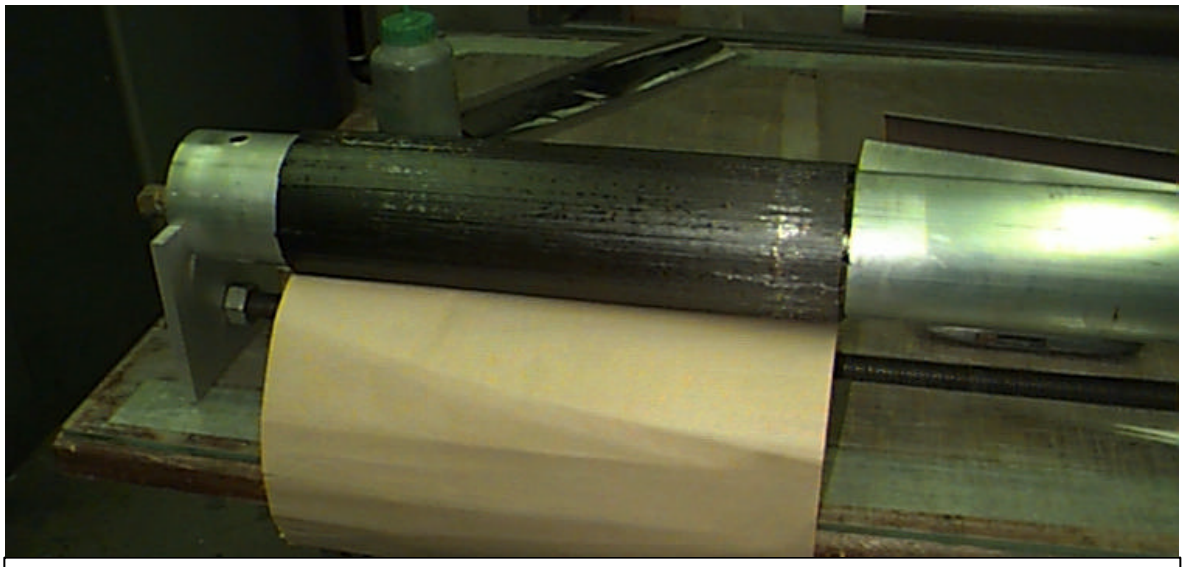

Figure 5.3: Picture of layed-up mandrel

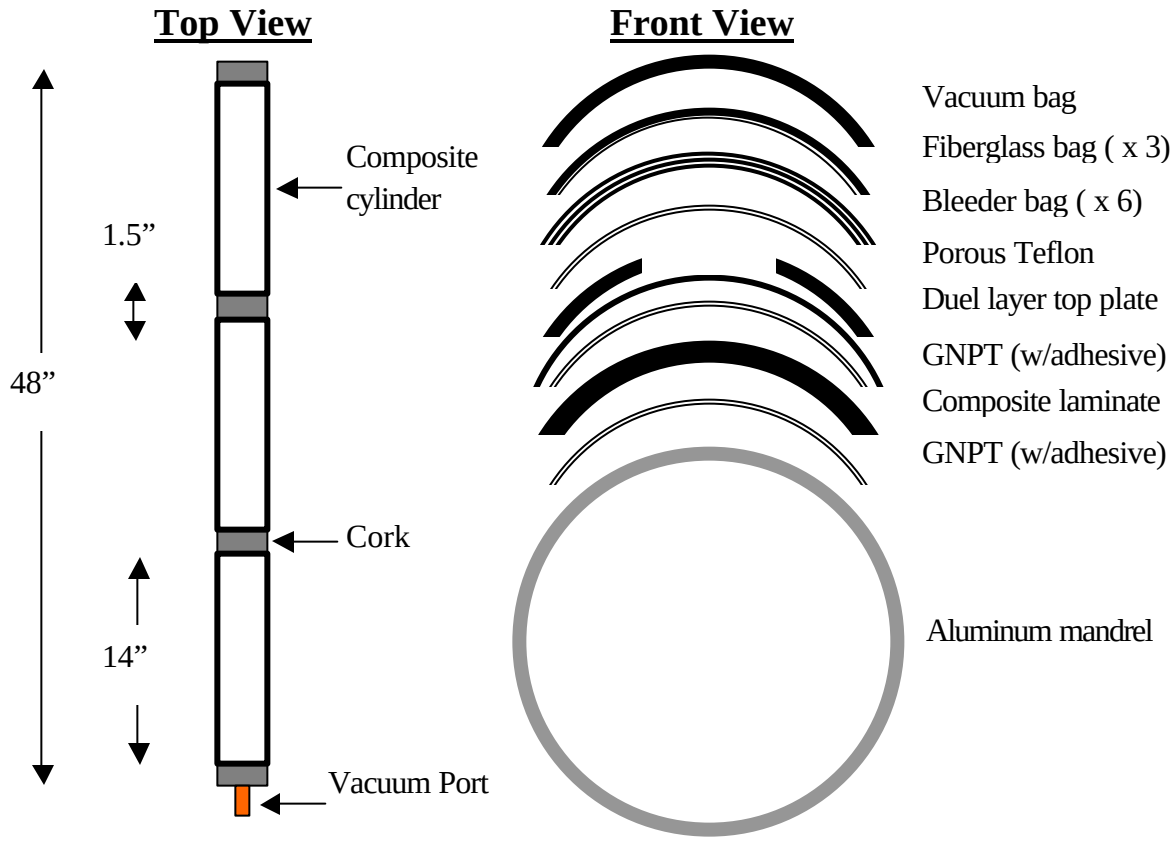

Figure 5.4: Schematic of bagging material placement

survival of the cure were the layers of bleeder paper, which prevented the other layers from being epoxied to the mandrel. The vacuum bag was oversized so that wrinkles could be deliberately introduced instead of using a “doggy ear” method of bagging. Vacuum tape was placed on the mandrel at either end, and a short section was exposed to tack down the vacuum bag, which was then rolled onto the mandrel. A long piece of vacuum tape was then placed along the length of the mandrel on the vacuum bag where the seam was to be made. This length then extended down the circumference at either end where it overlapped the small section of tape that was already exposed. Finally all of the backing was removed, and the vacuum bag was tacked down at regular intervals in order to produce several small wrinkles, which could then be drawn to the side and pushed down.

The cure cycle used for these specimens is the standard TELAC cure cycle used for AS4/3501-6. The mandrel was placed in the TELAC autoclave, standing on the legs that were built for it. First a vacuum of as close to 30” Hg as possible was pulled on the specimens (no less then 25” Hg was tolerated), and then a pressure of 85 psig was applied. Once the correct pressure was attained, the temperature was ramped to 240°F and held for 1 hour to allow the epoxy to gel and remove the voids. Then another ramp to 350°F was imposed where the cure was held for two hours while the matrix cross-linked and the composite material is cured. Lastly a 5°F per minute cool down was used to cool the autoclave down to 180°F, at which point the

pressure was removed and the autoclave was turned off. The standard cure temperature, pressure and vacuum profiles and be seen in **Figure 5.5**.

5.1.6 Post-cure procedures

Once the mandrel was removed from the autoclave, all of the bagging materials were removed. This was done by making a lengthwise incision using a utility knife through the region of the bag that appears to have the least epoxy on the surface. If the incision was made deep enough, all of the layers of material were then peeled and unwrapped off the mandrel at once, and the specimens were still protected by the top plates. The top plates were then removed, which only left the composite tubes on the mandrel. The mandrel was then placed in a large freezer for approximately 15 minutes in order to shrink the aluminum tube even further, while the composite tubes would stay at relatively the same diameter.

The process for taking the tubes off the mandrel also took much trial and error. The final process, which worked the quickest and easiest, was to use the mandrel legs to pull off the composite tubes. First the bolts holding on the legs were all loosened and one of the legs was put flush against the near side of the tube furthest from the vacuum port. Next an aluminum block was placed on the end of the mandrel opposite the vacuum port, and the other leg was against this block. A furniture clamp was then mounted on each of the legs, and cranked so as to bring them closer together. This pulling action was

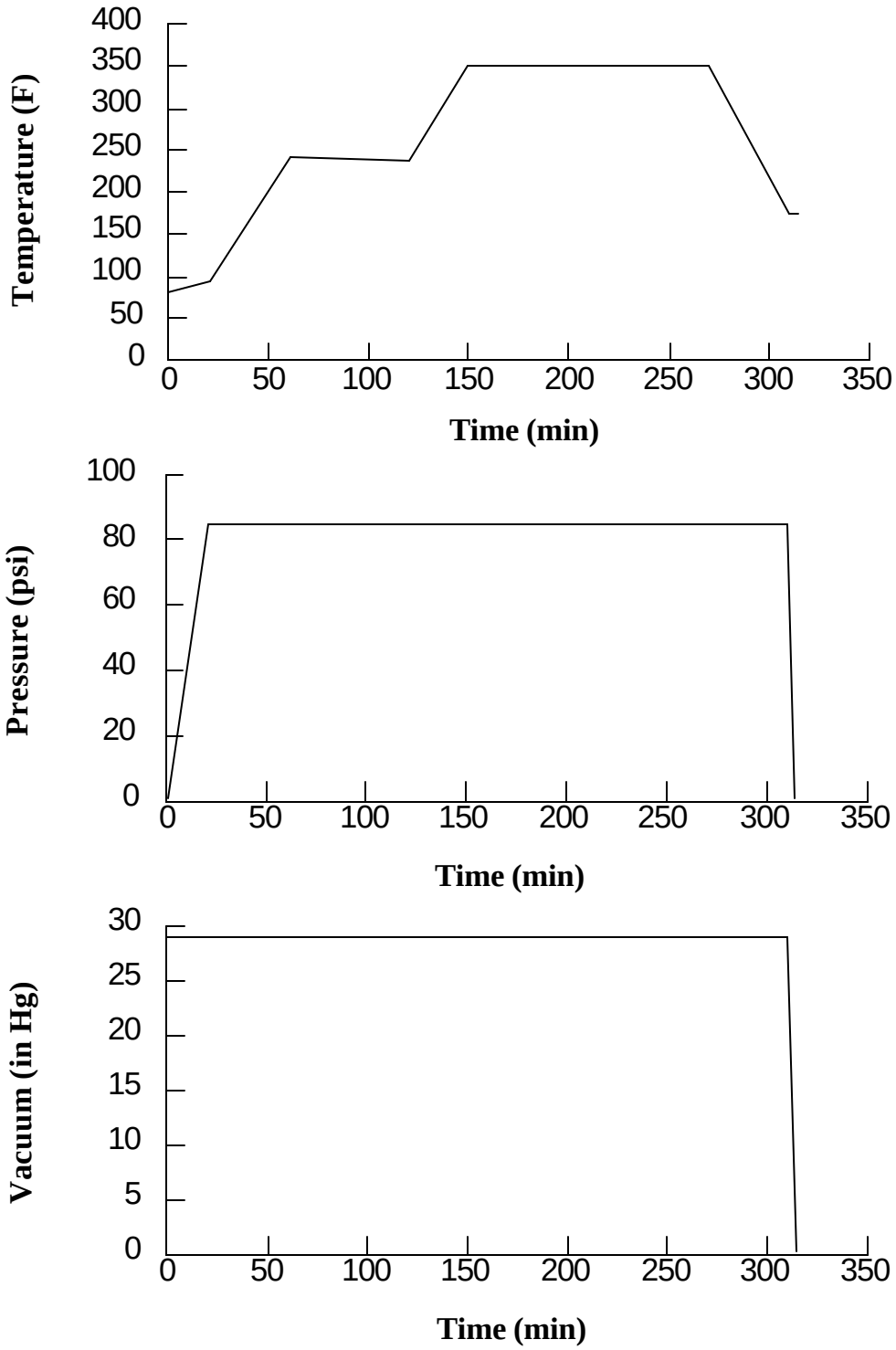

Figure 5.5: Standard cure temperature, pressure and vacuum plots[1]

enough to overcome the static friction and charge holding the tubes on the mandrel, and they would slide right off. Sometimes however, the tubes had to be cranked all the way off the Guaranteed Non-Porous Teflon™ (GNPT) underneath them before they would slide off. Each tube was removed in this fashion one by one, each being moved away from the vacuum port side of the mandrel. Once removed, the 3 tubes were placed in the post-cure oven for 8 hours at 350°F.

5.1.7 Machining the specimens

After being post-cured, the samples were brought to the central machine shop where the initial machining took place. Two 5½" specimens were cut out of each composite tube using a continuous carbide grit band-saw blade. The edges were then smoothed using fine grit sandpaper to make the sides parallel to each other for testing purposes. Both of these tasks were contracted out to be performed by the machinists of that shop.

The six specimens were then taken to the student machine shop where the appropriate slot formations would be milled into them. Marks were placed on the tubes at locations where slots would be cut using a silver pen and a lathe tool head to measure the angles. The tubes were then clamped onto a milling machine, which was draped with bleeder paper to protect the machine. The tool used to cut the slots was a ¼" 2-flute carbide endmill obtained from Harbor Tools. The tool was first inserted half way into the

composite wall at the middle of the tube in order to prevent edge delaminations, and then moved towards the end of the slot. There the tool was lowered while out of the tube to the full thickness, and another pass of the tool was made from the outside to the inside to complete the slot. This two pass method alleviated much of the torque on the system, thus reducing the amount of delamination and displaced edge fibers. Lastly a file was used to round the edges of the slots and to remove any stray fibers. The specimens were then cleaned, labeled, and were ready for testing.

5.2 Test Fixtures

To simulate the appropriate boundary conditions during testing, two sets of test fixtures were manufactured. Both of these sets of parts were designed on AutoCad4™, and were machine at Draper Laboratory.

5.2.1 Mass simulator

This part, as seen in **Figure 5.6**, was placed on the top surface of the specimens. It served the dual purpose of restraining the samples from compressing in the radial direction and to provide a uniform line load along the upper surface for both mechanical and air-gun testing. The dimensions of the cylindrical block were chosen to be 3” long by 3.8” diameter with a protruding ½” long cylinder of 3.5” diameter to fit inside the composite specimen with an

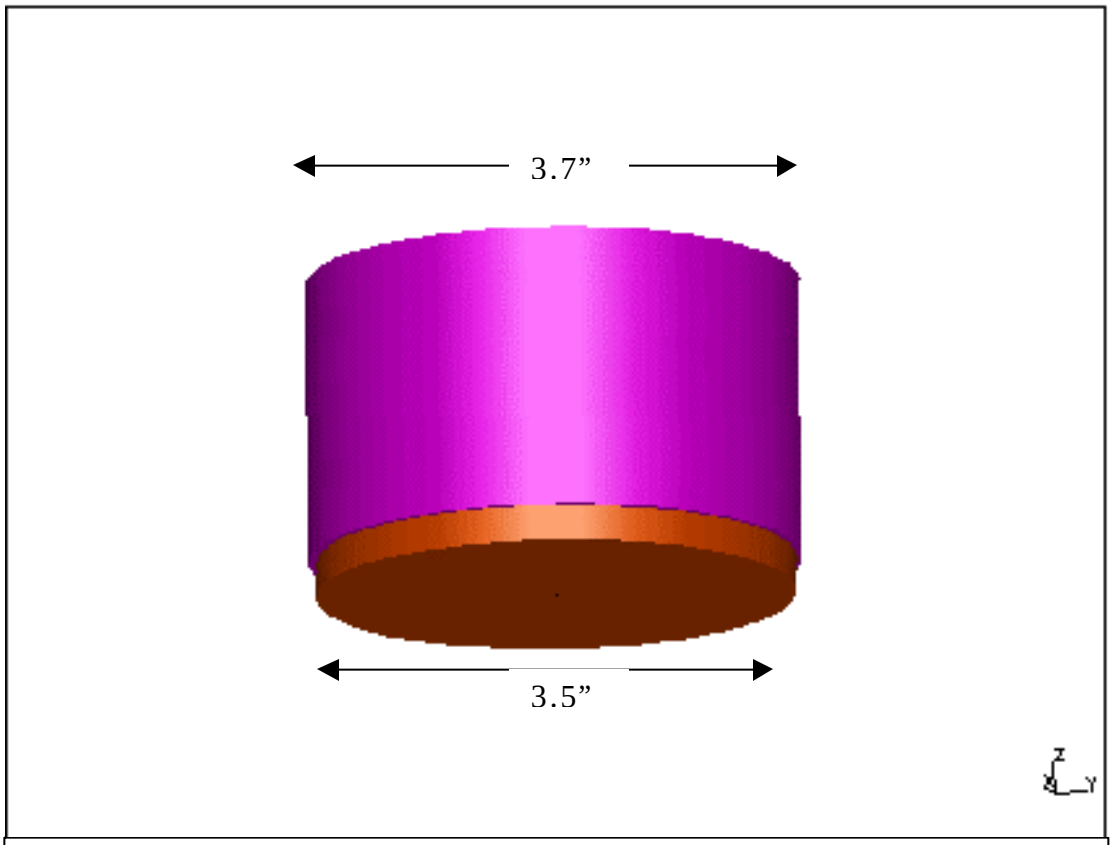

Figure 5.6: Aluminum mass simulator for tests

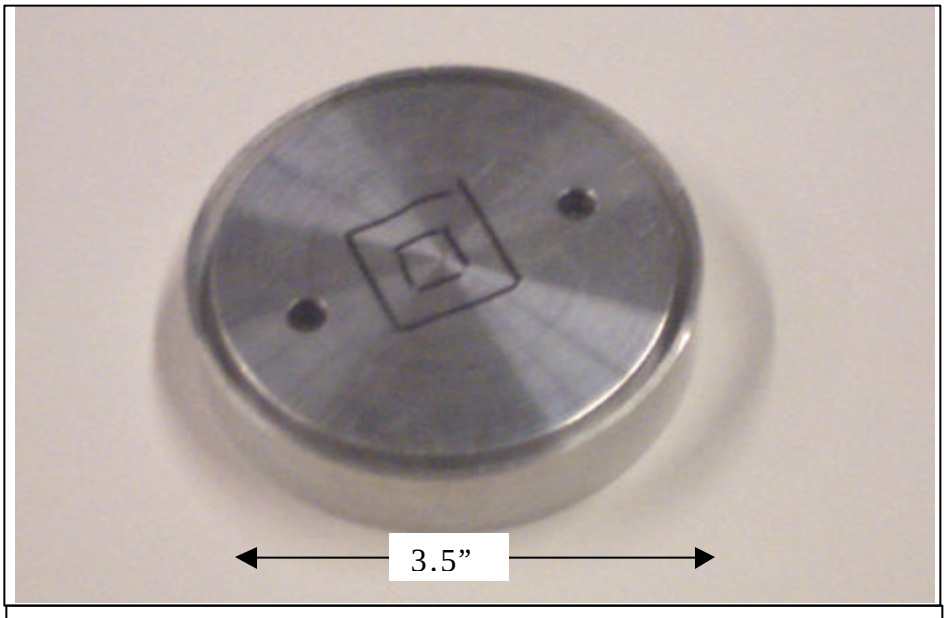

Figure 5.7: Aluminum clamp simulator for tests

interference fit. The overall part weighed 4.0 lbs, was designed to obtain appropriate stress levels at feasible g-levels during air-gun testing. Two of these parts were machined to allow for replacement in the case of damage during air-gun testing.

5.2.2 Clamp simulator

This second part was also machined out of aluminum, although its dimensions were dictated to minimize its volume. As seen in **Figure 5.7**, each bottom fixture is ¾" x 3.8" diameter with a ½" deep and .15" groove turned into it to allow tubes to be seated in it. Six of these parts were machined to save time during testing. The samples were held into this fixture by a crystalline wax (CA #790) manufactured by Greater Southwest Chemicals, Inc. A small amount of wax was melted in a glass petrie dish on a hotplate at 150°F, and then poured to fill the bottom of each groove of the fixture. The fixtures were then placed on the hotplate at 250°F, and after allowing the wax to become clear, each specimen was inserted and then the system was cooled in a water bath. This wax could be continually reheated and cooled to place new specimens in the fixture, and the water-soluble wax was easily wiped cleaned.

5.3 Testing

This section describes the two series of tests that were performed. A total of 12 specimens were tested, half at MIT using a mechanical compression machine, and the rest at Picatinny Arsenal in a 155 mm air-gun.

5.3.1 Test Matrix

As described in previous chapters, two specimen configurations were investigated: long slotted and short slotted. From this we derive a fairly simple test matrix to validate the analytical codes, as seen in **Figure 5.8**. The details of each test will be described in the following sections, as well as why not all of these tests were successful.

5.3.2 Mechanical Compression tests

Six axial compression tests were performed in displacement control on the MTS testing machines in TELAC. These tests were carried out until failure, at a rate of .025" per minute. The load-displacement data was recorded using LabView5™. Compression platens were placed on both heads of the MTS, and each specimen was loaded with mass and clamp fixtures in place, as

show in **Figure 5.9**. For safety, a Plexiglass™ box was placed around the setup since the failure of the tubes tended to be quite violent.

5.3.3 Air-Gun tests

Air-Gun testing was conducted in order to simulate the actual launch conditions the specimen would experience in service. Testing was performed at Picatinny Arsenal in New Jersey, where two guns were used: a 5" diaphragm air-gun and a 155mm air-gun as seen in **Figure 5.10**.

For the 5" diaphragm air-gun, Draper Labs machined custom canister shells to be launched out of the gun, as seen in **Figure 5.11**, which would allow larger samples to be tested. There was a large threaded section in the back of the shell along with a large nut, between which an appropriate diaphragm would be fastened. The diaphragm was nothing more than an aluminum disk with a certain depth groove turned into it, which determined the burst pressure of the disk. The specimens were loaded in a canister shell, a diaphragm was selected and the system was placed into the breech of the gun. Pressure is built up in the breech until the critical burst pressure is reached, while at the same time a small backpressure is maintained in the muzzle on the other end of the barrel in order to stop the canister once it has been launched. This gun was only used for one test however, since the recoil of the mass simulator jammed the canister after the first shot.

	Mechanical Testing	Air-Gun Testing
Long Slots	3	3
Short Slots	3	3

Figure 5.8: Test matrix for cylindrical composite sections

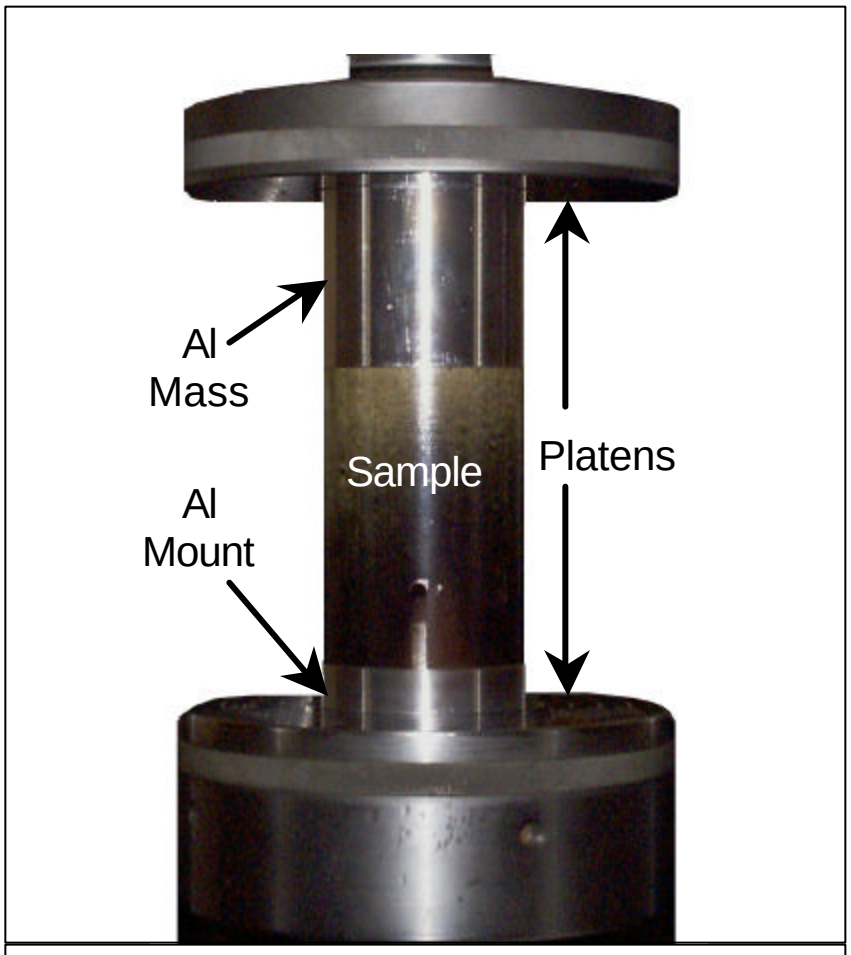

Figure 5.9: Static compression test configuration

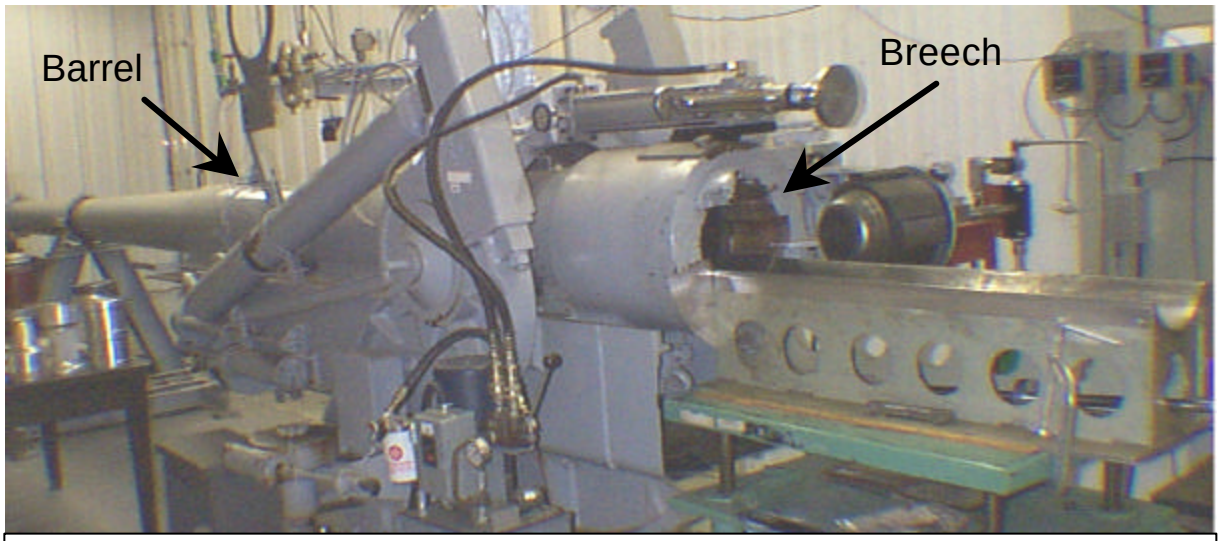

Figure 5.10: 155-mm air-gun at Picatinny Arsenal in New Jersey

Figure 5.11: Custom machined canisters for air-gun tests

For the remainder of the shots, a 155mm air-gun was used. This used a similar setup to the other gun, although a different firing mechanism. The canister, which was supplied by Picatinny Arsenal, was loaded with the specimen and then placed in a titanium sleeve with an o-ring on either end. This sleeve had several directional guide vanes, which directs the pressure in the breech to the back of the shell once released, to obtain the desired calculated acceleration. This test took a little longer to perform than on the other gun since the barrel had to be cleaned after each shot, and the sleeve insertion process was labor intensive. Three more shots were successfully completed from this gun before both of the borrowed canisters had become unusable. **Figure 5.12** summarizes the successful tests at Picatinny Arsenal. Chapter 6 presents the results for both the analytical and experiment tests.

	Long Slots	Short Slots
5” gun high-g	0	1
155mm gun 10,000 g’s	1	1
155mm gun 15,000 g’s	1	0

Figure 5.12: Table of air-gun tests performed

[This page intentionally left blank]

CHAPTER 6

RESULTS

This chapter outlines the results that were collected from both the analytical models and the experimental procedures described in the previous two chapters. For the analytical models, results are presented for both the static and dynamic models that were processed in ABAQUS™. The experimental results include axial compression tests and air-gun test results.

6.1 Analytical Results

In Chapter 4, the procedure for the finite element analysis was described. Stresses from the static model results were combined with the Tsai Wu failure criteria to solve for first ply failure for the two slot configurations. For the dynamic model, a series of trade studies were executed to observe the sensitivity of the buckling load to different variables. For all models a convergence study was performed, but only the results for the most efficient model are presented in this thesis (≈ 2,000 elements).

6.1.1 Static Model Stresses

The first ply to fail in both models was found to be the outermost 45° ply in the laminate; this was due to the combination of stresses present in that element. **Figure 6.1** presents the stress resultants that were found in these elements, which included the largest negative axial stress, the largest positive circumferential stress, and largest absolute shear stress. The failure factor, which was described in Chapter 4, was obtained from the quadratic Tsai-Wu formulation in Mathmatica™ and then multiplied by the applied load to calculate the failure strength of the structure. Since the nominal compressive load of 1,000 lbs/in^2 was applied to the finite element model over a 3.5" diameter .1" thick cross-section, the original load transmitted through the structure was 9,620 pounds. Thus, the calculated failure strength for the short slot model was 51,900 pounds, and for the long slot model 64,100 pounds. These results will be explained further in the discussion chapter.

6.1.2 Dynamic Model Buckling Loads

The dynamic model results were very straightforward. After processing the model in ABAQUS™, the buckling load factor would be found in the message file. This buckling load factor was multiplied by 9620 pounds to obtain the buckling load, which is the same constant calculated in the previous

section for obtaining the static failure load. Several different variables were then considered in a trade study, to test the sensitivity of the buckling load to lay-up, material, and dimensions of the tubes. These trades were only performed for the long slotted model, since those slots would be the driving factor of the true WASP vehicle. The buckling load factors for all of the variations studied can be found in **Figure 6.2**, along with a comparison to the control case. When the control buckling load factors are multiplied by the applied force, a buckling load of 92,700 pounds is obtained for the short slotted model, and 56,400 pounds for the long slotted one. In the discussion chapter, the implications of this trade study will be considered.

6.2 Experimental Results

This section describes the results obtained from the experiments that were carried out according to the procedures described in Chapter 5. This includes the elastic responses and failure loads of the axial compression tests, as well as the critical g-levels as obtained from the air-gun tests at Picatinny Arsenal. Some of the failures were caused by fracture, some by buckling, and some by a combination of both. In the discussion chapter the probable causes of failure for the particular failure modes will be analyzed in more depth.

Model	S11	S22	S12	**Failure Factor**	**Failure Load**
	(Psi)	(Psi)	(Psi)		**(Lbs)**
Short Slot Model	-19,012	444	-1,634	**5.40**	**51,900**
Long Slot Model	-20,587	2	1,536	**6.66**	**64,100**

Figure 6.1: Table of failure loads predicted by ABAQUS™ static model

Slot Length	Variation	Load Factor	% of Control
Short	Control	9.64	N/A
Long	Control	5.86	100%
Long	10% reduction in E	5.26	90%
Long	90° plies replace 0°	4.43	76%
Long	Two more 0° plies	7.13	122%
Long	4.5” diameter	3.85	66%
Long	6.0” tube length	5.56	95%
Long	S8R5 elements	5.80	99%

Figure 6.2: Table of buckling load factors predicted by ABAQUS™

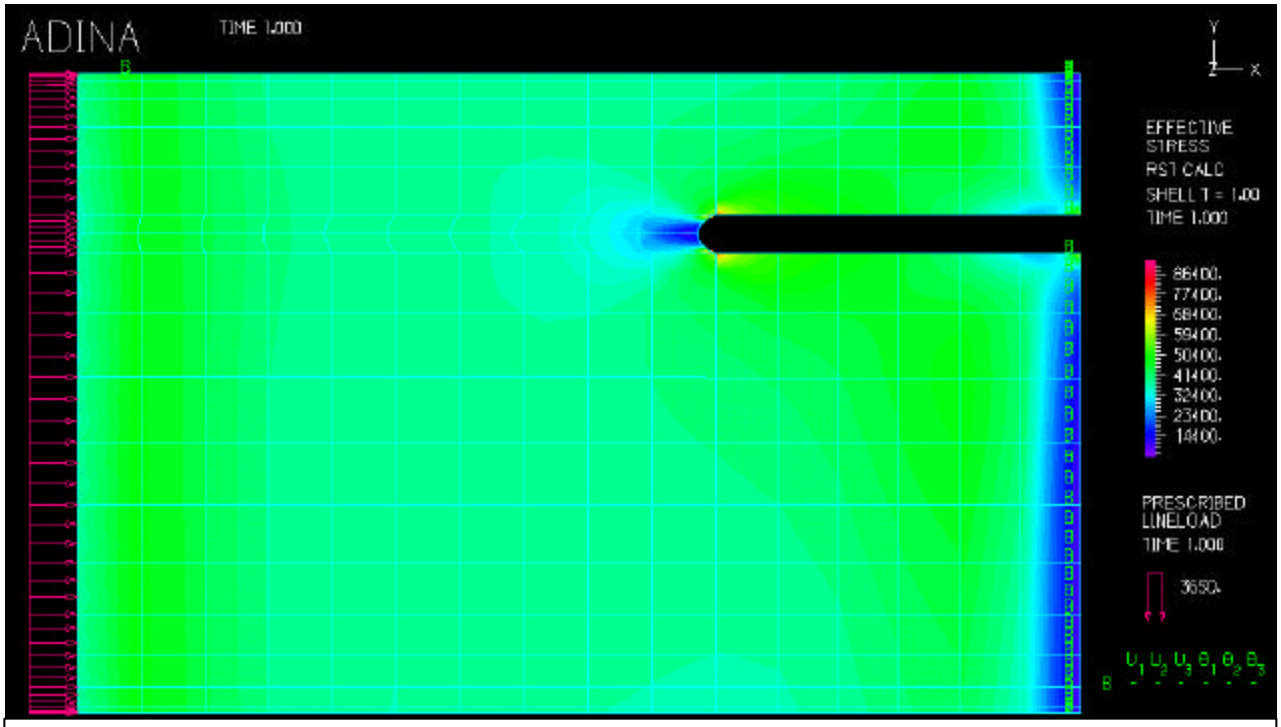

Figure 6.3: Finite element stress contours for short slotted model

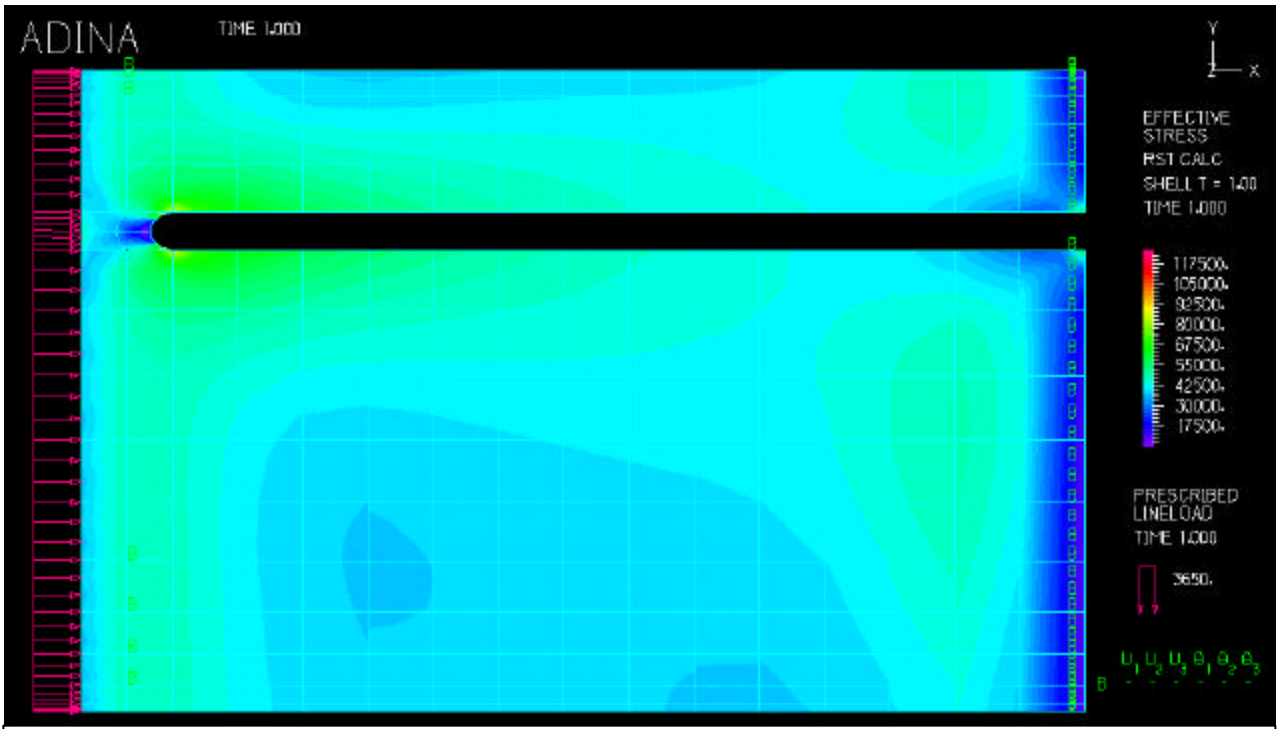

Figure 6.4: Finite element stress contours for long slotted model

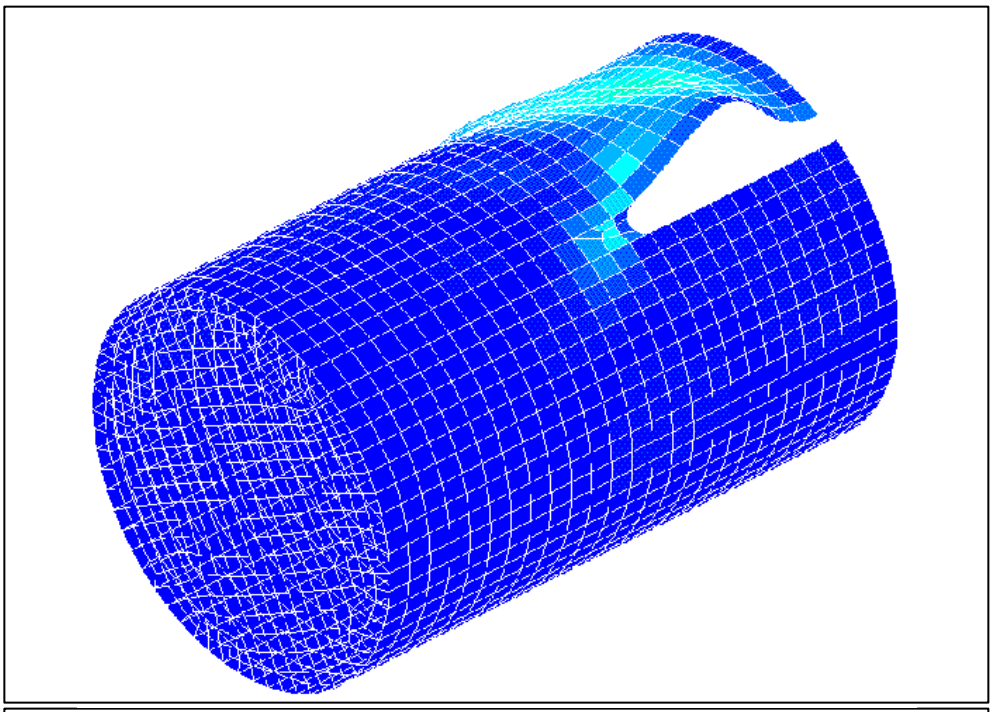

Figure 6.5: First buckling mode of short slotted model

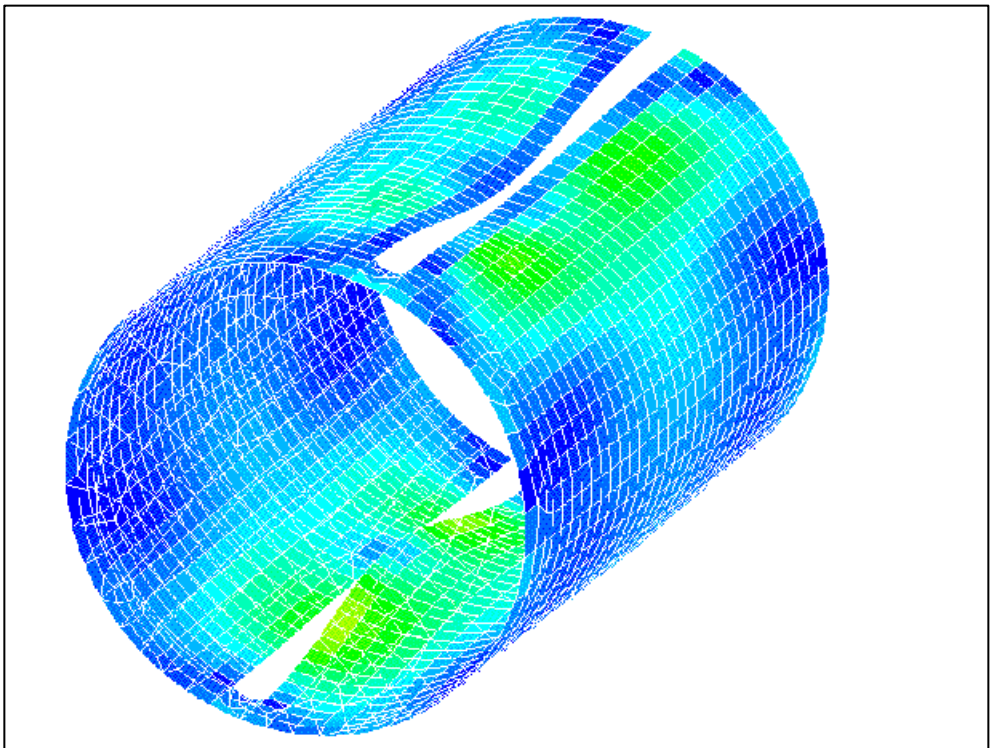

Figure 6.6: First buckling mode of long slotted model

6.2.1 Load-Displacement Response

During the axial compression tests, Labview™ was used to collect the load and displacement data. A plot of load versus displacement for one representative test can be seen in **Figure 6.7**; the remainder can be found in **Appendix C**. For all of the tests, both of the short and long slotted specimens, this plot exhibited identical results. The load reaction to the constant displacement remained linear until damage occurred, which was determined by first audible ply failure. The slight non-linear region at low loads corresponds to the self-alignment of the springs on the upper compression platen.

6.2.2 Short Slot Failure

Three short slotted samples were tested in displacement control in axial compression. Each of these samples exhibited a similar failure mode, as seen in **Figure 6.8**, as well as failure loads. The three samples failed at 43,975 pounds, 45,194 pounds, and 44,434 pounds respectively. The initial damage event was at approximately 44,500 pounds, at which point the 45° plies near the slot tip fractured and damage began to propagate towards the bottom clamped edge. Once these plies failed catastrophically, the structure was no longer able to carry any load and began to buckle about the slots.

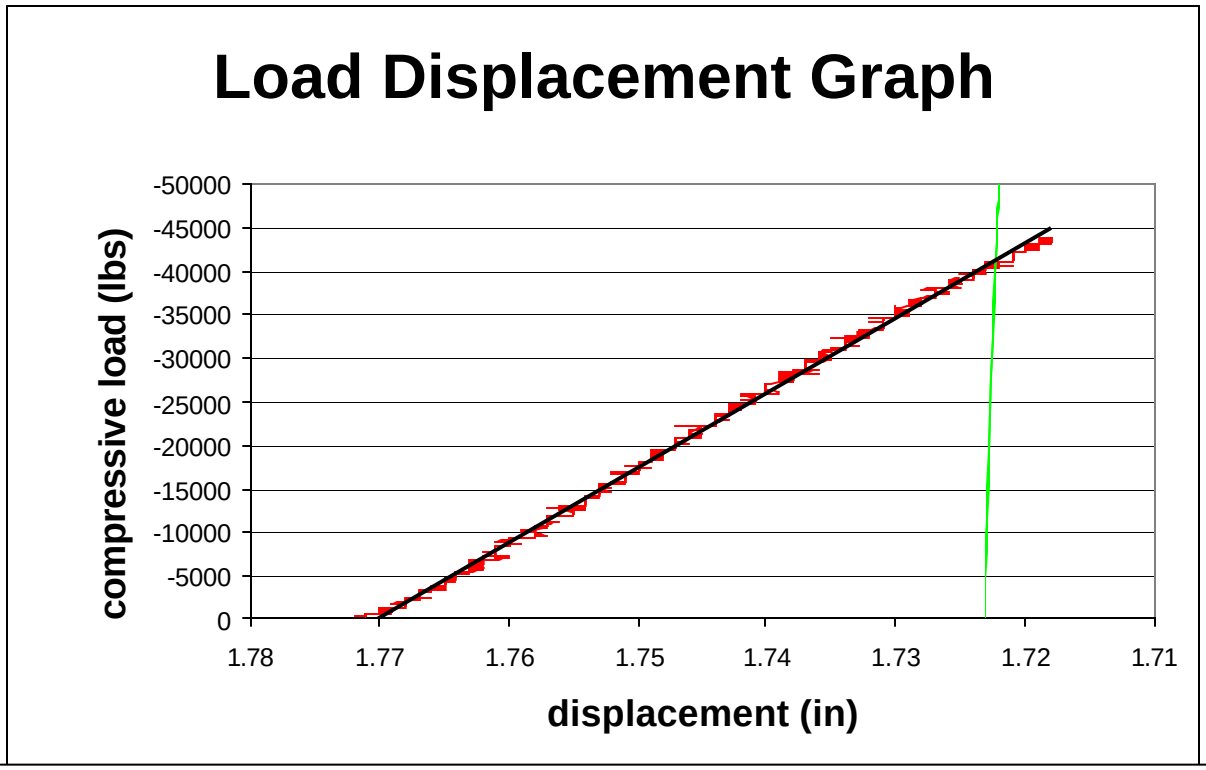

Figure 6.7: Load-displacement graph for a representative compression test

Figure 6.8: Fractured short slotted specimen

Figure 6.9: Buckled long slotted specimen

6.2.3 Long Slot Failure

Three long slotted samples were also tested in the MTS machine. These specimens exhibited the same phenomenon as the short slotted ones, demonstrating identical failure modes at similar critical loads, as seen in **Figure 6.9**. The three samples failed at 54,598 pounds, 51,791 pounds, and 61,220 pounds respectively. For these specimens, the failure apparently commenced at approximately 55,900 pounds, at which point the entire thickness of the structure buckled outward near the upper section of the slots. At the point of the largest magnitude of buckling, fracture initiated in the 45° plies, and again the damage propagated towards the bottom clamped edge. After the angle plies had fractured for almost the entire length of the structure, it could not carry any more load, and began to buckle even further. Collapse occurred instantaneously and catastrophically in all cases.

6.2.4 Air-Gun Results

Of the six samples that were supposed to be tested at Picatinny Arsenal, only four actually were tested due to one gun jamming, and the fracturing of both canisters of the second gun. For the tests that were performed, a 155 mm air-gun was used, whose acceleration profile can be seen in **Figure 6.10** along with a comparison of it to the actual 155 mm gun to be

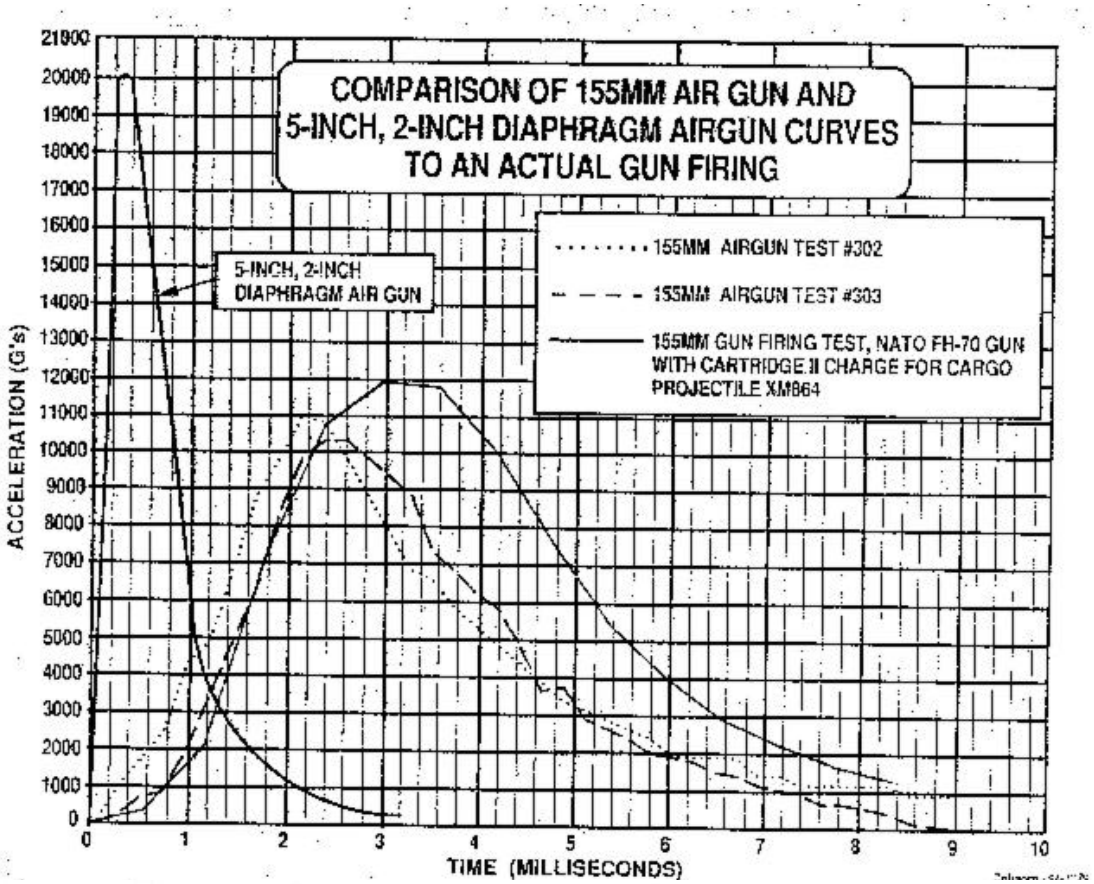

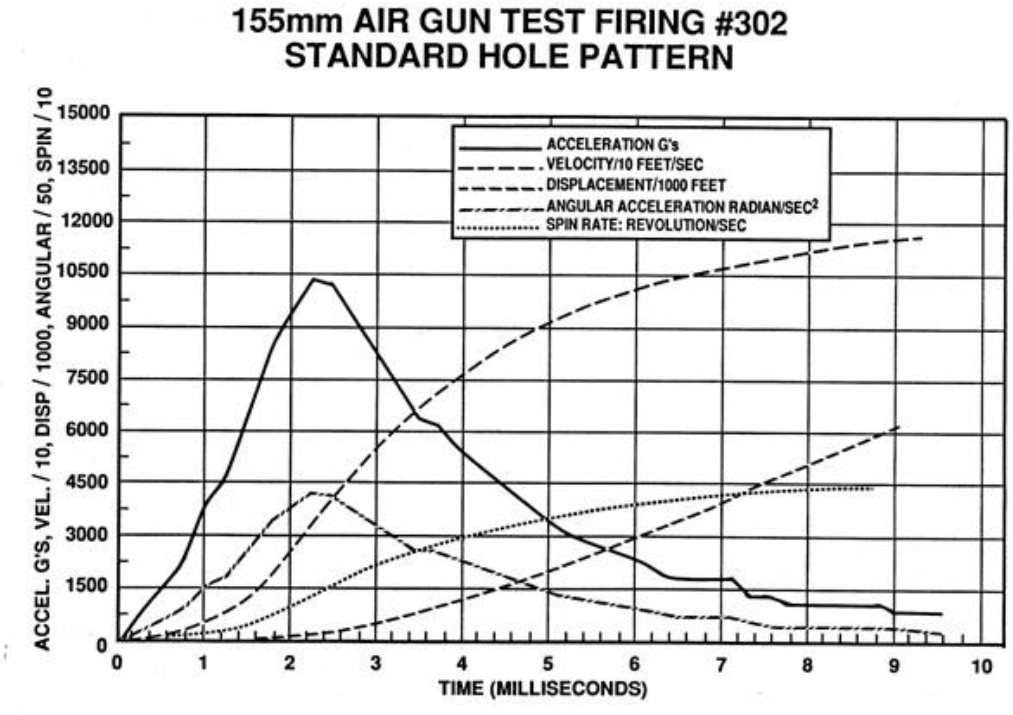

Figure 6.10: Air-gun acceleration profile graph

used to fire the WASP vehicle. This figure shows that the loads experienced by the specimens were very similar to what they would experience in a true launch, making these tests very relevant. **Figure 6.11** shows the g-levels experienced by the specimens fired, and the corresponding effect on the sample.

The pressure listed in the table is the pressure which was used by the gun in order to obtain the desired acceleration, and the load was calculated based on the 4 pound block of aluminum sitting on each specimen being accelerated while the bottom of the specimen is fixed against the back of the shell. The samples that survived here had no apparent damage of any sort after the tests; however, the samples that failed shattered catastrophically, as seen in **Figure 6.12** so that only graphite dust and small broken fibers remained. After a sample failed, the aluminum weight was accelerated into the back of the canister, damaging the weight, the clamp bottom and even the canister itself on some occasions.

6.3 Summary

Due to the cost and time associated with manufacturing and testing these specimens, not many experiments were performed. However, the small representative group of tests performed did place useful bounds on the failure loads that would damage this tail section, and a clear view of the failure loads that can be expected. Note that the accelerations seen in these tests are not

Slot Length	Gun	g-level	Psi in gun	Calculated load	Condition
Long	155 mm	10,000	9,300	40,000	Survived
Short	155 mm	10,000	9,300	40,000	Survived
Long	155 mm	12,500	11,700	50,000	Shattered
Short	155 mm	12,500	11,700	50,000	Shattered

Figure 6.11: Table of air-gun test results

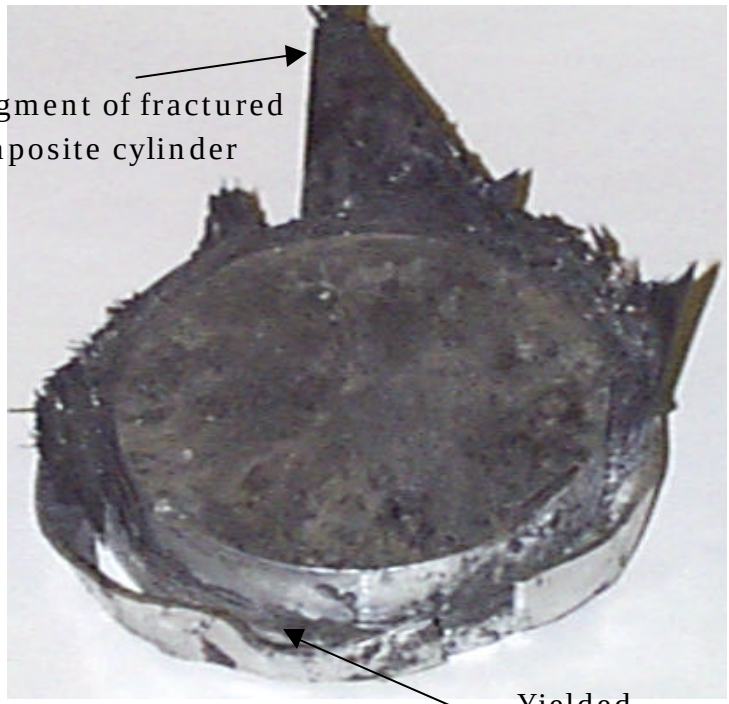

Figure 6.12: Catastrophically failed air-gun specimen

necessarily representative of the true accelerations experienced by the WASP vehicle; however, they provide appropriate load levels and loading conditions to the cylinders to validate the design codes. By combining the analytical and experimental results, as seen in the following discussion chapter, a comprehensive understanding of the failure of the tail section is obtained, which can be confidently used for design criteria.

[This page intentionally left blank]

CHAPTER 7

DISCUSSION

The following chapter provides a discussion of the results presented in the previous chapter. There are two major comparisons presented: first the predictions of failure obtained using the finite element model together with the CLPT code and failure theory is validated against the experimental data, and then the compression test results are compared to the air-gun results. Finally the influences of key variables on the failure modes are scrutinized, and a preliminary design tool is formulated.

7.1 Comparison Of FEA To Compression Tests

As described in previous chapters, some tuning had to be performed on the failure prediction scheme. However, there was a good correlation between the failure predicted—based on FEA together with CLPT and failure theory—and the compression tests results once this tuning was accomplished. The most consistent result was the correct selection of dominant failure mode,

which was predicted by comparing the results of the dynamic and static models. Theoretically one could find the point where a tube would start to fail in buckling instead of fracture using these codes by adjusting the length of the slot in the cylinder, however that was not the point of this analysis. For the two slot lengths of concern in this project, a value could be obtained for the load needed to cause fracture and the load needed to cause buckling; the lower of which being the first and dominant failure mode. For the short-slotted case, the static failure load was predicted to be 51,900 lbs while the buckling load was given as 92,700 lbs, clearly indicating that this cylinder would fail in fracture. Similarly, the static fracture load calculated for the long slotted tube was 64,100 lbs and the buckling load was predicted to be 56,400 lbs. While not as obvious as the previous case, these loads still designate the correct failure mode as buckling for the long slotted tube.

Next, one must compare these predicted failure loads with the actual loads experienced during testing. For the short slotted cylinder, the predicted fracture load was 51,900 lbs while the actual average failure load was at 44,710 lbs, a difference of 16%. The long slotted cylinders were predicted above to buckle at 56,400 lbs, whereas the actual average buckling load was at 55,870 lbs, a difference of 9%. With the margin of error between these results being so small, these codes have been validated to predict reasonably the appropriate failure load for cylinders of this geometry and loading. While not proving itself a reliable substitute for testing, these codes do provide insight to help design which specimens to test.

7.2 Comparison Of Compression To Air-Gun Tests

Since air-gun tests are very expensive and time consuming, one of the goals of this project was to be able to prove that compression tests could serve as an accurate surrogate. The air-gun tests performed for this project were only able to provide a bound for inertial failure; both cylinders tested could survive a launch load of 40,000 lbs, and neither could survive the load of over 60,000 lbs. This range does indicate however that the failure experienced during the compression tests was in the same ballpark as would be seen in a real gun launch. The results presented in this thesis also suggest that for this composite section, the air-gun testing environment was "quasi-static." This was because the resonant frequency of the system was much higher than the gun-shot frequency, so it was not excited. While this does not conclusively rule out the necessity for final air-gun testing of composite sections to prove g-hardness, it does provide a valid argument to enable the use of compression tests as a quick and cheap experimental design tool. Compression tests also help to compare the survivability of competing configurations, thereby drastically reducing the number of air-gun tests that will need to be performed.

7.3 Influence Of Variables On Failure

There were several variables that were analyzed for these composite cylinders. The rationale behind these trade studies was to provide a rubric to predict the effect of certain probable design changes on the failure load. These "rule-of-thumb" numbers would be critical to a quick and efficient design strategy. They would provide a guideline for the eventual entire re-design of the WASP II fuselage.

The first variable investigated was the effect of changing the slot length on the failure load. Since this is a geometric change, it could be assumed to alter both the static failure due to a new stress concentration at the slot tip and the buckling load. Somewhat contrary to expectation, the resulting stresses indicated that lengthening the slot did not have much of an effect on the fracture strength of the cylinder, and in fact somewhat relieved the stress concentration. The long slotted cylinder was predicted to fail at a lower stress level than the short slotted cylinder however, because the buckling load was significantly reduced by the slot length, causing the change in dominating failure modes. This reduction in buckling load can be explained through the Euler buckling equation, where the length here would be the local length of the slot, which accounts for the large reduction in failure load.

Next, several changes in the material properties of the composite were altered to explore the significance of the cylinder's stiffness to its final buckling

load. Again the response was found to follow the Euler equation, with a 10% reduction in E lowering the load factor by 10%. Similarly, a laminate with 0° plies replacing 90° ones, and a laminate with two additional 0° plies were modeled to show the respective linear decrease and increase in load factor. The tube dimensions were then adjusted to find their effect on the buckling load. It was discovered that increasing the tube diameter by 1" would decrease the buckling load factor by 33%; however, increasing the overall tube length had virtually no effect as long as the slot lengths remained constant. Again, these results proved critical when designing the actual WASP II structure, circumventing the need to perform a separate analysis to see the effect of each part of the design.

7.4 Design Tools For High-g Fuselage Sections

One of the most fundamental goals of this project was to prepare a design tool for high-g fuselage sections, which can be followed in the flow chart in **Figure 7.1**. First of all, using the trade-studies discussed above, one could piece together a reasonably survivable section, which could then be verified using the static and dynamic modeling tools presented in this paper. Then, iteratively using the results from the failure prediction procedure outlined, the design could be further "tweaked" using the trade-studies until an acceptable failure strength prediction is outputted. From there specimens would be

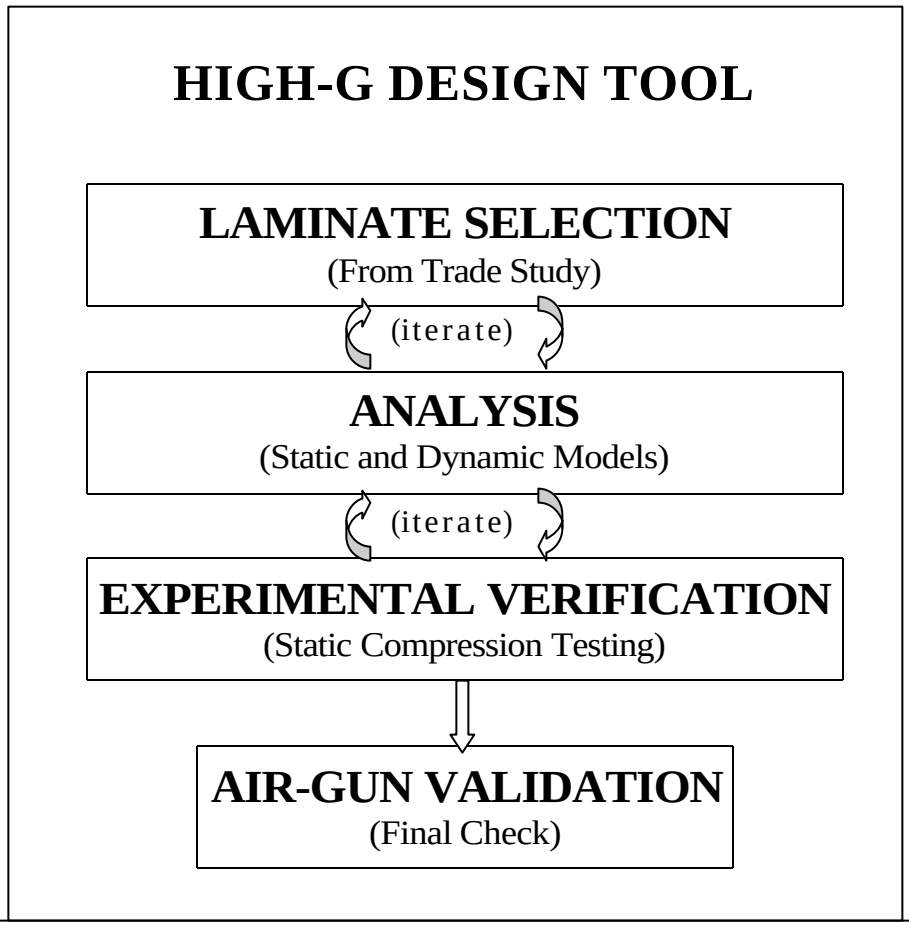

Figure 7.1: High-g design tool flow chart

manufactured to verify those results in a compressive test, where again it could be redesigned slightly if necessary. Finally, once the desired configuration is obtained, the updated fuselage section would only need to be fired out of an air-gun a few times to verify its g-hardness. Using the analysis procedure presented in this thesis, a high-g survival part could be designed with much less time and effort than with previous techniques. The final result of this conglomerated design tool is a method that allows more changes in the design process with fewer penalties, a savings in design and testing time, and significantly fewer expensive air-gun tests. Future uses of this design tool will be explored more thoroughly in the future work chapter.

[This page intentionally left blank]

CHAPTER 8

AIRFOIL MANUFACTURING

The following chapter outlines the manufacturing procedures used to make all of the aero-surfaces for the WASP II vehicle. This includes the main wings, the horizontal fins and the vertical rudder. All of these sections are constructed by wet-layup of carbon fibers, and are connected by various metal spring-loaded joints.

8.1 Overview

The decision to make the wings in composite material was made for the same reason as the fuselage sections; for the high stiffness to weight ratio. These sections were manufactured of graphite/epoxy prepreg at first, however the curvature and taper of these airfoils drove the design to the conformability of wet-layup composite fabric. There were two types of dry carbon fibers used, both ordered from CST in Tehachapi, CA[25]. The first was a 2.9 oz/yd^2 unidirectional carbon web that was used to increase the bending stiffness in

Gougeon Brothers Corporation Manufacturer's Data Sheet	**WEST SYSTEM EPOXY**			
	ASTM	105/205	105/206	105/209
Mix Ratio (by weight)		5.07:1	5.0:1	3.56:1
Mix Viscosity (cps @ 72°F)	D-2393	1300	580	775
Pot Life (100g @ 72°F)	D-2471	12 min.	21.5 min	51 min.
Specific Gravity of Cured Resin		1.18	1.18	1.163
Hardness (Shore D) (1 day)	D-2240	80	80	68
(2 weeks)	D-2240	83	83	79
Compression Yield (psi) (1 day)	D-695	10,120	7,990	1,226
(2 weeks)	D-695	11,418	11,500	10,027
Tensile Strength (psi)	D-638	7,846	7,320	7,105
Tensile Elongation (%)	D-638	3.4	4.5	4.0
Tensile Modulus (psi)	D-638	4.08E+05	4.60E+05	3.65E+05
Flexural Strength (psi)	D-790	14,112	11,810	11,923
Flexural Modulus (psi)	D-790	4.61E+05	4.50E+05	4.40E+05
Heat Deflection Temperature (°F)	D-648	117.8	123	129.5
Annular Shear Fatigue (lbs @ 100,000 cycles)			9,300	8,440
Izon Impact, notched (Ft-lb/in)	D-256	.93	.54	1.1

Figure 8.1: Table of West System™ epoxy cured properties

the airfoils. The second was a 5.6 oz/yd² carbon woven fabric, which was cut out in ±45° strips to provide torsional stiffness in the outside plies of the airfoil sections. The West System™ epoxy system was used to bind the fibers together, using the 105 adhesive with the 209 extra slow hardener for the main wings to allow more volatiles to escape and to achieve improved compaction, and the 206 slow hardener for the other sections. The properties of this epoxy system can be found in **Figure 8.1**. Several epoxy thickeners were used for various sections as well, including colloidal silica, micro-fiber powder and chopped carbon fibers.

All of the composite airfoil parts were fabricated inside the aluminum mold shown in **Figure 8.2**, and peel ply was applied and drawn smoothly across the top of the surfaces, which was followed by a layer of porous teflon and a dozen sheets of bleeder paper to absorb the excess epoxy. A vacuum bag was placed over the setup, which was then pulled down to 29.5" Hg slowly while the part was being smoothed through the bag to eliminate wrinkles and spread the epoxy. All of the cures were performed at room temperature to prevent residual thermal stresses, and were cured for either 24 hours with the 209 hardener or 12 hours with the 206, both under a 1-micron Hg vacuum.

Upon being cured, the bagging materials were removed, and a "cookie-cutter" piece, as seen in **Figure 8.3** was placed over the mold to guide a utility knife in cutting the excess fabric away from the part to define the appropriate shapes. Subsequently, there were several secondary cures to bond different sections together, to apply hinges, fill in gaps, and to define a good leading

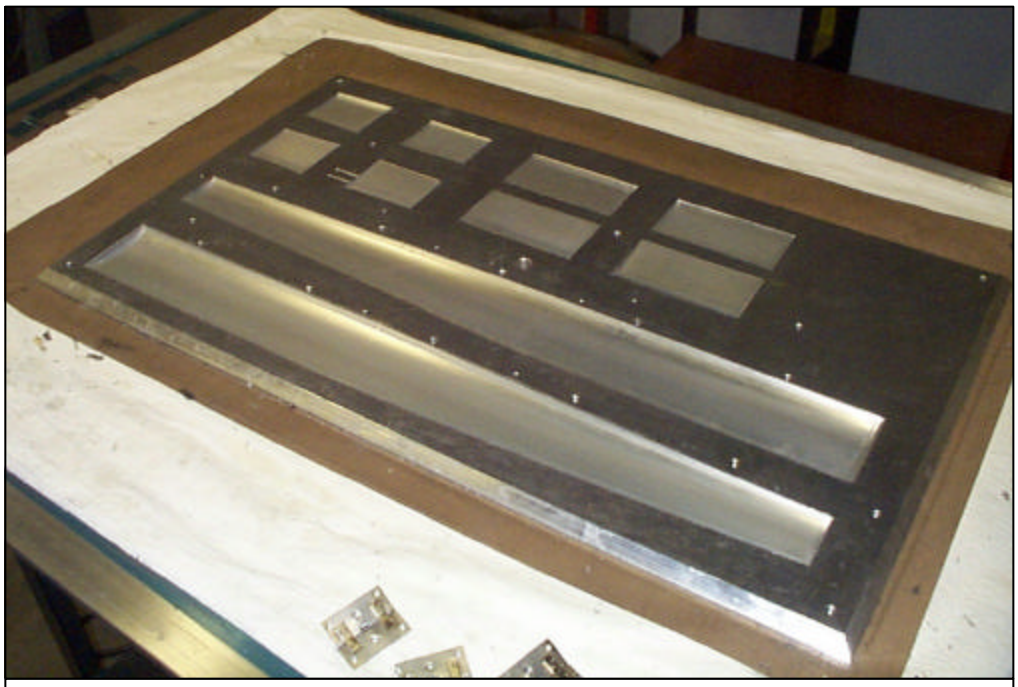

Figure 8.2: Aluminum mold for curing WASP II aerosurfaces

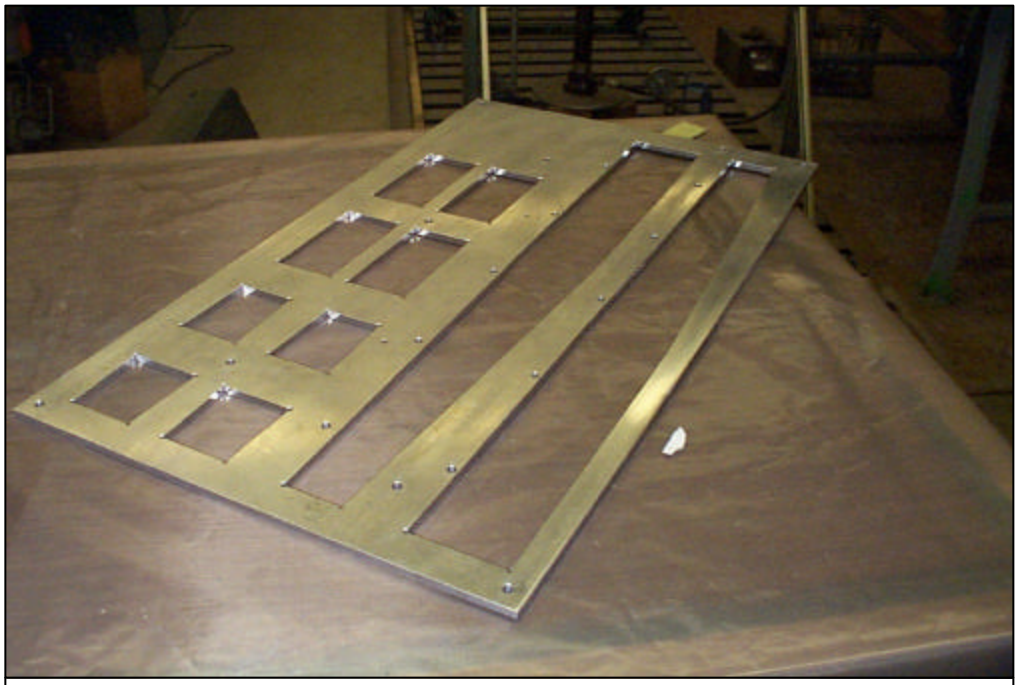

Figure 8.3: Aluminum “cookie-cutter” template

edge. Finally, fine sand paper was used to smooth the rough edges of the airfoil sections.

8.2 Main Wings

The two main wings of the WASP II vehicle, as seen in **Figure 8.4**, extended for a 55" wingspan. Each half span was comprised of three sections; the first was a straight cambered airfoil with a chord length of about 3", and the next two were tapered down to a tip chord of about 3.5" at a 16° dihedral. The wing was composed of three sections so that they could fold and stow to fit in the WASP artillery shell, as seen in **Figure 8.5**. The cross section of the wing was a T16 thin airfoil, selected by the aerodynamics group of the original WASP team[26] for its high camber (12%) and maximum lift coefficient (1.8). The first section below describes how these wings were manufactured, followed by a description of the hinging mechanism implemented.

8.2.1 Manufacture of structure

The milled aluminum mold cavities were first thoroughly cleaned and covered with 5 layers of Frekote™ to provide a smooth and easily released surface. Then the 105 epoxy and 209 hardener were blended together in a 3:1 by volume ratio, some of which was set aside and mixed with colloidal silica until a vaseline-like consistency was obtained. This thickened epoxy was

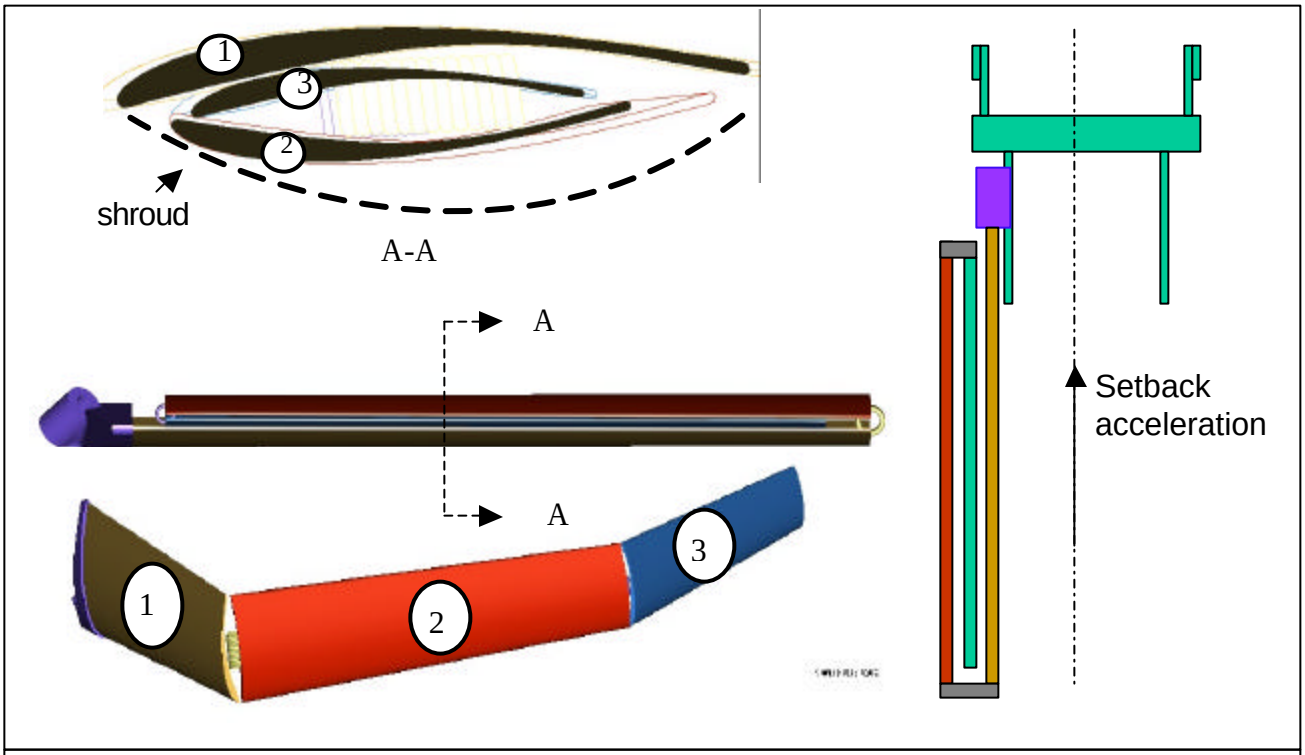

Figure 8.4: Main wing for WASP II vehicle in unfolded and stowed positions[2]

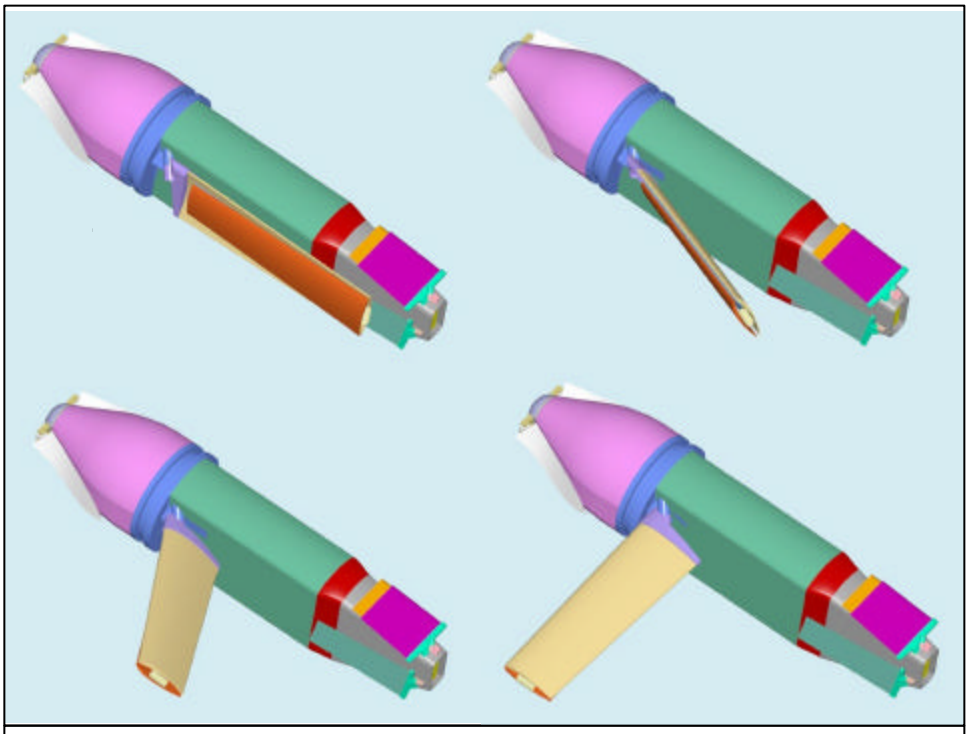

Figure 8.5: WASP II wing folding scheme[2]

applied in a thin coat over the entire mold with a tongue depressor to help stop the initial ply layers from moving, and to ensure a glossy surface finish on the part. The first ply layer was placed in the mold, which covered the entire cavity both in span and chord, and a plastic wedge was used to squeeze the excess epoxy through the woven fabric. Next an acid brush was used to apply a uniform layer of epoxy along the top surface of the first layer, and the second layer of fabric was laid down and smoothed into place. This procedure was followed through each ply layer as seen in **Figure 8.6**, which lists the layer angles and widths. Each ply was laid down starting at the leading edge and then smoothed down carefully towards the trailing edge, being careful not to stretch the weave. Since many of the center layers had shorter chord widths, the smallest only being 0.5" wide, some plies only contributed to the leading edge thickness. In this fashion the airfoil cross-section was defined.

The layers were applied symmetrically, so that at the leading edge there was a maximum of 28 plies (counting a ±45° layer as two plies), and a minimum of 12 at the trailing edge. Upon completion of laying down all of the carbon fabric, a generous amount of epoxy was poured on the upper surface and painted uniformly to guarantee that there would be no dry fabric after the cure. The bagging procedure was then carried out as described in the overview section, and the wings were cured under vacuum and trimmed using the template "cookie-cutter." Then an additional piece of aluminum, as seen in **Figure 8.7** was bolted onto the mold, which helped to define the lower half of the leading edge. A mixture of epoxy and micro-fiber power was prepared to a

Symmetry Line	
$0°_2$	0.5”
$0°_2$	1.0”
±45°	1.5”
$0°_2$	2.0”
$±45°_3$	3.0”
Mold Face	

Figure 8.6: Main wing layup

Figure 8.7: Aluminum rails for defining leading edge

thick peanut-butter-like consistency, and placed under this new piece with a tongue depressor and cured. Lastly, the wings were removed from the mold and cut into the three prescribed sections as seen in **Figure 8.8** on a horizontal milling machine with a diamond grit blade.

8.2.2 Manufacture of hinge

The hinges for the main wings presented one of the greatest challenges of both WASP vehicle designs. The objective was to have a hinge mechanism that would integrate a solid pivot, be spring loaded, hold a reliable dihedral and have a locking mechanism. In the original WASP vehicle, all of this functionality was integrated directly into the aluminum wing design. For the WASP II vehicle however, it was deemed too difficult to develop a similar system for the composite section in such little time. In the end, a similar mechanism to the original design was implemented using secondary cures.

Standard spring-loaded stainless steel cabinet hinges were purchased from McMaster-Carr, and were cleaned and sanded to provide a good bonding surface. First, to obtain the correct pivot line while maintaining a low surface profile on the bottom of the wing, the hinges were bent to an appropriate angle. A micro-fiber thickened epoxy mixture was used to build up a small platform, and holes were drilled through the hinges to allow the flowing epoxy to form a rivet like connection between the platform and the hinge. As seen in **Figure 8.9** these hinges covered a 3/4" span on either side of the hinge

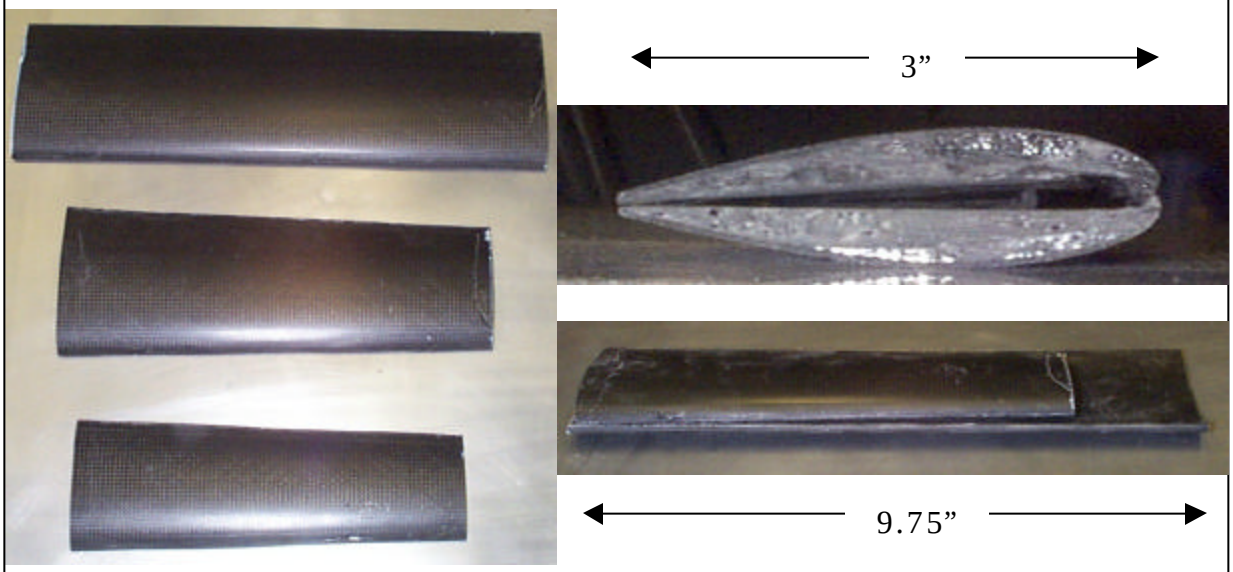

Figure 8.8: Main wing cut into three sections with cross sectional view

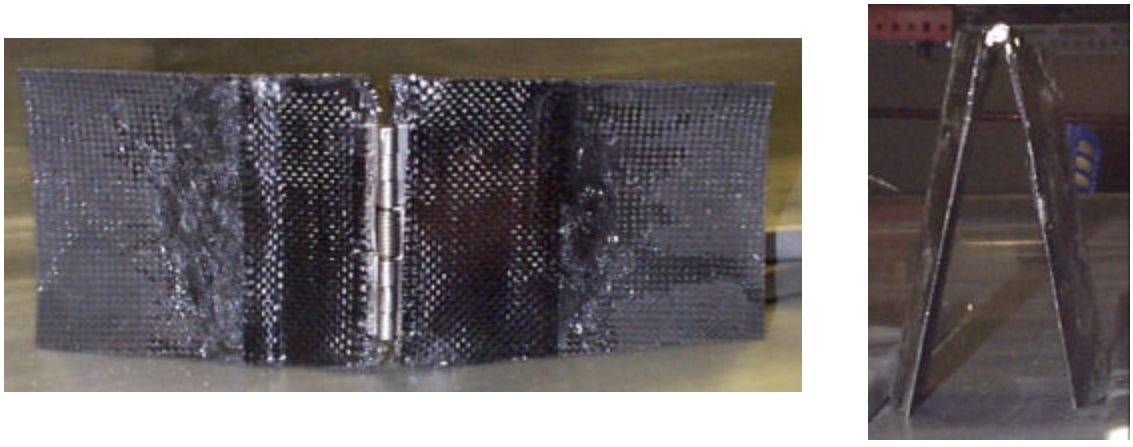

Figure 8.9: Main wing hinge cured onto test section airfoil

line, which amounted to the entire area of the chord from just below the leading edge down to the trailing edge. The hinge was also covered by a small piece of woven carbon fabric to help prevent delamination of the bond. The two sides of the hinge were cured simultaneously with their pin and spring removed to relieve the spring tension. After the cure the pin and spring, along with two additional springs were replaced on the hinge to hold up the wings with an appropriate amount of force.

In order to set the dihedral angle, the butted wings were sanded down to the appropriate angle using a belt-sander with fine grit paper. Once unfolded, the hinge was only capable of opening to the prescribed dihedral angle of 17° for the first section joint, and 0° for the second joint. It was determined that aerodynamic forces would be sufficient to support these wings during flight[27], so no lock mechanism was developed.

8.3 Horizontal Fins

The horizontal fins were manufactured in a similar fashion to the main wings, as described in the overview. Since the aerodynamic loading was not as high, these sections did not have to be as stiff as the main wings. Therefore they were cured with less plies to reduce weight. The layup was as seen in **Figure 8.10**. The fins were manufactured in four sections, each using a top and bottom matching piece to form a completed symmetric airfoil for each side. These pieces, as seen in **Figure 8.11** were joined together in a secondary

0°	0.5”
0°	1.0”
$\pm 45°_2$	2.5”
Mold Face	

Figure 8.10: Tail fin layup

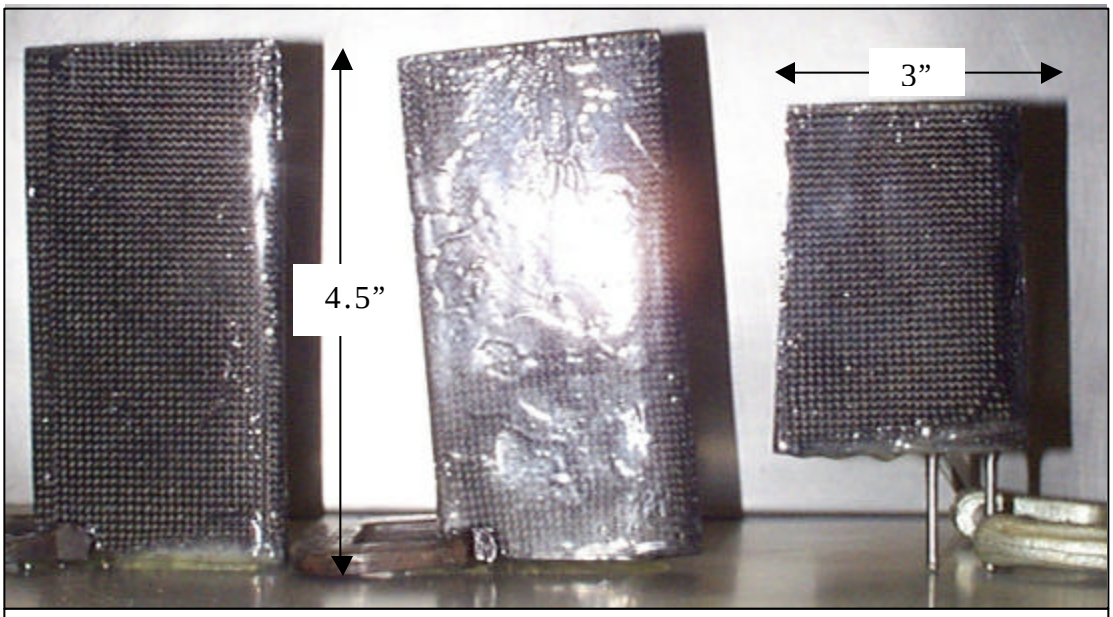

Figure 8.11: Tail fins and rudder for WASP II demonstration flyer

0°	3.0”
±45°	3.0”
Mold Face	

Figure 8.12: Rudder layup

curing procedure performed in the mold under vacuum, with an epoxy and chopped fiber mixed filling the gap. Once removed from the mold, the leading and trailing edges were sanded with fine grit paper to smooth the transitions.

8.4 Rudder

The vertical rudder was also fabricated identically to the other aerodynamic surfaces. The rudder was constructed in 3 pieces; two symmetric halves for the top section with lay-up as seen in **Figure 8.12**, and a bottom piece made in stereo lithography (SLA) and reinforced with a single layer of woven carbon. The top section was joined in a secondary cure process the same way the horizontal fins were—filled with chopped fiber and epoxy. Two freekoted .093" steel rods were placed in these top sections during cure to leave guide-pole holes for the telescoping mechanism. Since there was a telescoping scheme to stow the top section of the rudder, the bottom section had to be hollow which presented a challenge. A separate SLA mandrel was used to maintain this gap, which was machined slightly larger than the top section to allow smooth sliding in and out of the bottom section. This piece was then laminated with a single layer of woven carbon fabric along each side. Again, the leading and trailing edges were sanded with fine paper afterwards to better define them. The rudder was one of the pieces that needed some additional development, which will be discussed further in the future recommendations section.

[This page intentionally left blank]

CHAPTER 9

VEHICLE SUPPORTS, ATTACHMENTS AND JOINTS

The following chapter details how the composite sections described previously were attached together, and how other components were attached to them. This includes the fixed joints between the cylindrical fuselage sections, the hinged joints between the wing sections, and the joint between the airfoils and the body. Component attachment tests were also performed, bonding and bolting materials onto the fuselage sections. Also described in this chapter is the supporting shroud which is intended to mechanically isolate the fuselage sections during acceleration, making it possible to reduce structural mass from these components.

9.1 Overview

Two methods of attachment were explored: adhesive bonds and bolting. It was decided early on that the initial test vehicle would be constructed with all bolted joints so that it could be easily disassembled for display or repairs.

The future operational vehicle however, will have all adhesive joints, as they are much lighter and easier to manufacture for a single use vehicle such as the WASP II. On the flight demonstration vehicle, several #6 flat-head screws were used, distributed around each section to hold them in place. Each of these screw holes were countersunk using a diamond grit beveled end-mill. The following sections will describe the attachment schemes that were designed for the operational and production line vehicle.

9.2 Tube Sections

Since the WASP vehicle undergoes very high accelerations, it was important to design several "hard-points" into the vehicle for payload attachment. The most convenient place to put these "hard-points," which were to be machined out of aluminum, was between each of the composite sections and at the nose of the vehicle. That way, the aluminum blocks would serve the purposes of both holding the sections together, and providing mounting points for the heavier components in the vehicle.

9.2.1 Joining tube sections

There were two main bulkheads used to attach the tube sections together: the main bulkhead, which connected the nose and body sections, and the aft bulkhead, which joined the body and tail sections. The main bulkhead was a relatively complicated component, as seen in **Figure 9.1**,

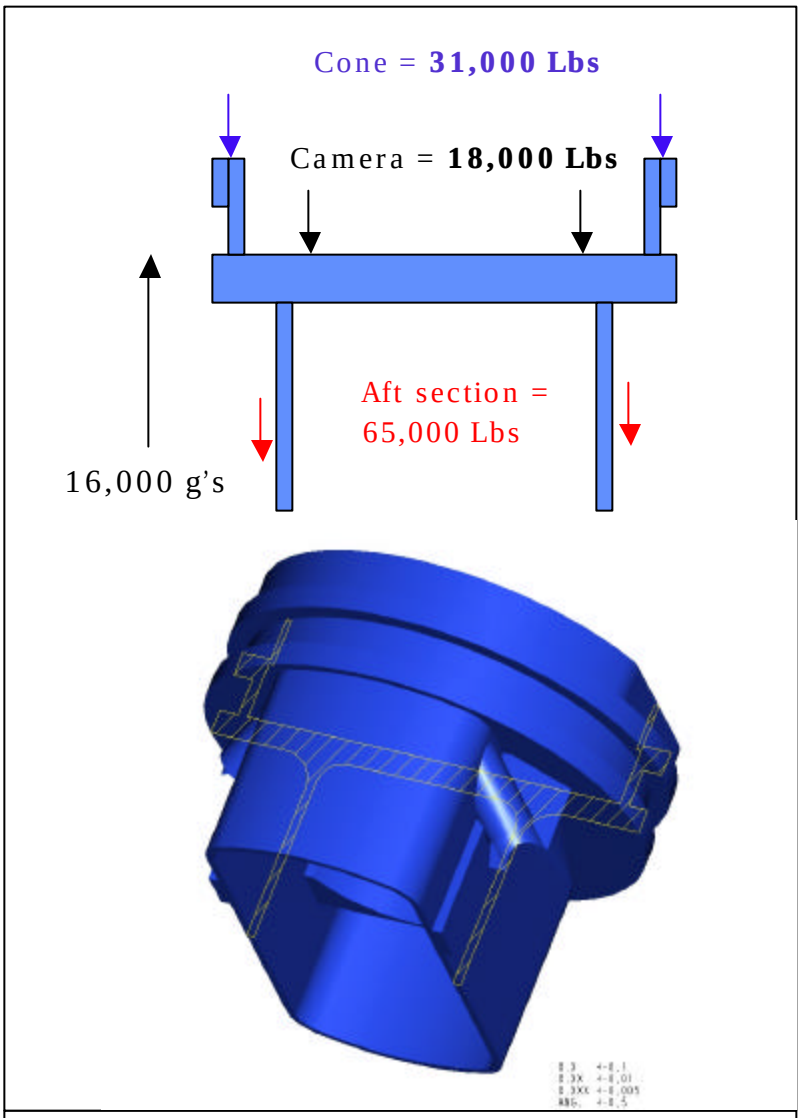

Figure 9.1: Aluminum fore-bulkhead[2]

needing to be machined on a computerized milling machine. The fore-area of this bulkhead was where the composite nose section attached to the bulkhead, using FM-123 elevated temperature cure film adhesive. The metal part was undersized slightly to accommodate the manufacturing tolerances in the composite, and the epoxy was allowed to flow into the gaps during the gel time of the cure cycle.

The next section of the main bulkhead was referred to as the shelf, and was a piece of metal that protruded slightly from the vehicle to provide an attachment area for the shroud, a part which will be described later in this chapter. Aft of the shelf section of the bulkhead was a long contoured piece that matches the inside curvature of the body section, and was bonded to that section in the same fashion as described for the fore-area of the bulkhead. This main bulkhead also served for attachment purposes, which will be explained in the following section. The aft-bulkhead was similar to the main-bulkhead, and joined the composite sections in the same fashion using film adhesive. The main difference between the two pieces was that the aft-bulkhead did not have the shelf piece, since the shroud only contacted the vehicle in the front.

9.2.2 Inside attachments

There are two general ways that components were attached to the composite sections inside of the vehicle: either they were mounted to the "hard-points," or adhesively bonded. The heaviest component inside the WASP II vehicle was the battery, which is inserted into a cut-out inside the main bulkhead which supports it from all sides. The front side of this bulkhead was also where the cameras and the photo-electronics were fastened. The next heaviest component was the motor, which was housed in the nose plate, a piece of aluminum that was placed in the front of the vehicle protruding from the nose cone. The last large components to be mounted into a "hard-point" were the servos and gyros, which were fixed onto the aft bulkhead in the rear of the vehicle to provide them with a rigid support.

There were a few more components that needed to be mounted into the vehicle, such as guidance and navigation systems. These parts, which were mostly miscellaneous electronic components, either had their casings machined to match the contour of the composite wall, or they were mounted by welding or soldering onto a piece of metal piping which matched this contour as close as possible. This metal part was then bonded with FM-123 onto the composite wall, using a standard surface preparation of cleaning and sanding.

9.3 Wing Sections

As described in the previous chapter, the wings were one of the most important and challenging parts of this program. How the wing sections would attach together and to the body of the vehicle was a topic of great debate for the WASP team. It has already been described how the test flyer's wings were attached together, and in this section future configurations will be discussed.

9.3.1 Joining wing sections

Chapter 8 describes the hybrid metal/epoxy joint used to join the wing sections together, as well as the telescoping rudder in depth. This was a very challenging part since not only did it have very specific volume restrictions because of the shell and the folding scheme, but it had to provide a rigid support to transfer the bending stress across the joint, as well as being a spring loaded pivot with a reliable dihedral lock. The original design of the WASP II vehicle had planned to use custom machined inserts with hinges to attach the wing sections together, which was similar to what the final configuration ended up being for the test flyer. For several months, the hinge design had switched to a Kevlar flexure, a single piece of woven cloth brushed over with epoxy to become a compact hinge with internally stored potential energy when folded. This scheme worked well for smaller test sections, but once implemented into the full chord length, the flexure became too torsionally

weak and did not hold the wings to a tight level tolerance. The question of dihedral remained for this design as well.

For the flight demonstration vehicle, the solution was determined to be a standard spring-loaded cabinet hinge epoxied onto the underside of the wing, with matched sanded angles on the cross section of the wing providing the dihedral. For the final production vehicle, which will most likely be made by resin transfer molding or a similar process, these hinges should be an integral part of the wing, with a spring loaded pin providing the necessary force, and the dihedral lock molded into the cross-section of the wing.

9.3.2 Wing pivot attachment

For wings, tail fins and rudder the same attachment scheme was used to connect them to the flyer. An oversized cavity is machined into a mounting piece, which is used to control the folding mechanism, and the aerosurface is then potted into the metal. In the case of the wings, this mounting piece protrudes from the sides of the main bulkhead as seen in **Figure 9.2**, and for the tail surfaces they were special separated pieces. For the test vehicle all of the aluminum pieces were thoroughly freekoted, and fast-hardening epoxy was used to pot all of these pieces so it would be easier to replace parts if necessary. In the final configuration of the vehicle, a wet epoxy system would be used to mount the parts without the release agent.

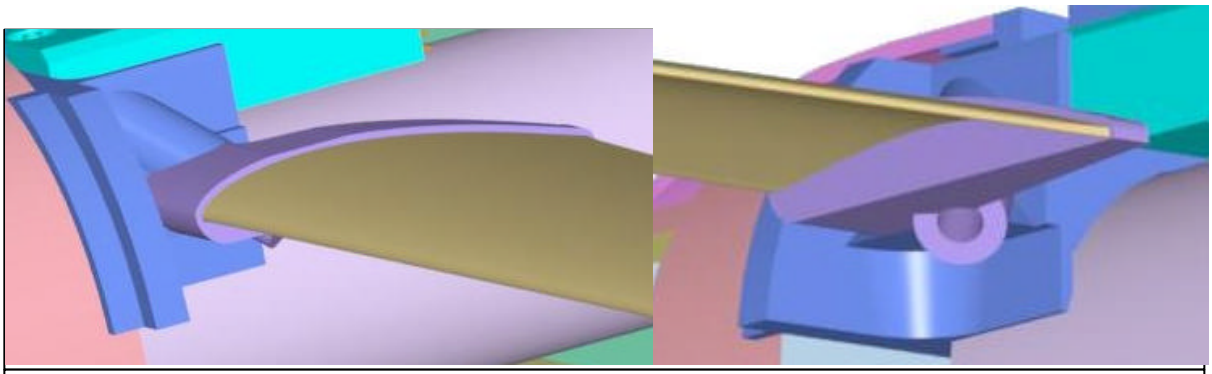

Figure 9.2: Main wing aluminum root[2]

TEST	Description	Bearing Area (in^2)
Square	1”x1” Al pipe	1
Long	1”x2” long Al pipe	2
Wide	2”x1” wide Al pipe	2
Clamp1	Bonded inside and outside of tube for 0.5”	11
Clamp2	Bonded inside and outside of tube for 0.5”	11
Clamp3	Bonded inside and outside of tube for 0.5”	11
Ring1	Bonded inside of both sides, 0.5”	5.5
Ring2	Bonded inside of both sides, 0.5”	5.5
Ring3	Bonded inside of both sides, 0.5”	5.5
Bolt	Same as clamped section, with 4 - ¼” bolts	0.1

Figure 9.3: FM-123 adhesive attachment test matrix

9.4 Test Matrix

Several tests were performed in order to obtain the shear strength of the FM-123 film adhesive, which can be seen in the **Figure 9.3**. There were basically two categories of tests performed. The first type of test was to experimentally bond metal pieces to the inside walls of the composite as described in the component attachment section above. There were three different shape of pieces as described in the table. The second type of test performed was to bond two sections together. Three variations of this test were also performed; the clamped section having bonding surfaces on both sides of the tube wall, the ring sections just being bonded into the insides of the tubes, and lastly a clamped section with 4 ¼" bolts going through the composite and metal sandwich.

Special testing fixtures were machined for each of these three tests. As seen in **Figure 9.4**, a steel test stand was constructed for the three composite curved panels with the pipe sections bonded onto them. These ¼ cylinders were constrained from lateral movement by two metal posts in the front, and one adjustable post in the back to hold it tightly in place. Then a special grip was made for the MTS hydraulic testing machine, which had a 1 in^2 flat square cross-section, which bore down on the bonded aluminum pieces until they failed. As seen in **Figures 9.5** and **Figure 9.6** the aluminum clamps and rings had bolt holes cut through them, through which the steel top and bottom

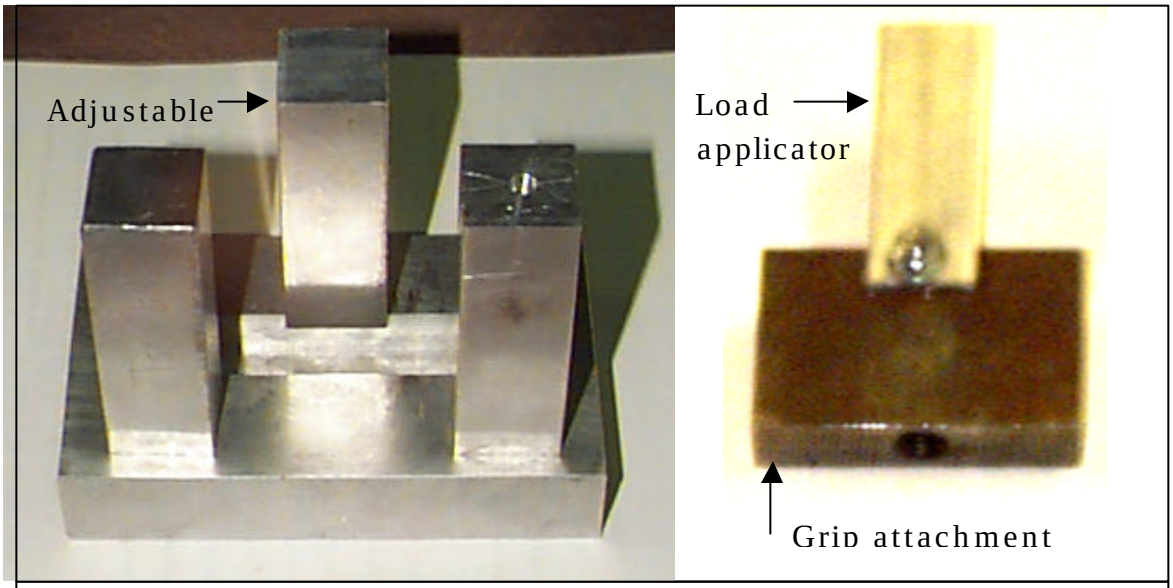

Figure 9.4: Curved panel test stand and load applicator

Figure 9.5: Aluminum clamp

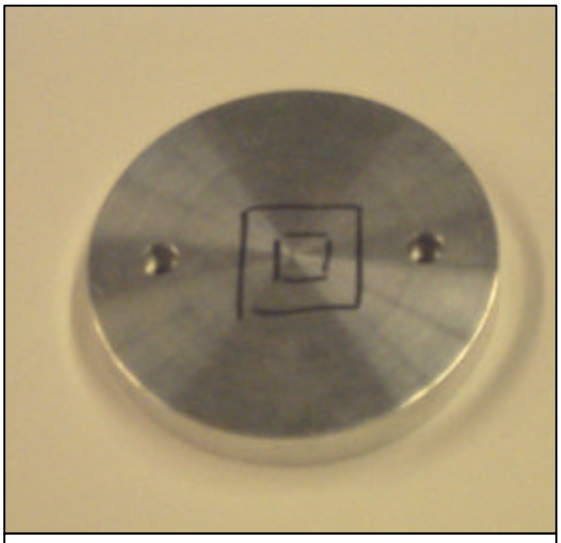

Figure 9.6: Aluminum ring

specialty grips where attached to interface with the testing machine. All of these tests were performed in stroke control at .05” per minute, and the failures load and modes were recorded.

9.5 Results

The results for these adhesive tests were rather discouraging. Most of the bonds failed at much lower stresses than expected, as seen in **Figure 9.7**, which presents the failure load with its corresponding stress and mode. All of the failures were adhesive failures as opposed to cohesive failures, which partially explains the divergence from the expected 5,000 Psi shear strength. The age of the material along with the surface preparation used are believed to have played an important role in the failure, and need to be experimented further with this, and other adhesive films. Clearly though, the bolt test did prove to be a good attachment method for these composite parts, with a bearing strength of nearly 25 Ksi. More attachment tests are specified in the future work section of this thesis.

TEST	Failure Load (Lbs)	Failure Stress (Psi)	Failure Mode
Square	1,091	1,091	Composite delamination
Long	2,343	1,172	Weld yield
Wide	1,690	845	Composite delamination
Clamp1	169	15	Bad bond
Clamp2	11,200	1,018	Adhesive delamination
Clamp3	4,039	367	Slipped out of top
Ring1	10,210	1,856	Inner ply failure
Ring2	5,912	1,075	Inner ply failure
Ring3	6,882	1,251	Inner ply failure
Bolt	2,454	24,540	Bearing rip through

Figure 9.7: Table of results for adhesive attachment tests

9.6 Shroud

A protective steel shroud was designed to surround the vehicle, bearing on the main bulkhead's "shelves," to serve several purposes. The primary role of the shroud was to support the vehicle during the gun launch as seen in **Figure 9.8**, providing a load path for the axial acceleration force and placing most of vehicle in tension, which eliminates buckling as a dominant failure mode. This has the consequence of relieving the tail section strength requirements, which improves the many vehicle characteristics that were described in length in Chapters 2-5. The shroud also bears the 60,000 lbs compressive force of expulsion charge the vehicle would normally feel before leaving the shell. Secondary purposes of the shroud include protecting the vehicle during spin launch balloting, and adding ballistic weight to the shell/flyer combination to match ballistic trajectory tables.

9.6.1 Material selection

There were four basic failure modes for the shroud that had to be considered in order to select the appropriate metal for its construction:

1. Yielding
2. Euler column buckling
3. Local shell buckling of the cylinder
4. Local shell buckling of the half clamshell

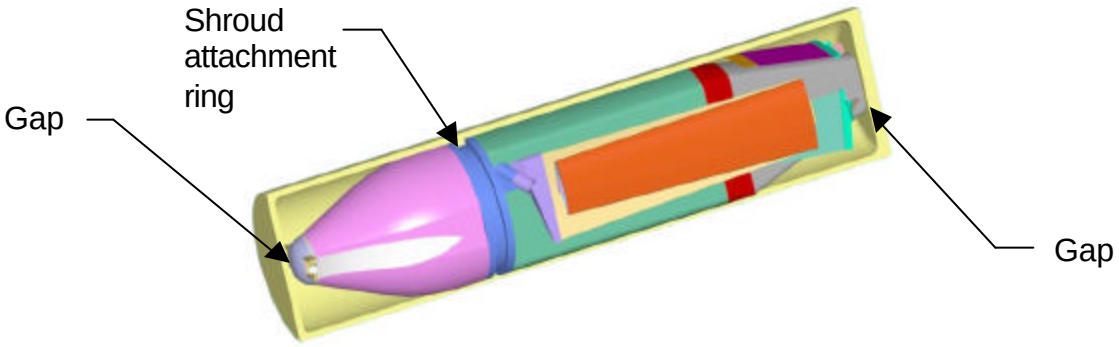

Figure 9.8: Protective shroud surrounding WASP II vehicle[2]

Allowable g-Level for Shrouds of Different Metals
(16,000 required)

	Steel AISI 4140H	Tungsten W-25Re	Moly Mo-47.5Re	Titanium Ti 6211	AL AL 7075T6
Yield	24,000	8,000	9,000	16,000	12,000
Euler Column Buckling	583,000	643,000	725,000	443,000	331,000
Local Shell Buckling	145,000	160,000	180,000	110,000	82,000
Local Clamshell Buckling	30,000	33,000	37,000	23,000	17,000

Figure 9.9: Table of materials investigated for shroud design

There were 2 loading conditions to be considered as well:

a. Expulsion charge of 3000 Psi
b. Acceleration load of 16,000 g's on shroud and 12 Lbs vehicle

All of these failure criterion and loading conditions are explored for several candidate metals, the result of which can be found in **Figure 9.9**. A demonstration of the various calculations performed is shown in **Figure 9.10**, using steel as an example. The outcome of this trade-study was that in order for the vehicle to be statically and dynamically stable, the shroud metal would have to have an Young's Modulus, E, greater than 16.0 Msi and a yield stress, σ_y, greater than 160 Ksi. AISI 4140H Steel, with a 500°F temper was selected as the best candidate, however several different high grade steels would have been appropriate, the trade-off being in their fracture toughness versus their yield strength. All of these steels have a modulus of 30 Msi, and a density of around 0.283 lbs/in^3; this particular grade has a yield stress of 240 Ksi and fracture toughness of 53 $Ksi*in^{½}$ (giving a critical crack length of 0.07" at the design stress level of 160 Ksi).

9.6.2 Analysis

After the material for the shroud had been selected, the attachment ledge, which was the part that mated with the main bulkhead shelf, was sized for bearing loads and shear. A finite element analysis was

$\rho_{steel} = .283\ \text{lbs/in}^3 \quad R_{outer} = 2.5" \quad R_{inner} = 2.3" \quad t = .2" \quad A = 3\ \text{in}^2 \quad I = 8.7\ \text{in}^4 \quad L = 21\ \text{in}$

1. a. $\sigma_{max} = \dfrac{A_{5"cyl}}{A_{.2"tube}} \times 3{,}000\ \text{psi} \approx 20\ \text{ksi}$

   b. $V_{.2"tube} = 63.3\ , \quad F_{max} = 16{,}000(63.3\rho + 12) \quad \Rightarrow \quad \sigma_{max} = 5{,}305(63.3\rho + 12) \approx 160\ \text{ksi}$

2. $\sigma_{cr} = \dfrac{\pi^2 EI}{L^2} \quad \Rightarrow \quad \dfrac{\sigma_{cr}}{E} = .195$

   a. $E \geq 0.1\,\text{msi}$

   b. $E \geq 0.8\,\text{msi}$

3. $\sigma_{cr} = \dfrac{Et}{R\sqrt{3(1-\nu^2)}} \quad \Rightarrow \quad \dfrac{\sigma_{cr}}{E} = .0484$

   a. $E \geq 0.4\,\text{msi}$

   b. $E \geq 3.3\,\text{msi}$

4. Structural Handbook chart using $\dfrac{t}{R} = .08$ and $\dfrac{L}{R} = 8.4 \quad \Rightarrow \quad \dfrac{\sigma_{cr}}{E} = .01$

   a. $E \geq 2.0\,\text{msi}$

   b. $E \geq 16.0\,\text{msi}$

Figure 9.10: Shroud material requirement calculations

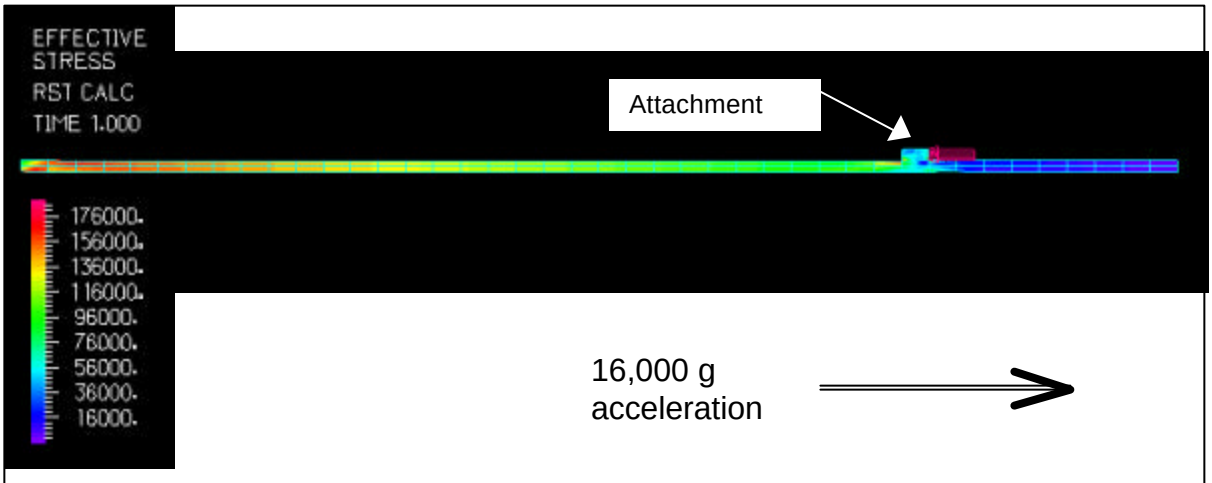

Figure 9.11: Finite element analysis stress solution of shroud design

performed in ADINA™ to solve for the stresses experienced by the shroud during loading. It was modeled as a 2-D axisymmetric cross section, with mass-proportional load along its length with the weight of vehicle applied as a distributed force on the ledge. As seen in **Figure 9.11**, the maximum stress of 180 Ksi occurs at base of the shroud and at the point where it attaches to the vehicle. All of these stresses in the finite element model agree with the calculations presented in the previous section as well. This analysis confirms the fact that steel was an appropriate material selection for the shroud, and that it will protect the WASP vehicle with a large margin of safety.

[This page intentionally left blank]

CHAPTER 10

CONCLUSIONS AND RECOMMENDATIONS

The work in this thesis investigated the design and manufacture of the major structural components of the WASP II vehicle. These parts included the nose, mid-body and tail sections, all of the aerodynamic surfaces, and the hinge and joint mechanisms. This chapter presents conclusions based upon the research presented in this thesis, and offers recommendations for further work. First, here is a list of key contributions documented by this thesis:

Analysis

- Verified significant advantages of composite materials over aluminum in WASP vehicle design
- Trade study on material and geometry variable sensitivity for quick design change evaluation
- Shroud concept and design crucial for WASP II survival
- Framework for composite failure analysis code

Testing

- Tested 6 composite cylinder samples statically, 4 dynamically
- Validated survivability of composite cylinders in high-g environment
- Showed static tests can substitute for air-gun tests in many situations

Manufacturing

- Streamlined procedure for manufacturing graphite/epoxy cylinders
- Prescribed materials and requirements for manufacturing body sections by external vendor
- Developed procedure for manufacturing complicated aerosurfaces accurately using room temperature vacuum cures on a single faced mold
- Developed new folding hinged wings and dihedral mechanisms
- Manufactured 3 functional sets of all WASP II aerosurfaces

Design

- Building block approach to improve high-g composite component design

10.1 Conclusions

The structural design of the WASP vehicle was a very challenging problem since it not only had to sustain flight, but survive a gun launch with a sensitive payload. A basic finite element model was created to evaluate the advantages of utilizing composite materials over aluminum in the design of the tail section. It was found that a significant saving in weight and a slight increase in strength could be achieved by this material substitution. Further finite element models were subsequently made to investigate more thoroughly the static and dynamic effects of high-g loading on these fuselage sections. Static and air-gun tests were then performed to validate these models. From

these tests and models, a "building-block" procedure for designing high-g composite components was proposed utilizing CLPT, an ABAQUS™ model, and a few validating tests. Also, the correlation between the static tests and air-gun launches provided the confidence to save both time and money by hydraulically testing these sections to refine their design.

From these studies performed at the conclusion of the WASP I vehicle, it was decided that the entire structure (except for the bulkheads) of the WASP II flyer would be constructed of composite material. The developed high-g procedure was employed to design the three main sections of the vehicle, which were then manufactured by an external vendor by compression molding. Wet-layup was identified as the appropriate fabrication method for the aerodynamic surfaces of the vehicle, and a manufacturing technique was developed to obtain the correct cross-section and stiffness. These parts were vacuum-cured in an open-faced aluminum mold, and secondary cures were used to join sections and to add features. Attachment and hinge mechanisms were also investigated to allow a minimum volume vehicle to stow in an artillery shell.

Finally, the concept of a protective shroud was introduced that significantly reduced the requirements of the composite components. It accomplished this by decreasing the load experienced by many of the sections, and by putting most of the components whose failure mode in the original design was dominated by buckling, into tension. The shroud was designed to survive both the set-back and forward accelerations, the spin loads, and the global and local buckling of its thin shell walls. It would also serve as ballistic

weight, being built out of steel, to trim the center of gravity of the projectile and to adjust the overall weight for the use of standard ballistic range tables.

10.2 Recommendations for Future Work

This work represents a preliminary attempt to develop a full design tool for composites in a high-g environment. Further refinement is needed in the ABAQUS™ code presented to more accurately predict the failure load observed during testing, and the Matlab™ CLPT code utilized could be integrated into a failure analysis routine embedded in ABAQUS™ to make this procedure more compact. Other composite materials utilizing higher strength fibers and tougher matrices (e.g. IM7/977-2 or T300/914C), and manufacturing techniques, such as filament winding, should be investigated as well to confirm that this model is appropriate for more than just the hand laid-up AS4/3501-6 used for these tests. Also, further static tests should be performed with different boundary conditions and loading rates to attempt to more accurately match the air-gun launch profile.

The airfoil sections, which in this investigation were manufactured by wet-layup, will most likely need to be developed using a different procedure or at least using a different adhesive system, since it is unlikely that the ones made here are g-hardened. A probable solution for manufacture of the entire detailed WASP vehicle in the future would be resin-transfer-molding (RTM), which would consist of designing of a closed mold which is injected with a

graphite and epoxy mixture. This procedure has high development costs, but would significantly reduce the cost and time of making each unit, and allows more complicated details in the design as well as quasi-isotropic material properties in all directions. If the demands for the WASP vehicle are not high enough to justify the high initial costs, or if testing proves that RTM is not suitable for high-g applications, compression molding should also be considered as a possible candidate for all of the components.

Lastly, much testing and re-design remains for the attachment and hinge mechanisms of this vehicle. The methods presented in this paper will achieve the current flight goals of the WASP II flight demonstrator, however are thought not to be survivable for a high-g environment. Testing is needed to find an appropriate adhesive to attach the different composite sections, since the bolts and wax used for the current flyer were only meant for demonstration so that the vehicle would be easily disassembled or repaired. Also, testing is needed on the hinge sections to examine their response to all the loads on the vehicle, and a more integrated system should be developed since the current hinge/dihedral/lock mechanism is very labor intensive and requires 4 separate cures. Overall, the work presented in this thesis offers much insight into the preliminary design of a high-g composite structure, however more work is necessary to fully qualify a protocol for designing a g-hardened vehicle.

[This page intentionally left blank]

REFERENCES

1) Jenkins, S. *Investigation of Curved Composite Panels Under High-G Loading*. Massachusetts Institute of Technology. Cambridge, MA, USA, 1999.

2) Kirkos, G. "Wide Area Surveillance Projectile (WASP) Critical Design Review," Charles Stark Draper Laboratory, Presented to DARPA SPO, Cambridge, MA, Oct. 1999.

3) Van Dyke, P. "Stress about a Circular Hole in a Cylindrical Shell." *AIAA Journal,* Sept. 1964, pp. 1733-1742.

4) Young, W.C. *Roark's Formulas for Stress and Strain*. 6th ed., McGraw-Hill Book Company, Inc., New York, 1989.

5) Pilkey, R.D. *Peterson's Stress Concentration Factors*. 2nd ed., John Wiley & Sons, New York, 1997.

6) Hoff, N.J. "Low Buckling Stresses of Axially Compressed Circular Cylindrical Shells of Finite Length." *Journal of Applied Mechanics,* Sept. 1965, pp. 533-541.

7) Hilburger, M.W. *Numerical and Experimental Study of the Compression Response of Composite Cylindrical Shells with Cutouts*. University of Michigan, Ann Arbor, MI, USA, 1998.

8) Noor, A.K., and W.S. Burton. "Assessment of Computational Models for Multilayered Composite Shells." *Applied Mechanics Reviews,* Vol. 43, 1990, pp. 67-97.

9) Noor, A.K., and J.M. Peters. Tress, Vibration, and Buckling of Multilayered Cylinders." *Journal of Structural Engineering,* Vol. 115, 1989, pp. 69-88.

10) Hu, H.T., and S.S. Wang. "Optimization for Buckling Resistance of Fiber-Composite Laminate Shells With and Without Cutouts." *Composite Structures,* Vol. 22, 1992, pp. 3-13.

11) Timoshenko, S., and J.N. Goodier. *Theory of Elasticity*. A McGraw-Hill Classic Textbook Reissue. 3rd ed., McGraw-Hill Book Company, Inc., New York, 1987.

12) Timoshenko, S., and S. Woinowsky-Krieger. *Theory of Plates and Shells.* A McGraw-Hill Classic Textbook Reissue. 2nd ed., McGraw-Hill Book Company, Inc., New York, 1987.

13) Donnell, L. H. "A New Theory for the Buckling of Thin Cylinders Under Axial Compression and Bending." *Transactions of the American Society of Mechanical Engineers,* Vol. 56, 1934, pp. 795-800.

14) Tong, L. "Buckling of Filament Wound Composite Conical Shells Under Axial Compression." *AIAA Journal,* Vol. 37, 1999, pp. 778-781.

15) Tennyson, R.C. "Buckling of Laminated Composite Cylinders." *Composites*, Vol. 1, 1975, pp. 17-25.

16) Jegley, D. C., and O.F. Lopez. "Comparison of hand laid-up tape and filament wound composite cylinders and panels with and without impact damage." *Structural Dynamics, and Materials Conference*, AIAA/ASME/ASCE/AHS/ASC Structures, 32nd, Baltimore, MD, Apr. 1991, pp. 1144-1152.

17) Tennyson, R.C. "The Effects of Unreinforced Circular Cutouts on the Buckling of Circular Cylindrical Shells Under Axial Compression." *Journal of Engineering for Industry*, Vol. 90, 1968, pp. 541-546.

18) Toda, S., "Buckling of Cylinders with Cutouts Under Axial Compression." *Experimental Mechanics*, Vol. 23, 1983, pp. 414-417.

19) Katch, S. *Concept Development, Mechanical Design, Manufacturing and Experimental Testing for a Cannon-Launched Reconnaissance Vehicles.* Massachusetts Institute of Technology. Cambridge, MA, USA, 1998.

20) Tsai, S. W. *Theory of Composites Design*. Think Composites, Dayton, OH, 1992.

21) Jones, R. M. *Mechanics of Composite Materials.* 2nd ed., Taylor & Francis, Blacksburg, VA, 1999.

22) Lagace, P.A., Brewer, J.C., and Varnerin, C., "TELAC Manufacturing Course Notes." TELAC Report 88-4B, Massachusetts Institute of Technology, 1990.

23) TW metals, Chicago, IL. 1-800-545-5000

24) Dunn, C. *The Analysis, Design, Manufacture, and Testing of a Composite Micro-Satellite*. Massachusetts Institute of Technology. Cambridge, MA, USA, 2000.

25) Composite Structure Technology (CST), Tehachapi, CA. 1-800-338-1278

26) Casiez, T. *Compact, High-G, High Efficiency Folding Wing for a Cannon Launched Reconnaissance Vehicle*. Massachusetts Institute of Technology, Cambridge, MA, USA, 1998.

27) Radcliffe, T. *Aeroelastic Study of a Folding Wing*. Massachusetts Institute of Technology, Cambridge, MA, USA, 2000.

APPENDIX A: Matlab® CLPT failure analysis codes

MATLABÔ CLPT Laminate Bulk Orthotropic Properties Code

```
layup = input('Enter nonSymetric Half Layup: [0 45 -45 ...]s ');
**(material property definitions)**
E = [144.5E9 9.63E9 .34 5.85E9 .000134];
F = [2167E6 -1720E6 53.7E6 -185.8E6 86.7E6];
St = [2.167/144.5 -1.72/144.5 .0537/9.63 -.1858/9.63 .0867/5.85];

El = E(1,1);
Et = E(1,2);
vlt = E(1,3);
vtl = Et/El*vlt;
G = E(1,4);
t = E(1,5);
ply = size(layup,2);
**(plane stress coefficients)**
q = zeros(3,3);
q(1,1) = El/(1-vlt*vtl);
q(2,2) = Et/(1-vlt*vtl);
q(1,2) = (Et*vlt)/(1-vlt*vtl);
q(2,1) = q(1,2);
q(3,3) = G;

sym = 0;

QBAR = [0 0 0
    0 0 0
    0 0 0];
**(ply coordinate transformation and Q matrix assembly)**
for z = 1 : ply;

            x = layup(1,z)*pi/180;

            a = [cos(x)*cos(x) sin(x)*sin(x) cos(x)*sin(x)
                sin(x)*sin(x) cos(x)*cos(x) -cos(x)*sin(x)
              -2*cos(x)*sin(x) 2*cos(x)*sin(x) (cos(x)*cos(x)-sin(x)*sin(x))];

            b = transpose(a);

            Q = b*q*a;

            QBAR = QBAR + Q;
end
if sym == 1;
            QBAR = 2*QBAR;
end
```

QBAR;
A=QBAR/(ply*2);
As=A^-1;
Es11=As(1,1);
Es22=As(2,2);
Es33=As(3,3);
Es12=As(1,2);
(Bulk orthotropic material properties)*
E11=Es11^-1
E22=Es22^-1
G=Es33^-1
v=-Es12*E11
t=ply*2*t

MATLABÔ CLPT Ply-by-Ply Laminate Failure Analysis Code

```
**(Material property definition)**
E = [144.5E9 9.63E9 .34 5.85E9 .000134];
F = [2167E6 -1720E6 53.7E6 -185.8E6 86.7E6];
St = [2.167/144.5 -1.72/144.5 .0537/9.63 -.1858/9.63 .0867/5.85];
layup = [0 45 -45 0 45 -45 0 45 -45];
mass = 1.795;

sym=1;
kt = input('kt1 kt2 kt12:  ');
method = input('0 for Tsai-Wu or 1 for Max-Strain:  ');

v1 = kt(1,1);
v2 = kt(1,2);
v12 = kt(1,3);
V = [v1 0 0; 0 v2 0; 0 0 v12];
**(Plane stress coefficients)**
El = E(1,1);
Et = E(1,2);
vlt = E(1,3);
vtl = Et/El*vlt;
G = E(1,4);
t = E(1,5);
ply = size(layup,2);
area = pi*(2*t*ply*2*.04445 + (t*ply*2)^2);

Xt = F(1,1);
Xc = F(1,2);
Yt = F(1,3);
Yc = F(1,4);
S = F(1,5);

xt = St(1,1);
xc = St(1,2);
yt = St(1,3);
yc = St(1,4);
s = St(1,5);
**(Tsai-Wu Failure Constants)**
F1 = (1/Xt)+(1/Xc);
F11 = -1/(Xc*Xt);
F2 = (1/Yt)+(1/Yc);
F22 = -1/(Yc*Yt);
F66 = 1/S^2;
F12 = -.5/sqrt(Xt*Xc*Yt*Yc);

q = zeros(3,3);
q(1,1) = El/(1-vlt*vtl);
q(2,2) = Et/(1-vlt*vtl);
q(1,2) = (Et*vlt)/(1-vlt*vtl);
q(2,1) = q(1,2);
q(3,3) = G;
```

```
begin_accel_check = 0

broke = zeros(1,ply);
brokelast = ones(1,ply);
stress = zeros(3,1);
strain = zeros(3,1);
done = 0;

T=0;
g=0;
load = zeros(3,1);

while done ~= 1,
        index = 0;
        while index ~= 1,
                **(Remove broken plies from stiffness matrix)**
                if sum(brokelast) ~= sum(broke)
                        therm = zeros(3,1);
                        QBAR = zeros(3,3);
                        for z = 1 : ply,

                                if broke(1,z) == 1
                                        Q = zeros(3,3);
                                else
                                        x = layup(1,z)*pi/180;
                                        a = [cos(x)*cos(x) sin(x)*sin(x) cos(x)*sin(x)
                                            sin(x)*sin(x) cos(x)*cos(x) -cos(x)*sin(x)
                                         -2*cos(x)*sin(x) 2*cos(x)*sin(x) (cos(x)*cos(x)-sin(x)*sin(x))];
                                        b = transpose(a);
                                        Q = b*q*a;

                                end

                                tforce = T*Q*a^-1*al;
                                therm = therm + tforce;

                                QBAR = QBAR + Q;
                        end

                        if sym == 1
                                QBAR = 2*QBAR;
                                therm = 2*therm;
                        end
                end

                brokelast = broke;

                strain = QBAR^-1*((load*ply*2)+therm);
                **(ply coordinate transformation and Q matrix assembly)**
                jump = 0;
                for z = 1 : ply,
                        if broke(1,z) ~= 1
                                x = layup(1,z)*pi/180;
                                a = [cos(x)*cos(x) sin(x)*sin(x) cos(x)*sin(x)
                                    sin(x)*sin(x) cos(x)*cos(x) -cos(x)*sin(x)
                                 -2*cos(x)*sin(x) 2*cos(x)*sin(x) (cos(x)*cos(x)-sin(x)*sin(x))];
```

```
                        b = transpose(a);
                        Q = b*q*a;

                        mstrain = strain-(T*a^-1*al);
                        sigmal = Q*mstrain;
                        sigma = b^-1 * sigmal;
                        sigma = V*sigma;
                    else
                        sigma = zeros(3,1);
                    end
                    **(Tsai-Wu Failure Criteria)**
                    if method == 0
                        TSAI = F1*sigma(1,1) + F2*sigma(2,1) + F11*sigma(1,1)^2 +
F22*sigma(2,1)^2 + F66*sigma(3,1)^2 + 2*F12*sigma(1,1)*sigma(2,1);
                        if TSAI >= 1;
                            jump = 1;
                            broke(1,z) = 1;
                            layup(1,z)
                        end
                    end
                    **(Max Strain Failure Criteria)**
                    if method == 1
                        epsilon = q^-1 * sigma;
                        if (epsilon(1,1) >= xt) | (epsilon(1,1) <= xc)
                            jump = 1;
                            broke(1,z) = 1;
                            layup(1,z)
                        elseif (epsilon(2,1) >= yt) | (epsilon(2,1) <= yc)
                            jump = 1;
                            broke(1,z) = 1;
                            layup(1,z)
                        elseif (epsilon(3,1) >= s) | (epsilon(3,1) <= -s)
                            jump = 1;
                            broke(1,z) = 1;
                            layup(1,z)
                        end
                    end
                end


                if jump == 1
                    g
                    index = 1;
                    break
                end
                **(Increment mass and thus acceleration load)**
                g = g + 250;
                load(1,1) = mass*9.8*g/area;
            end

            if broke == ones(1,ply)
                done = 1;
                break
            end

end
```

APPENDIX B: ABAQUS® FEA input files

ABAQUS Ô Static Finite Element Analysis Input File (static.inp)

```
*HEADING
SDRC I-DEAS ABAQUS FILE TRANSLATOR  04-Jun-99   11:38:57
*NODE, SYSTEM=R
       1, 1.7500000E+00,-6.8296200E-17, 5.0000000E-01
                                    •
                                    •
                                    •
     6895,-1.7453480E+00,-9.0608547E-02, 2.2443526E-01
*ELEMENT,TYPE=S8R     ,ELSET=E1
  2141,   6056,   6055,   6058,   6057,   6417,   6427,   6105,   6419
                                    •
                                    •
                                    •
  1948,   5643,   5645,   5971,   5967,   5690,   6061,   6062,   6063
*ELEMENT,TYPE=S8R     ,ELSET=E2
  2194,   6473,   6479,    369,    461,   6600,   6601,    430,   6596
                                    •
                                    •
                                    •
  1097,   3406,   3408,   3500,   3498,   3407,   3452,   3499,   3451
*SHELL SECTION,ELSET=E1,MATERIAL=STEEL
 0.5, 3
*MATERIAL,NAME=STEEL
*ELASTIC,TYPE=ISOTROPIC
 2.0E+12, 0.3
*DENSITY
 0.1
*SHELL GENERAL SECTION,ELSET=E2,COMPOSITE,ORIENTATION=SECORI
.005,,LAMINA, 90.
.005,,LAMINA,+45.
.005,,LAMINA,-45.
.005,,LAMINA, 90.
.005,,LAMINA,+55.
.005,,LAMINA,-45.
.005,,LAMINA, 90.
.005,,LAMINA,+45.
.005,,LAMINA,-45.
*** CENTER LINE
.005,,LAMINA,-45.
.005,,LAMINA,+45.
.005,,LAMINA, 90.
.005,,LAMINA,-45.
.005,,LAMINA,+45.
.005,,LAMINA, 90.
.005,,LAMINA,-45.
.005,,LAMINA,+45.
.005,,LAMINA, 90.
**defined 90 degrees rotated
```

```
*MATERIAL,NAME=LAMINA
*ELASTIC,TYPE=LAMINA
21E6, 1.4E6, .34, 0.85E6, 0.85E6, 0.5E6
*DENSITY
 0.06
*ORIENTATION,SYSTEM=CYLINDRICAL,NAME=SECORI
0.,0.,0., 0.,0., 1.
1, 0.
*NSET,NSET=CLAMPED
   61,   92,  153,  184,  245,  276,  337,  368,  429,  460,  521
                                    •
                                    •
                                    •
 5091, 5122, 5183, 5214, 5275, 5306, 5367, 5398, 5459, 5490, 5551
*ELSET,ELSET=FORCE
 1948, 1949, 1950, 1951, 1952, 1953, 1954, 1955, 1956, 1957, 1958
                                    •
                                    •
                                    •
 2124, 2125, 2126, 2127, 2128, 2129, 2130, 2131, 2132, 2133, 2134
*STEP
*STATIC
*BOUNDARY
CLAMPED, ENCASTRE
*DLOAD
FORCE, P, -1000.0
*RESTART,WRITE,OVERLAY
*EL FILE,ELSET=E2,DIRECTIONS=YES
SDV,FV
S,E
*NODE FILE, FREQUENCY=1, LAST MODE=1
U
*EL PRINT,ELSET=E2
S,E
*NODE PRINT
U
RF
*END STEP
**-------
```

ABAQUS Ô Dynamic Finite Element Analysis Input File (dynamic.inp)

```
*HEADING
SDRC I-DEAS ABAQUS FILE TRANSLATOR  04-Jun-99   11:38:57
*NODE, SYSTEM=R
        1, 1.7500000E+00,-6.8296200E-17, 5.0000000E-01
                                    •
                                    •
                                    •
      6895,-1.7453480E+00,-9.0608547E-02, 2.2443526E-01
*ELEMENT,TYPE=S8R     ,ELSET=E1
  2141,   6056,   6055,   6058,   6057,   6417,   6427,   6105,   6419
                                    •
                                    •
                                    •
  1948,   5643,   5645,   5971,   5967,   5690,   6061,   6062,   6063
*ELEMENT,TYPE=S8R     ,ELSET=E2
  2194,   6473,   6479,    369,    461,   6600,   6601,  430,   6596
                                    •
                                    •
                                    •
  1097,   3406,   3408,   3500,   3498,   3407,   3452,   3499,   3451
*SHELL SECTION,ELSET=E1,MATERIAL=STEEL
 0.5, 3
*MATERIAL,NAME=STEEL
*ELASTIC,TYPE=ISOTROPIC
 2.0E+12, 0.3
*DENSITY
 0.1
*SHELL GENERAL SECTION,ELSET=E2,COMPOSITE,ORIENTATION=SECORI
.005,,LAMINA, 90.
.005,,LAMINA,+45.
.005,,LAMINA,-45.
.005,,LAMINA, 90.
.005,,LAMINA,+45.
.005,,LAMINA,-45.
.005,,LAMINA, 90.
.005,,LAMINA,+45.
.005,,LAMINA,-45.
*** CENTER LINE
.005,,LAMINA,-45.
.005,,LAMINA,+45.
.005,,LAMINA, 90.
.005,,LAMINA,-45.
.005,,LAMINA,+45.
.005,,LAMINA, 90.
.005,,LAMINA,-45.
.005,,LAMINA,+45.
.005,,LAMINA, 90.
**defined 90 degrees rotated
```

```
*MATERIAL,NAME=LAMINA
*ELASTIC,TYPE=LAMINA
18.54E6, 1.287E6, .3, 0.785E6, 0.785E6, 0.785E6
*DENSITY
 0.06
*ORIENTATION,SYSTEM=CYLINDRICAL,NAME=SECORI
0.,0.,0., 0.,0., 1.
1, 0.
*NSET,NSET=CLAMPED
   61,   92,  153,  184,  245,  276,  337,  368,  429,  460,  521
                                    •
                                    •
                                    •
 5091, 5122, 5183, 5214, 5275, 5306, 5367, 5398, 5459, 5490, 5551
*ELSET,ELSET=FORCE
 1948, 1949, 1950, 1951, 1952, 1953, 1954, 1955, 1956, 1957, 1958
                                    •
                                    •
                                    •
 2124, 2125, 2126, 2127, 2128, 2129, 2130, 2131, 2132, 2133, 2134
*STEP
*BUCKLE
1,,3,30
*BOUNDARY
CLAMPED, ENCASTRE
*DLOAD
FORCE, P, -1000.0
*RESTART,WRITE,OVERLAY
*MODAL FILE
*END STEP
**-------
```

ABAQUS Ô Dynamic Finite Element Analysis Message File (dynamic.msp)

STEP 1 INCREMENT 1 STEP TIME 0.

S T E P 1 C A L C U L A T I O N O F E I G E N V A L U E S

F O R B U C K L I N G P R E D I C T I O N

THE SUBSPACE ITERATION METHOD IS USED FOR THIS ANALYSIS
NUMBER OF EIGENVALUES 1
MAXIMUM NUMBER OF ITERATIONS 30
NUMBER OF VECTORS IN ITERATION 3
ONLY INITIAL STRESS EFFECTS ARE INCLUDED IN THE
STIFFNESS MATRIX

RESTART FILE WILL BE WRITTEN EVERY 1 INCREMENTS

ONLY THE LATEST INCREMENT WILL BE RETAINED

THIS IS A LINEAR PERTURBATION STEP.
ALL LOADS ARE DEFINED AS CHANGE IN LOAD TO THE REFERENCE STATE

EXTRAPOLATION WILL NOT BE USED

CHARACTERISTIC ELEMENT LENGTH 0.175

PRINT OF INCREMENT NUMBER, TIME, ETC., TO THE MESSAGE FILE EVERY 1 INCREMENTS

ITERATION 1 CURRENT ESTIMATES OF EIGENVALUES

1 69.195 2 102.83 3 167.53

ITERATION 2 CURRENT ESTIMATES OF EIGENVALUES

1 43.362 2 45.897 3 60.184

ITERATION 3 CURRENT ESTIMATES OF EIGENVALUES

1 9.8411 2 10.655 3 13.792

ITERATION 4 CURRENT ESTIMATES OF EIGENVALUES

1 5.6051 2 6.0827 3 6.7424

ITERATION 5 CURRENT ESTIMATES OF EIGENVALUES

1 5.4248 2 5.5082 3 6.0477

•
•
•

ITERATION 20 CURRENT ESTIMATES OF EIGENVALUES

1 5.2596 2 5.2906 3 5.3473

ITERATION 21 CURRENT ESTIMATES OF EIGENVALUES

1 5.2595 2 5.2892 3 5.3470

ITERATION 22 CURRENT ESTIMATES OF EIGENVALUES

1 5.2594 2 5.2880 3 5.3468

ITERATION 23 CURRENT ESTIMATES OF EIGENVALUES

1 5.2594 2 5.2871 3 5.3466

THE FIRST 1 EIGENVALUES HAVE CONVERGED

RESTART INFORMATION WRITTEN IN STEP 1 AFTER INCREMENT 1

THE ANALYSIS HAS BEEN COMPLETED

ANALYSIS SUMMARY:
TOTAL OF 1 INCREMENTS
0 CUTBACKS IN AUTOMATIC INCREMENTATION
25 ITERATIONS
25 PASSES THROUGH THE EQUATION SOLVER OF WHICH
2 INVOLVE MATRIX DECOMPOSITION, INCLUDING
0 DECOMPOSITION(S) OF THE MASS MATRIX
0 ADDITIONAL RESIDUAL EVALUATIONS FOR LINE SEARCHES
0 ADDITIONAL OPERATOR EVALUATIONS FOR LINE SEARCHES
33 WARNING MESSAGES DURING USER INPUT PROCESSING
0 WARNING MESSAGES DURING ANALYSIS
0 ANALYSIS WARNINGS ARE NUMERICAL PROBLEM MESSAGES
0 ANALYSIS WARNINGS ARE NEGATIVE EIGENVALUE MESSAGES
0 ERROR MESSAGES

THE SPARSE SOLVER HAS BEEN USED FOR THIS ANALYSIS.

JOB TIME SUMMARY
USER TIME (SEC) = 944.19
SYSTEM TIME (SEC) = 40.640
TOTAL CPU TIME (SEC) = 984.83
WALLCLOCK TIME (SEC) = 505

APPENDIX C: Load-Displacement Curves

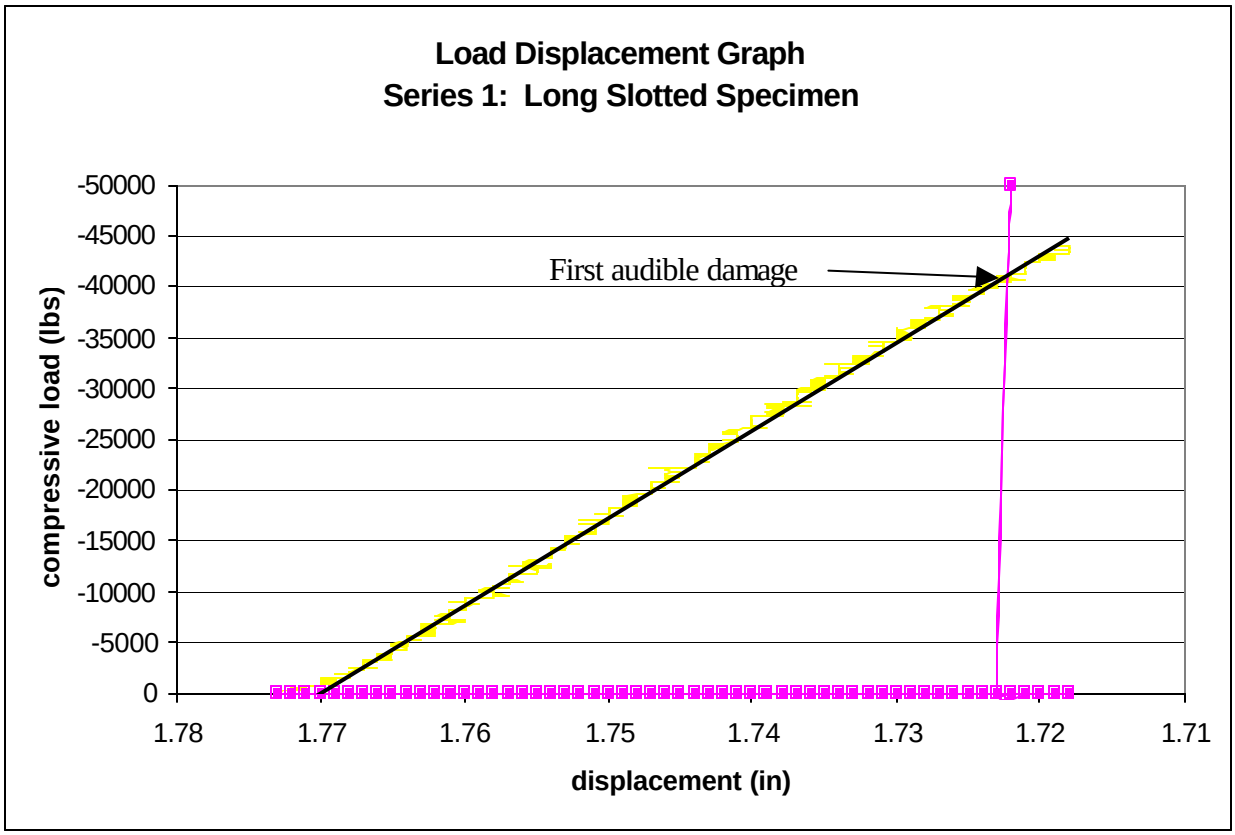
Load Displacement Graph
Series 1: Long Slotted Specimen
compressive load (lbs)
-50000
-45000
-40000
-35000
-30000
-25000
-20000
-15000
-10000
-5000
0
First audible damage
1.78
1.77
1.76
1.75
1.74
1.73
1.72
1.71
displacement (in)

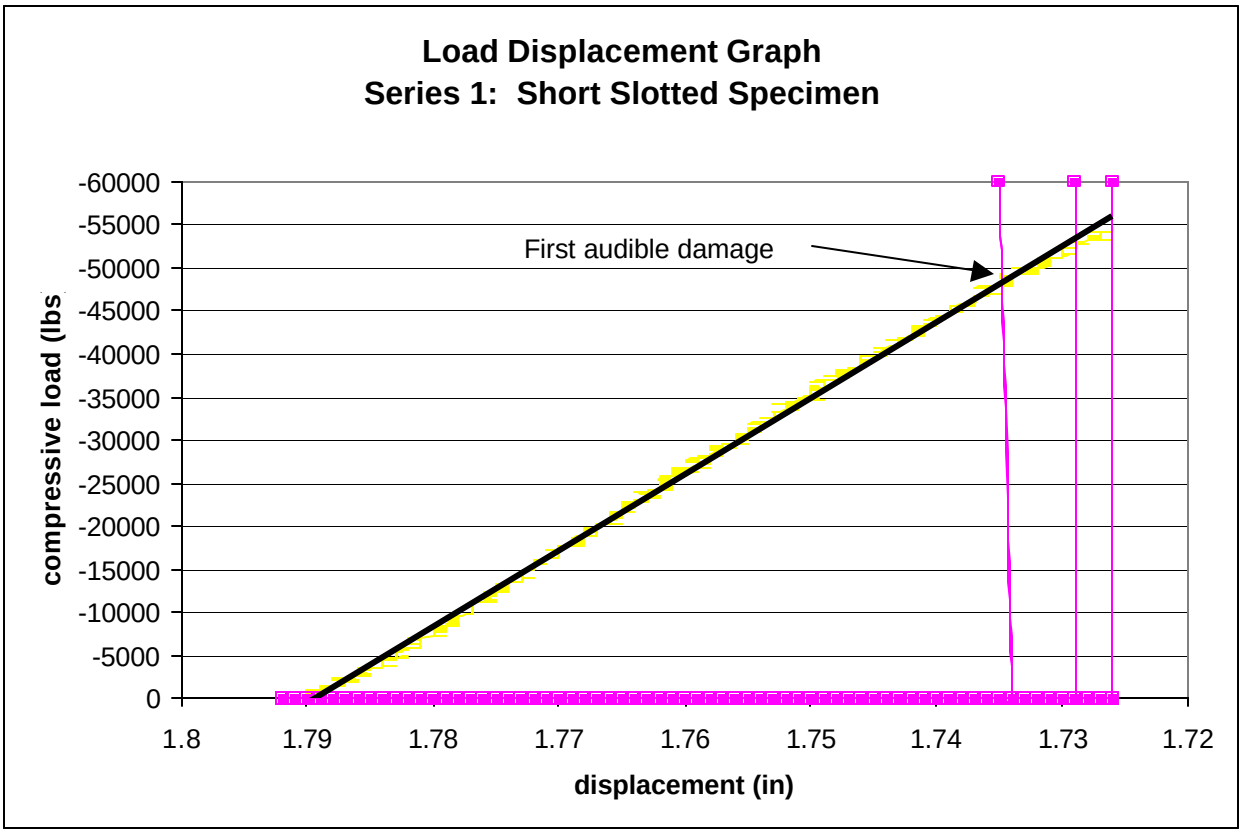
Load Displacement Graph
Series 1: Short Slotted Specimen
compressive load (lbs
-60000
-55000
-50000
-45000
-40000
-35000
-30000
-25000
-20000
-15000
-10000
-5000
0
First audible damage
1.8
1.79
1.78
1.77
1.76
1.75
1.74
1.73
1.72
displacement (in)

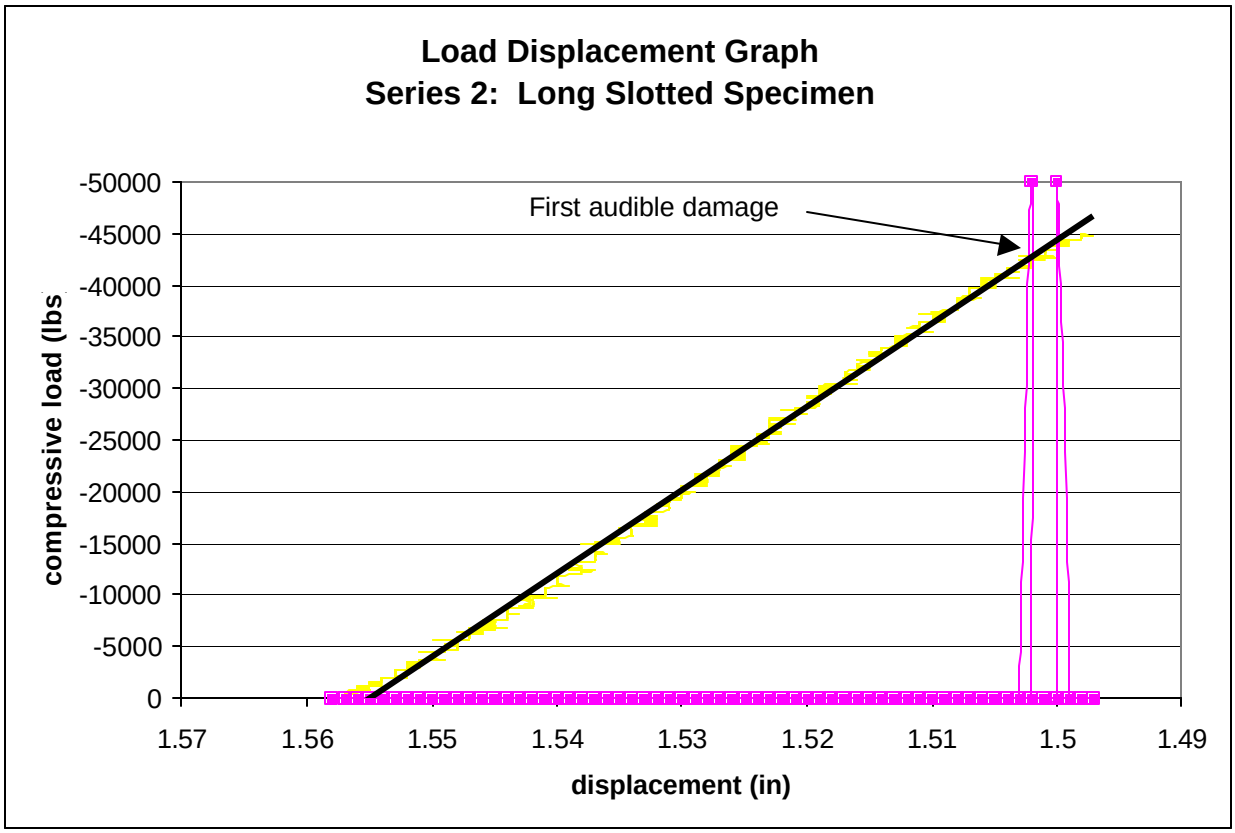
Load Displacement Graph
Series 2: Long Slotted Specimen
First audible damage
compressive load (lbs
-50000
-45000
-40000
-35000
-30000
-25000
-20000
-15000
-10000
-5000
0
1.57
1.56
1.55
1.54
1.53
1.52
1.51
1.5
1.49
displacement (in)

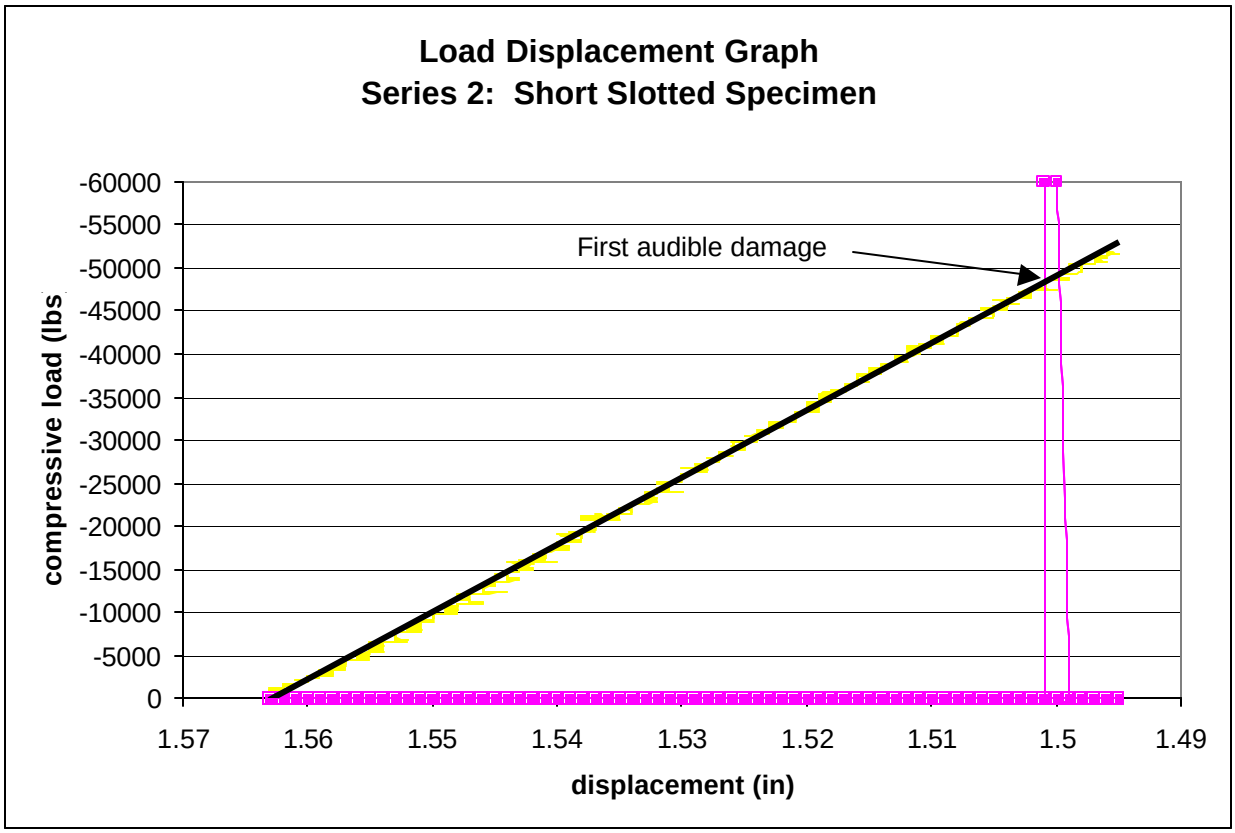
Load Displacement Graph
Series 2: Short Slotted Specimen
First audible damage
compressive load (lbs
-60000
-55000
-50000
-45000
-40000
-35000
-30000
-25000
-20000
-15000
-10000
-5000
0
1.57
1.56
1.55
1.54
1.53
1.52
1.51
1.5
1.49
displacement (in)

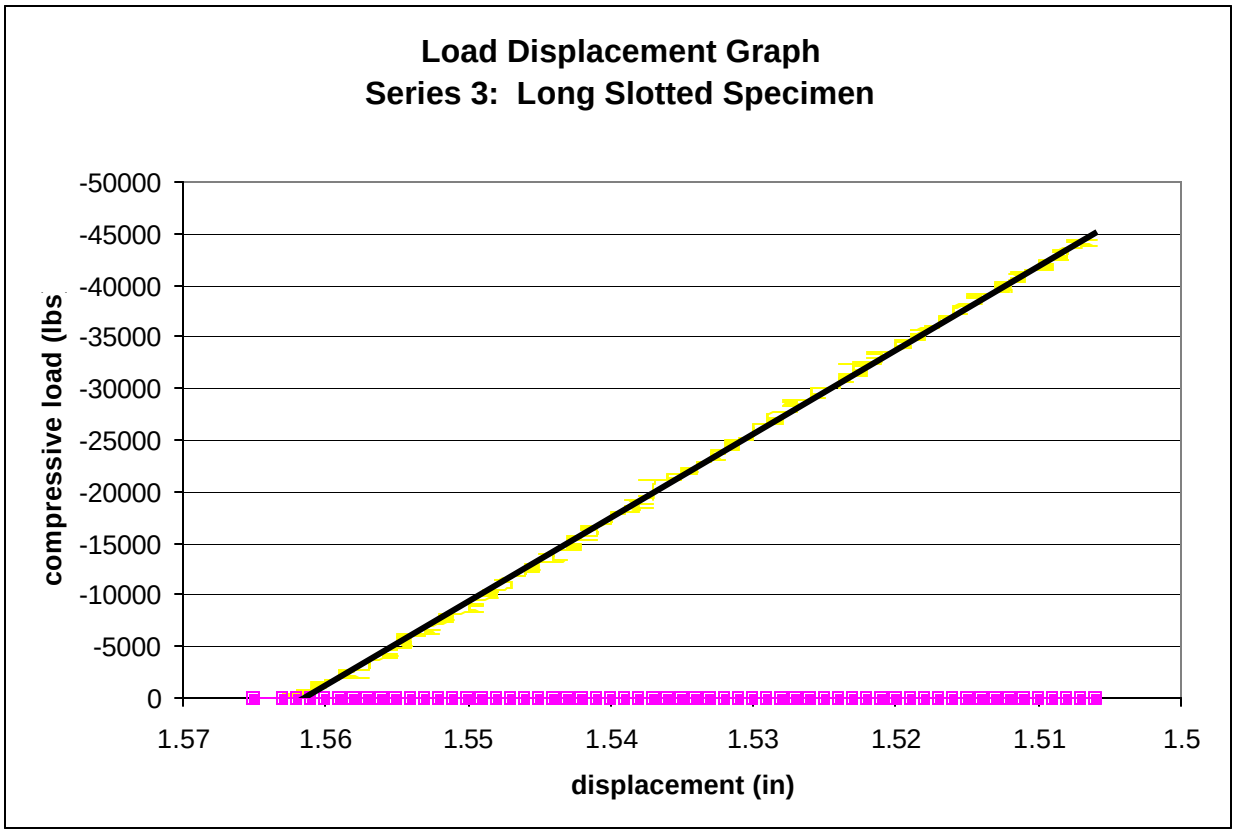
Load Displacement Graph
Series 3: Long Slotted Specimen
compressive load (lbs
-50000
-45000
-40000
-35000
-30000
-25000
-20000
-15000
-10000
-5000
0
1.57
1.56
1.55
1.54
1.53
1.52
1.51
1.5
displacement (in)

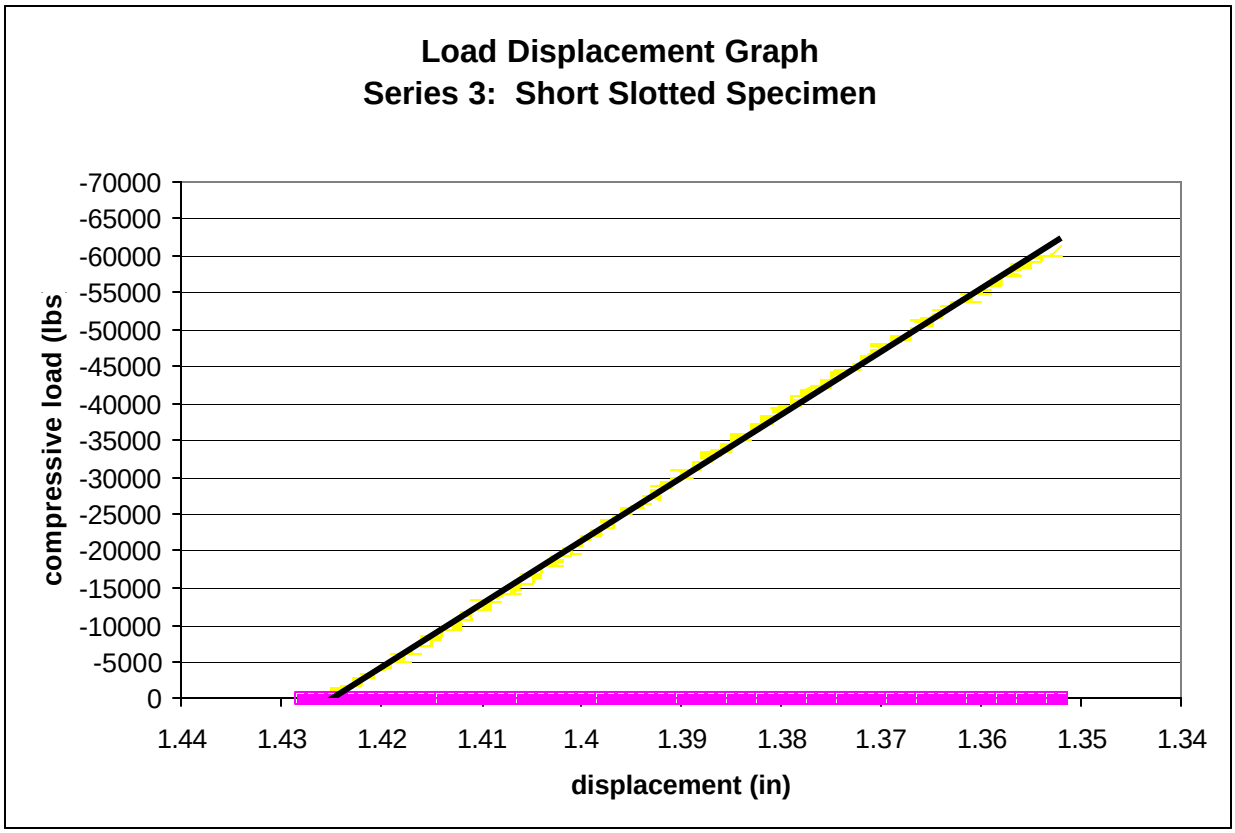
Load Displacement Graph
Series 3: Short Slotted Specimen
compressive load (lbs
-70000
-65000
-60000
-55000
-50000
-45000
-40000
-35000
-30000
-25000
-20000
-15000
-10000
-5000
0
1.44
1.43
1.42
1.41
1.4
1.39
1.38
1.37
1.36
1.35
1.34
displacement (in)

[This page intentionally left blank]